



HAL
open science

Generation of static magnetic fields per current and permanent magnet. Method of calculating field synthesis and realization of any profile.

Alexandre Labiche

► **To cite this version:**

Alexandre Labiche. Generation of static magnetic fields per current and permanent magnet. Method of calculating field synthesis and realization of any profile.. Computational Physics [physics.comp-ph]. Université Paris-Sud Orsay, 1998. English. NNT: . hal-02570229v1

HAL Id: hal-02570229

<https://hal.science/hal-02570229v1>

Submitted on 12 May 2020 (v1), last revised 28 Sep 2021 (v2)

HAL is a multi-disciplinary open access archive for the deposit and dissemination of scientific research documents, whether they are published or not. The documents may come from teaching and research institutions in France or abroad, or from public or private research centers.

L'archive ouverte pluridisciplinaire **HAL**, est destinée au dépôt et à la diffusion de documents scientifiques de niveau recherche, publiés ou non, émanant des établissements d'enseignement et de recherche français ou étrangers, des laboratoires publics ou privés.

ORSAY

N° D'ORDRE: 4963

**UNIVERSITE DE PARIS-SUD
U.F.R. SCIENTIFIQUE D'ORSAY**

THESE
présentée

Pour obtenir

Le GRADE de DOCTEUR EN SCIENCES

DE L'UNIVERSITE PARIS XI ORSAY

PAR

Alexandre LABICHE

SUJET: Génération de champs magnétiques statiques par courant et aimant permanent. Méthode de calcul de la synthèse de champ et réalisation de profil quelconque.

Soutenue le Mercredi 7 Janvier 1998 devant la Commission d'examen

MM. COULOMB	Jean Louis	Rapporteur
JEANDEY	Christian	Membre du jury
L'HUILLIER	Jean Pierre	Rapporteur
SAUZADE	Michel	Président du jury

Generation of static magnetic fields per
current and permanent magnet.
Method of calculating field synthesis and
realization of any profile.

LABICHE Alexandre

October 23rd 1997

Acknowledgements

I would like to thank my thesis supervisor, Mr Taquin, for his availability and his support throughout this thesis. His experience in the field of magnetic field calculations was indispensable and the orientations chosen were beneficial. These three years have therefore been very rich in teaching.

I am very grateful to the directors of the laboratory, Dr M. Sauzade and Dr J. Bittoun, for accepting me into their unit and providing the means necessary for this work.

I am very grateful to Mr. S.K. Kan for teaching me a related field. such as radiofrequency field calculation.

I would also like to thank the entire laboratory team for its support and his great kindness.

I would like to thank the members of the jury, especially Mr. Coulomb and Mr. L'huillier. for taking on the extra burden of report writing thesis.

I would like to thank the Ecole Spéciale des Travaux Publics (Special School of Public Works) which has been instrumental in bringing this work to fruition.

A big thank you to my parents Raymonde and Jacques who helped me to continue my studies until this achievement.

Contents

Introduction	5
1 Determination of the field \vec{B}	7
1.1 Scalar potential	7
1.2 Generalized coordinates	7
1.2.1 Matrix determination F	9
1.3 Cylindrical coordinates	10
1.3.1 Matrix F in cylindrical coordinates	10
1.4 Cartesian coordinates	13
1.4.1 Matrix F in cartesian coordinates	13
1.5 Shape of the magnets	15
1.6 Influence of the demagnetizing field	16
1.6.1 Calculation of the demagnetizing field	17
2 Field correction	21
2.1 Potential development	21
2.2 Conditions on the calculation of coefficients	24
2.3 Algorithm for calculating coefficients	27
2.4 Coefficients cancellation	30
2.5 Calculation of correction magnets	30
2.5.1 Legendre polynomial magnet development	31
2.5.2 Approximate Surface Integration	32
2.5.3 Cancellation of coefficients	33
2.5.4 Hardware configuration of the shims	35
2.6 First problem solved	36

2.7	Discussion on the direction of magnetization of the magnets relative to the main field	38
2.7.1	All magnets in the same direction:	38
2.7.2	One every two magnets in the same direction	39
2.7.3	One hemisphere one way and vice versa	39
2.8	Influence on transverse components	40
2.9	Bessel field development	42
3	Non-linear resolution	45
3.1	General Newton method	45
3.2	Roots of Legendre's equations	46
3.3	Inversion of the Jacobian matrix	48
3.4	Singular value decomposition of a square matrix	49
3.5	Software flowchart	50
4	Bivariates application	53
4.1	Curve appearance a_{00} , a_{10} , a_{20}	54
4.2	Selection of initial vectors	54
5	Field generation by means of current wires.	59
5.1	Field development of a wire segment	60
5.1.1	Calculation of component B_z (see Fig 5.1)	60
5.1.2	Calculation of the B_x component (see Fig 5.1)	61
5.1.3	Calculation of the B_y component (see Fig 5.1)	62
5.2	Uniform field generator	64
5.3	Field gradient generation $\frac{\partial B_x}{\partial x}$	66
5.4	Generation of a field gradient $\frac{\partial B_x}{\partial y}$	71
5.5	Field gradient generation $\frac{\partial B_x}{\partial z}$	74
5.6	Return arcs	78
5.7	Generation of a sinusoidal field	80
6	Experimentation	83
6.1	Measuring environment	83
6.2	Gradient measurement a_{11} version I	84
6.3	Gradient measurement a_{11} version II	84

6.4 Magnet cage validation	86
Conclusion	88

Introduction

This paper presents a technique for static magnetic field synthesis. Starting from a desired field profile, it is a matter of finding the position or certain characteristics of field sources. Since the equations used are those of the $1/R$ field development, we can extend this technique to electrostatic fields. From a numerical point of view, it is the search for the roots of these equations that interests us and not an optimization of a cost function. We have therefore followed the general heuristic that the number of equations must be equal to the number of unknowns. The degrees of freedom of the system (number of magnets, displacement in x,y of the conductors, value of the current, etc...) are therefore in agreement with the number of equations to be solved. But this is true in linear problems and in no case can we ensure a solution in non-linear systems even if we increase the number of degrees of freedom and then solve the problem by a least squares technique.. On this last point, it is a functional that will be minimized and nothing can be said a priori about the accuracy of the results.

We chose to search for the true roots of these equations. In this way, the solving system is able to give which equations cannot be canceled (or equal to a fixed value). By studying this problem in detail, some characteristics of field generation structures are necessary, they are presented throughout the document.

We will therefore start with the direct calculation of the magnetic field generated by a permanent magnet. This calculation does not really pose any difficulty, it is mainly a question of obtaining sufficient precision in relation to the real field. This step makes it possible later on to check the validity of a configuration without systematically needing to make a model. We will see that only one parameter must be experimentally determined, this is the remanent field of each magnet composing the correction structure. We will then study the inverse problem that will provide the position of the magnets, which is the very subject of the thesis

In practical cases, we can either check for field defects by measuring them

beforehand and then generate a profile in adequacy with the field already present, or generate a simple profile without taking into account possible defects related to the environment. We treated the first case with a magnet configuration and the second case with wires. The direct calculation of the field generated by conductors is not presented because we use Biot-Savart's law. The experimental validity is easy because there is no approximation and the current flowing in the conductors is easily controllable (as opposed to the value of the remanent field of the magnets).

Low-field magnetic resonance imaging requires a field of 1010 Gauss for a hydrogen resonance frequency at 4.3 MHz. In the context of imaging itself, the homogeneity of the static magnetic field must be extreme.

The maximum error in the useful area is plus or minus 10mG (10^{-6} T). This represents a relative error for a low-field imager of 10 parts per million (10 ppm per 1010 Gauss). In comparison, the Earth's magnetic field in our latitude is in the order of 500mG. Given the great homogeneity of this field, this does not pose major difficulties. On the other hand, in the presence of nearby metal structures (concrete iron for example) the Earth's magnetic field will be deflected locally. As a result, it alone will generate a very significant error in the useful area. It is then a matter of properly mapping these defects in order to have a reference when measuring a configuration. It appears that a setting at 10mG close does not allow at all to move the machine and especially not to turn it, once it is set.

In this study we will consider that the addition of magnets or conductors cannot magnetize surrounding structures and that magnetic permeability is constant in the correction area. It is slightly wrong with water contained in the body. A slight diamagnetism (water repels the magnetic field) is seen per a quantum mechanical effect in presence of very high magnetix fields.

Chapter 1

Determination of the field \vec{B}

We will study the validity of the direct calculation of the magnetic field generated by a permanent magnet. Although the magnets used are cylindrical, we will justify the use of a simple formula derived from the calculation in Cartesian coordinates. We will also study the demagnetization of the magnet itself and the possibility of integrating it by experimentally determining the value of the remanent field of each magnet.

1.1 Scalar potential

If in a given region there are no electrical sources (in movement), we can define a scalar potential ψ , such as:

$$\vec{B}(\vec{r}) = -\vec{\nabla}\psi(\vec{r}) \quad (1.1)$$

In the presence of magnetic media [41, p.37], the potential is written:

$$\psi(\vec{r}) = \frac{1}{4\pi} \int_V \vec{\nabla}' \cdot \frac{\vec{M}(\vec{r}')}{|\vec{r}_i - \vec{r}'|} dv' \quad (1.2)$$

If the magnetization \vec{M} is defined and localized, one integration per part gives:

$$\psi(\vec{r}) = \frac{1}{4\pi} \int_V \vec{M}(\vec{r}') \cdot \vec{\nabla}' \frac{1}{|\vec{r}_i - \vec{r}'|} dv' \quad (1.3)$$

1.2 Generalized coordinates

The magnetic field \vec{B} at a point i in space, determined from the field \vec{B}_{ext} created by currents and the field produced by a magnetized body of volume

V and magnetization \vec{M} is given by the expression:

$$\vec{B}(\vec{r}_i) = \vec{B}_{ext}(\vec{r}_i) - \frac{1}{4\pi} \vec{\nabla} \int_V \vec{M}(\vec{r}') \cdot \vec{\nabla}' \frac{1}{|\vec{r}_i - \vec{r}'|} dv' \quad (1.4)$$

where \vec{r}_i and \vec{r}' are respectively the coordinates of the point i and the internal coordinates of the volume V .

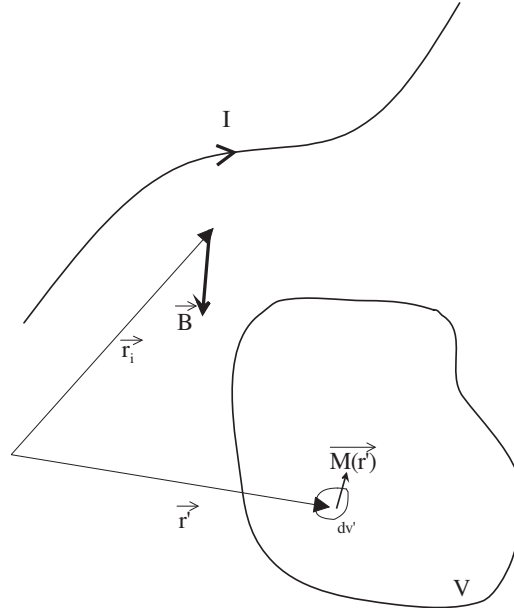


Figure 1.1: Magnetic field produced by a magnetic body and wired lines.

If we discretize the magnetized volume V into N elements V_i such that the magnetization can be considered as homogeneous, the magnetic field created at one point j of the volume V can be put in the following matrix form[41, p.9]:

$$[B_j] = [B_{0,j}] + \sum_{\substack{i=1 \\ i \neq j}}^N [F_{ij}] \cdot [M_i] - [D_j] \cdot [M_j] \quad (1.5)$$

The F matrix is used to calculate the field created by the magnetization M_i of a volume V_i at any point outside the said volume. Formally, the D matrix is identical to the F matrix, it expresses the influence of the field generated by an elementary volume on itself. This translates into by a decrease

in the magnetization of the material and thus the external excitation field \vec{B} . To simplify the calculations, the D row matrix is determined according to the calculation point located in the center of the element and thus[39], the matrix is made up of the diagonal terms of the F matrix. It is imperative to take into account the demagnetization if we are looking for the magnetization $\vec{M}(r')$ induced in the material by an external field, $\vec{M} = f(\vec{H})$, because the errors can be consequent and depend on the shape of the magnetized volume. As we will see later, the field can decrease by 1% in the case of a cubic magnetic volume. The matrix form of this last relation is written as follows

$$[M_j] = [\chi_j] \cdot [B_j] \quad (1.6)$$

The simultaneous resolution of the two equations (1.5) and (1.6) allows to calculate the magnetizing field in each element. In the thesis[41] and the article[39], the solution is based on an iterative calculation allowing at each step to refine the magnetizations $[M_j]$.

1.2.1 Matrix determination F

The calculation of the gradient of a scalar function $f(u_1, u_2, u_3)$ in orthogonal curvilinear coordinates whose reference is supported by the normalized vectors $\vec{e}_1, \vec{e}_2, \vec{e}_3$ is written [50, p.72]

$$\vec{\nabla} f(u_1, u_2, u_3) = \sum_{i=1}^3 \frac{1}{\sqrt{g_{ii}}} \frac{\partial f}{\partial u^i} \vec{e}_i \quad (1.7)$$

The magnetic field \vec{B} is then determined by the equation

$$\begin{aligned} \vec{B}(\vec{r}_i) &= \vec{B}_{ext}(\vec{r}_i) - \frac{1}{4\pi} \\ &\times \sum_{k=1}^3 \sum_{l=1}^3 \frac{M(r')}{\sqrt{g_{kk}}} \frac{\partial}{\partial u^k} \left(\int_V \frac{1}{\sqrt{g_{ll}}} \frac{\partial}{\partial u^l} \frac{1}{|\vec{r}_i - \vec{r}'|} dv' \right) \vec{e}_k \end{aligned} \quad (1.8)$$

1.3 Cylindrical coordinates

1.3.1 Matrix F in cylindrical coordinates

The metric tensor g_{ij} in cylindrical coordinates is written as follows

$$[g_{ij}] = \begin{bmatrix} 1 & 0 & 0 \\ 0 & \rho^2 & 0 \\ 0 & 0 & 1 \end{bmatrix} \quad (1.9)$$

We then identify the double-sum term in the equation (1.8) with the matrix $[F_{ij}]$ of the equation (1.5). The matrix D is obtained when the computation point r is inside the integration volume of the element. In cylindrical coordinates (ρ, ϕ, z) Figure (1.2), the matrix F can be written:

$$[F_{ij}] = \frac{1}{4\pi} \begin{bmatrix} F_{\rho\rho'} & F_{\rho\phi'} & F_{\rho z'} \\ F_{\phi\rho'} & F_{\phi\phi'} & F_{\phi z'} \\ F_{z\rho'} & F_{z\phi'} & F_{zz'} \end{bmatrix} \quad (1.10)$$

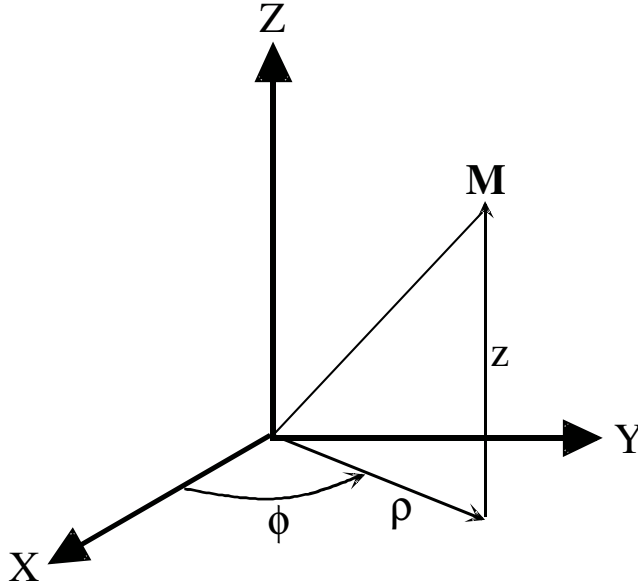


Figure 1.2: Variables used in cylindrical coordinates.

The identification of the elements of the matrix leads to the following expressions:

$$\begin{aligned}
F_{\rho\rho'} &= \frac{\partial}{\partial\rho} \int_V \frac{\partial\left(\frac{1}{R}\right)}{\partial\rho'} \rho' d\rho' d\phi' dz' \\
F_{\rho\phi'} &= \frac{\partial}{\partial\rho} \int_V \frac{1}{\rho'} \frac{\partial\left(\frac{1}{R}\right)}{\partial\phi'} \rho' d\rho' d\phi' dz' \\
&= \frac{\partial}{\partial\rho} \int_S \left[\frac{1}{R}\right]_{\phi_1}^{\phi_2} d\rho' dz' \\
F_{\rho z'} &= \frac{\partial}{\partial\rho} \int_V \frac{\partial\left(\frac{1}{R}\right)}{\partial z'} \rho' d\rho' d\phi' dz' \\
&= \frac{\partial}{\partial\rho} \int_S \left[\frac{1}{R}\right]_{z_1}^{z_2} \rho' d\rho' d\phi' \\
F_{\phi\rho'} &= \frac{1}{\rho} \frac{\partial}{\partial\phi} \int_V \frac{\partial\left(\frac{1}{R}\right)}{\partial\rho'} \rho' d\rho' d\phi' dz' \\
&= -\frac{1}{\rho} \int_S \left[\frac{\partial\left(\frac{1}{R}\right)}{\partial\rho'}\right]_{\phi_1}^{\phi_2} \rho' d\rho' dz' \\
F_{\phi\phi'} &= \frac{1}{\rho} \frac{\partial}{\partial\phi} \int_V \frac{1}{\rho'} \frac{\partial\left(\frac{1}{R}\right)}{\partial\phi'} \rho' d\rho' d\phi' dz' \\
&= \frac{1}{\rho} \frac{\partial}{\partial\phi} \int_S \left[\frac{1}{R}\right]_{\phi_1}^{\phi_2} d\rho' dz' \\
F_{\phi z'} &= \frac{1}{\rho} \frac{\partial}{\partial\phi} \int_V \frac{\partial\left(\frac{1}{R}\right)}{\partial z'} \rho' d\rho' d\phi' dz' \\
&= -\frac{1}{\rho} \int_L \left[\frac{1}{R}\right]_{\phi_1, z_1}^{\phi_2, z_2} \rho' d\rho' \\
F_{z\rho'} &= \frac{\partial}{\partial z} \int_V \frac{\partial\left(\frac{1}{R}\right)}{\partial\rho'} \rho' d\rho' d\phi' dz' \\
&= -\int_S \left[\frac{\partial\left(\frac{1}{R}\right)}{\partial\rho'}\right]_{z_1}^{z_2} \rho' d\rho' d\phi' \\
F_{z\phi'} &= \frac{\partial}{\partial z} \int_V \frac{1}{\rho'} \frac{\partial\left(\frac{1}{R}\right)}{\partial\phi'} \rho' d\rho' d\phi' dz' \\
&= -\int_L \left[\frac{1}{R}\right]_{\phi_1, z_1}^{\phi_2, z_2} d\rho' \\
F_{zz'} &= \frac{\partial}{\partial z} \int_V \frac{\partial\left(\frac{1}{R}\right)}{\partial z'} \rho' d\rho' d\phi' dz'
\end{aligned}$$

$$= \frac{\partial}{\partial z} \int_S \left[\frac{1}{R} \right]_{z_1}^{z_2} \rho' d\rho' d\phi'$$

where R is the distance between the measuring point and the integration point

$$R = \sqrt{\rho^2 + \rho'^2 - 2\rho\rho' \cos(\phi - \phi') - (z - z')^2}$$

After analytical integration, the following equations are obtained:

$$\begin{aligned} f_{\rho\rho'} d\phi' &= \frac{\rho\rho'z - \rho\rho'z' - \rho'^2z \cos(\phi - \phi') + \rho'^2z' \cos(\phi - \phi')}{(\rho^2 + \rho'^2 - 2\rho\rho' \cos(\phi - \phi')) R} \\ &+ \cos(\phi - \phi') \log(-z + z' + R) \\ &+ \arctan\left(\frac{(z - z')}{\rho \sin(\phi - \phi')}\right) \sin(\phi - \phi') \\ &+ \arctan\left(\frac{(z - z')(-\rho' + \rho \cos(\phi - \phi'))}{\rho R \sin(\phi - \phi')}\right) \sin(\phi - \phi') \\ F_{\rho\phi'} &= \cos(\phi - \phi') \log(-z + z' + R) \\ &- \frac{1}{2} \arctan\left(\frac{(z - z')}{\rho \sin(\phi - \phi')}\right) \sin(\phi - \phi') \\ &- \arctan\left(\frac{(z - z')(-\rho' + \rho \cos(\phi - \phi'))}{\rho R \sin(\phi - \phi')}\right) \sin(\phi - \phi') \\ f_{\rho z'} d\phi' &= \frac{\rho - \rho' \cos(\phi - \phi')}{R} \\ &+ \frac{\rho \cos(\phi - \phi') \left(-\cos(\phi - \phi') + \frac{\rho - \rho' \cos(\phi - \phi')}{R}\right)}{\rho' - \rho \cos(\phi - \phi') + R} + \\ &+ \cos(\phi - \phi') \log(\rho' - \rho \cos(\phi - \phi') + R) \\ f_{\phi\rho'} dz' &= -\frac{\frac{\rho'}{R} - \log(\rho' - \rho \cos(\phi - \phi') + R)}{\rho} \\ F_{\phi\phi'} &= -\left(\arctan\left(\frac{(z - z')}{\rho \sin(\phi - \phi')}\right) \cos(\phi - \phi')\right) + \\ &+ \frac{1}{2} \arctan\left(\frac{(-z + z')(-\rho' + \rho \cos(\phi - \phi'))}{\rho R \sin(\phi - \phi')}\right) \cos(\phi - \phi') \\ &+ \log(-z + z' + R) \sin(\phi - \phi') \\ F_{\phi z'} &= -\frac{R + \rho \cos(\phi - \phi') \log(\rho' - \rho \cos(\phi - \phi') + R)}{\rho} \\ f_{z\rho'} d\phi' &= -\frac{\rho'}{R} + \log(\rho' - \rho \cos(\phi - \phi') + R) \\ F_{z\phi'} &= -\log(\rho' - \rho \cos(\phi - \phi') + R) \end{aligned}$$

$$f_{zz'} d\phi' = \frac{z - z'}{R} + \frac{\rho (z - z') \cos(\phi - \phi')}{R(\rho' - \rho \cos(\phi - \phi') + R)}$$

We realize that it remains to be numerically integrated $f_{\rho\rho'}, f_{\rho z'}, f_{z\rho'}, f_{zz'}$ as ϕ' and $f_{\phi\rho'}$ as z' . As these are primitives, the bounds should be applied before any digital integration. For example, to obtain $f_{\rho\rho'} d\phi'$ the 4 terms resulting from the integration in ρ' and z' will be calculated beforehand.

1.4 Cartesian coordinates

1.4.1 Matrix F in cartesian coordinates

The metric tensor g_{ij} is in this case very simple and is equal to the identity matrix:

$$[g_{ij}] = \begin{bmatrix} 1 & 0 & 0 \\ 0 & 1 & 0 \\ 0 & 0 & 1 \end{bmatrix} \quad (1.11)$$

it shall be written that[51, p.59]

$$[F_{ij}] = \frac{1}{4\pi} \begin{bmatrix} F_{xx'} & F_{xy'} & F_{xz'} \\ F_{yx'} & F_{yy'} & F_{yz'} \\ F_{zx'} & F_{zy'} & F_{zz'} \end{bmatrix} \quad (1.12)$$

with

$$\begin{aligned} F_{xx'} &= \frac{\partial}{\partial x} \int_V \frac{\partial \left(\frac{1}{R} \right)}{\partial x'} dx' dy' dz' \\ &= \frac{\partial}{\partial x} \int_S \left[\frac{1}{R} \right]_{x_1}^{x_2} dy' dz' \\ F_{xy'} &= \frac{\partial}{\partial x} \int_V \frac{\partial \left(\frac{1}{R} \right)}{\partial y'} dx' dy' dz' \\ &= - \int_L \left[\frac{1}{R} \right]_{x_1, y_1}^{x_2, y_2} dz' \\ F_{xz'} &= \frac{\partial}{\partial x} \int_V \frac{\partial \left(\frac{1}{R} \right)}{\partial z'} dx' dy' dz' \end{aligned}$$

$$\begin{aligned}
&= - \int_L \left[\frac{1}{R} \right]_{x_1, z_1}^{x_2, z_2} dy' \\
F_{yx'} &= \frac{\partial}{\partial y} \int_V \frac{\partial \left(\frac{1}{R} \right)}{\partial x'} dx' dy' dz' \\
&= - \int_L \left[\frac{1}{R} \right]_{x_1, y_1}^{x_2, y_2} dz' \\
F_{yy'} &= \frac{\partial}{\partial y} \int_V \frac{\partial \left(\frac{1}{R} \right)}{\partial y'} dx' dy' dz' \\
&= \frac{\partial}{\partial y} \int_S \left[\frac{1}{R} \right]_{y_1}^{y_2} dx' dz' \\
F_{yz'} &= \frac{\partial}{\partial y} \int_V \frac{\partial \left(\frac{1}{R} \right)}{\partial z'} dx' dy' dz' \\
&= - \int_L \left[\frac{1}{R} \right]_{y_1, z_1}^{y_2, z_2} dx' \\
F_{zx'} &= \frac{\partial}{\partial z} \int_V \frac{\partial \left(\frac{1}{R} \right)}{\partial x'} dx' dy' dz' \\
&= - \int_L \left[\frac{1}{R} \right]_{x_1, z_1}^{x_2, z_2} dy' \\
F_{zy'} &= \frac{\partial}{\partial z} \int_V \frac{\partial \left(\frac{1}{R} \right)}{\partial y'} dx' dy' dz' \\
&= - \int_L \left[\frac{1}{R} \right]_{y_1, z_1}^{y_2, z_2} dx' \\
F_{zz'} &= \frac{\partial}{\partial z} \int_V \frac{\partial \left(\frac{1}{R} \right)}{\partial z'} dx' dy' dz' \\
&= \frac{\partial}{\partial z} \int_S \left[\frac{1}{R} \right]_{z_1}^{z_2} dx' dy' \tag{1.13}
\end{aligned}$$

The following analytical forms are obtained¹ :

$$\begin{aligned}
F_{xx'} &= \arctan \left(\frac{(y - y')(z - z')}{(x - x')R} \right) \\
F_{xy'} &= - \ln(-z + z' + R) \\
F_{xz'} &= - \ln(-y + y' + R) \\
F_{yx'} &= - \ln(-z + z' + R)
\end{aligned}$$

¹From these primitives we will integrate according to the bounds $x_1, x_2, y_1, y_2, z_1, z_2$, that will thus make 8 terms to be calculated for each integral.

$$\begin{aligned}
F_{yy'} &= \arctan\left(\frac{(x-x')(z-z')}{(y-y')R}\right) \\
F_{yz'} &= -\ln(-x+x'+R) \\
F_{zx'} &= -\ln(-y+y'+R) \\
F_{zy'} &= -\ln(-x+x'+R) \\
F_{zz'} &= \arctan\left(\frac{(x-x')(y-y')}{(z-z')R}\right)
\end{aligned}$$

Formulas in Cartesian coordinates are of great use in our study. We can quickly calculate the field generated by a small parallelepipedic magnet whose internal magnetization \vec{M} will be considered homogeneous and directed along the \vec{z} only. If we want to determine the z component of the external field generated by this magnet, starting from $F_{zz'}$ we get:

$$B_z(x, y, z) = \frac{M_z}{4\pi} \left[\arctan\left(\frac{(x-x')(y-y')}{(z-z')R}\right) \right]_{x_1, y_1, z_1}^{x_2, y_2, z_2} \quad (1.14)$$

$$\text{with } R = \sqrt{(x-x')^2 + (y-y')^2 + (z-z')^2}$$

The figure (1.3) represents the profile of the B_z field generated by a small magnet placed 10cm from the z axis. The cross section of this magnet is square and its side size = $\sqrt{0.004^2\pi/4}$. The following length z is 5mm and the remanent magnetization is 1.2 Tesla.

1.5 Shape of the magnets

The problem consists in proving the validity of the formula (1.14) for a magnet with a cylindrical section. This formula is rigorous for a magnet having the shape of a rectangular parallelepiped. It is much more economical in computing time to use this analytical form than the formula $F_{zz'}$ page 13 where an integration according to ϕ' remains to be performed. The geometry of the correcting magnets we use is a bar of cylindrical section with a diameter of 4mm and a length of 5mm. The magnetization is directed along the length of the bar and is equal to 1.2 Tesla for neodymium-iron-boron. The Figure (1.4) shows the relative difference between the field B_z calculated by the integration in cylindrical coordinates and the approximation of this field by the formula in cartesian coordinates. The cross-section and length

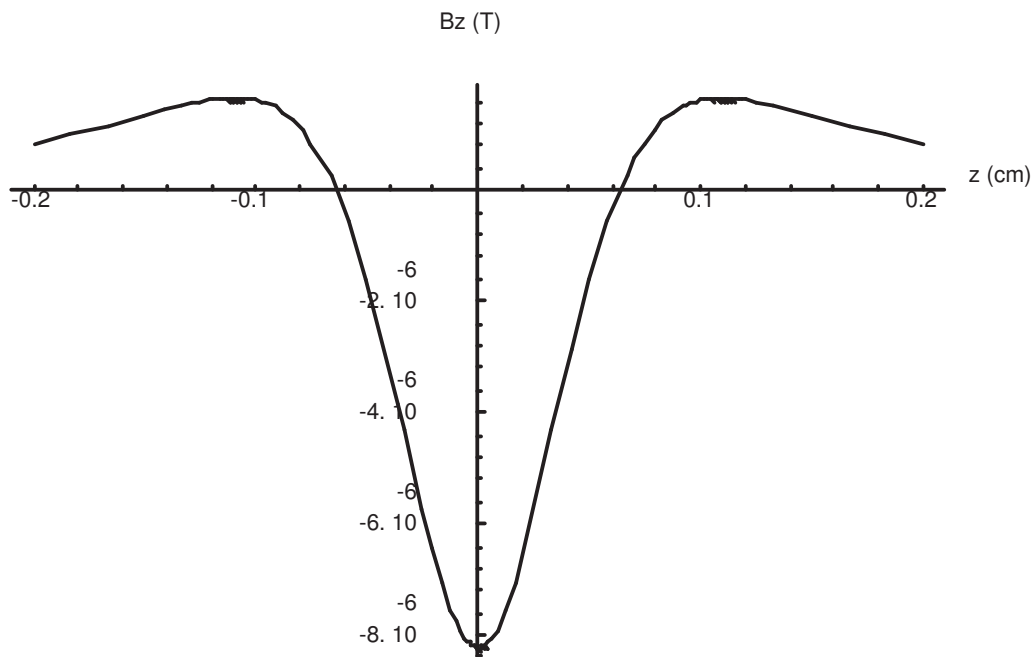


Figure 1.3: field Bz generated by a correction magnet.

of the cylindrical bar and the rectangular bar must be equal, i.e. the same volume of magnetized material which gives the same field at a great distance.

We notice that the maximum error is approximately one radius from the magnet surface. Since this is essentially a length ratio, the dimensions can be considered relative. The maximum error is 1%. However, the calculation point will generally be located at least 5cm from the magnet, i.e. about 10 times its size. We then achieve an accuracy of less than 1 per 1000, which is sufficient considering the dispersion of the remanent field of each magnet. This dispersion at manufacture is 5 % compared to the nominal value provided in the documentation. The maximum value of the residual field is often given by the manufacturer and magnets can vary between 1.15 and 1.2 Tesla.

1.6 Influence of the demagnetizing field

Using the formula (1.14), we consider that the magnetization inside the magnet is rigid and equal to its maximum value i.e. 1.2 Tesla in our case. In reality, we omit a very important term which is the demagnetization of the magnet on itself. We therefore propose to quantify the calculation error when

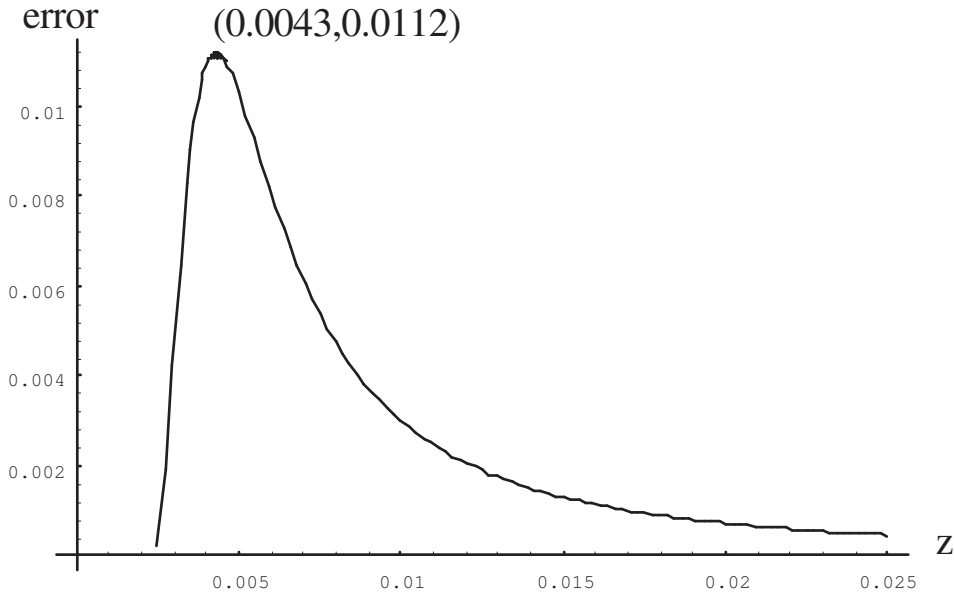


Figure 1.4: Difference $\frac{Bz_{cyl}-Bz_{rect}}{Bz_{cyl}}$

determining the far field by the arctangent analytical formula.

1.6.1 Calculation of the demagnetizing field

To determine the influence of the demagnetizing field, we will decompose the parallelepiped magnet into $n \times n \times n$ elements whose magnetization of each will be considered constant throughout the volume. In order to examine the result of the sampling, we will perform finer and finer decompositions.

We'll compare the calculated field on the \vec{z} axis by each of the decompositions with the magnet at the origin of the coordinates. The geometry and magnetic characteristics of the magnet are those mentioned above.

The table 1.1 shows that the decomposition quickly converges to the same field value, especially as we move away from the magnet. However, there is a difference between using the analytical formula in column (2) and the decomposed magnet involving the demagnetizing field. Column (7) is much more accurate but the calculation time is considerably longer than that needed to evaluate (1.14).

We notice in the table 1.2 that at great distance ($> 10cm$) the value given by the formula (1.14) and the field obtained taking into account the demagnetization differs by 1.018 % , Given the actual remanent field dispersion of

(1)	(2)	(3)	(4)	(5)	(6)	(7)	(8)
z mm	formula(1.14)	1x1x1	2x2x2	3x3x3	4x4x4	5x5x5	$\frac{(7)-(2)}{(7)}\%$
2.51	5.54e-01	5.49e-01	5.51e-01	5.46e-01	5.38e-01	5.44e-01	-1.81
3.51	2.96e-01	2.93e-01	2.92e-01	2.91e-01	2.91e-01	2.91e-01	-1.78
4.51	1.50e-01	1.48e-01	1.48e-01	1.48e-01	1.47e-01	1.47e-01	-1.53
5.51	8.16e-02	8.09e-02	8.07e-02	8.06e-02	8.05e-02	8.05e-02	-1.37
6.51	4.84e-02	4.80e-02	4.79e-02	4.79e-02	4.78e-02	4.78e-02	-1.28
7.51	3.09e-02	3.07e-02	3.06e-02	3.06e-02	3.06e-02	3.05e-02	-1.21
8.51	2.09e-02	2.07e-02	2.07e-02	2.07e-02	2.07e-02	2.07e-02	-1.17
9.51	1.48e-02	1.47e-02	1.46e-02	1.46e-02	1.46e-02	1.46e-02	-1.14
10.51	1.08e-02	1.07e-02	1.07e-02	1.07e-02	1.07e-02	1.07e-02	-1.12
11.51	8.21e-03	8.14e-03	8.13e-03	8.13e-03	8.12e-03	8.12e-03	-1.10
12.51	6.36e-03	6.30e-03	6.29e-03	6.29e-03	6.29e-03	6.29e-03	-1.09
13.51	5.02e-03	4.98e-03	4.97e-03	4.97e-03	4.97e-03	4.97e-03	-1.08
14.51	4.04e-03	4.00e-03	4.00e-03	3.99e-03	3.99e-03	3.99e-03	-1.07
15.51	3.29e-03	3.26e-03	3.26e-03	3.26e-03	3.26e-03	3.26e-03	-1.06
16.51	2.72e-03	2.70e-03	2.69e-03	2.69e-03	2.69e-03	2.69e-03	-1.06
17.51	2.27e-03	2.26e-03	2.25e-03	2.25e-03	2.25e-03	2.25e-03	-1.05
18.51	1.92e-03	1.90e-03	1.90e-03	1.90e-03	1.90e-03	1.90e-03	-1.05
19.51	1.64e-03	1.62e-03	1.62e-03	1.62e-03	1.62e-03	1.62e-03	-1.04
20.51	1.41e-03	1.39e-03	1.39e-03	1.39e-03	1.39e-03	1.39e-03	-1.04
21.51	1.22e-03	1.21e-03	1.21e-03	1.20e-03	1.20e-03	1.20e-03	-1.04
22.51	1.06e-03	1.05e-03	1.05e-03	1.05e-03	1.05e-03	1.05e-03	-1.04
23.51	9.33e-04	9.25e-04	9.24e-04	9.24e-04	9.24e-04	9.24e-04	-1.03
24.51	8.23e-04	8.16e-04	8.15e-04	8.15e-04	8.14e-04	8.14e-04	-1.03
25.51	7.29e-04	7.23e-04	7.22e-04	7.22e-04	7.22e-04	7.22e-04	-1.03
26.51	6.49e-04	6.44e-04	6.43e-04	6.43e-04	6.43e-04	6.43e-04	-1.03
27.51	5.81e-04	5.76e-04	5.75e-04	5.75e-04	5.75e-04	5.75e-04	-1.03
28.51	5.21e-04	5.17e-04	5.16e-04	5.16e-04	5.16e-04	5.16e-04	-1.03
29.51	4.70e-04	4.66e-04	4.65e-04	4.65e-04	4.65e-04	4.65e-04	-1.03
30.51	4.25e-04	4.21e-04	4.21e-04	4.21e-04	4.21e-04	4.21e-04	-1.02

Table 1.1: Comparison between more or less fine meshes

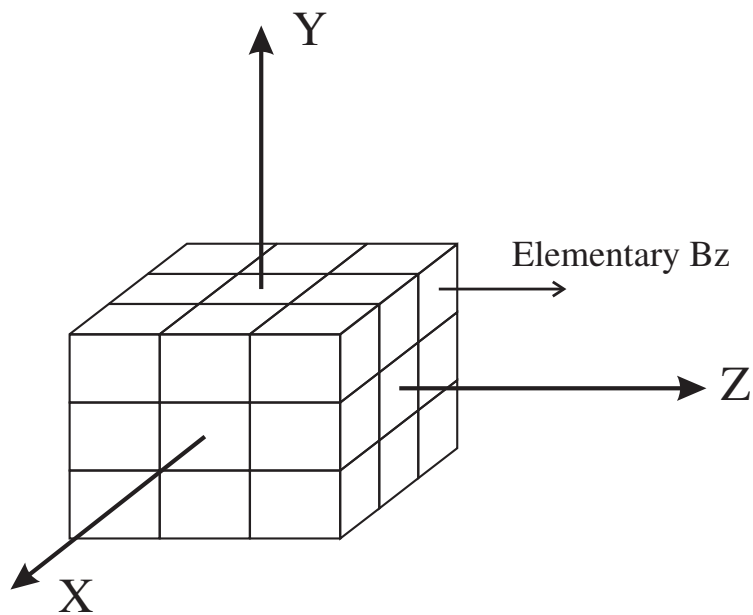


Figure 1.5: Elementary decomposition of a magnet

1.2 Tesla $\pm 5\%$, we must re-evaluate the remanent field using (1.14) and a few measurement points located if possible more than 10cm or 20 times the diameter of the magnet. Thanks to the regularity of column (4) at great distance, the demagnetization will be included in the evaluation of the residual field and an accuracy of about one per thousand will be maintained .

(1)	(2)	(3)	(4)
z (mm)	formula(1.14) T	5x5x5	$\frac{(3)-(2)}{(3)}\%$
10.00	1.269e-02	1.254e-02	-1.1327
20.00	1.523e-03	1.507e-03	-1.0464
30.00	4.475e-04	4.429e-04	-1.0302
40.00	1.882e-04	1.863e-04	-1.0245
50.00	9.624e-05	9.526e-05	-1.0218
60.00	5.565e-05	5.509e-05	-1.0204
70.00	3.503e-05	3.468e-05	-1.0195
80.00	2.346e-05	2.322e-05	-1.0190
90.00	1.647e-05	1.631e-05	-1.0186
100.00	1.201e-05	1.189e-05	-1.0183
110.00	9.020e-06	8.929e-06	-1.0181
120.00	6.947e-06	6.877e-06	-1.0179
130.00	5.464e-06	5.409e-06	-1.0178
140.00	4.375e-06	4.330e-06	-1.0177
150.00	3.557e-06	3.521e-06	-1.0176
160.00	2.930e-06	2.901e-06	-1.0176
170.00	2.443e-06	2.418e-06	-1.0175
180.00	2.058e-06	2.037e-06	-1.0175
190.00	1.750e-06	1.732e-06	-1.0174
200.00	1.500e-06	1.485e-06	-1.0174
210.00	1.296e-06	1.283e-06	-1.0174
220.00	1.127e-06	1.116e-06	-1.0173
230.00	9.864e-07	9.765e-07	-1.0173
240.00	8.681e-07	8.594e-07	-1.0173
250.00	7.681e-07	7.603e-07	-1.0173

Table 1.2: Error when using (1.14) from a great distance.

Chapter 2

Field correction

After validating the direct calculation, the field overview can therefore be checked numerically. Although we can start from the formula in arctangent and use a standard inverse method, we must choose an error function and especially determine how this error will be distributed. Moreover, this approach does not give any information on the number of magnets required for a given accuracy. For the localization of the error, we chose to move it as far as possible from the center and thus naturally to work on a Taylor series-type function base, which leads us directly, in the case of potentials, to the development of the field in Legendre polynomials.

2.1 Potential development

To make a magnetic field homogeneous, one solution is to express the measured field in a simpler series that will approximate it and try to cancel as many spurious terms as possible.

Solving the differential equation $\nabla^2\psi = 0$ in spherical coordinates gives the following double series:

$$\psi(r, \theta, \phi) = \frac{1}{4\pi} \sum_{n=0}^{\infty} \sum_{m=0}^n (A_{nm} \cos(m\phi) + B_{nm} \sin(m\phi)) r^n P_{nm}(\cos \theta) \quad (2.1)$$

where P_{nm} are the associated Legendre polynomials¹.

¹In the following calculations we will use the Abramowitz writing convention, $P_{nm} = (-1)^m P_n^m = (1-x^2)^{m/2} \frac{d^m}{dx^m} P_n(x)$.

On the unit sphere we determine the A_{nm} and B_{nm} by calculating the following integrals²:

$$A_{nm} = \frac{\int_0^{2\pi} \int_0^\pi f(\theta, \phi) P_{nm}(\cos(\theta)) \cos(m\phi) \sin(\theta) d\theta d\phi}{\int_0^{2\pi} \int_0^\pi (P_{nm}(\cos(\theta)) \cos(m\phi))^2 \sin(\theta) d\theta d\phi} \quad (2.2)$$

$$B_{nm} = \frac{\int_0^{2\pi} \int_0^\pi f(\theta, \phi) P_{nm}(\cos(\theta)) \sin(m\phi) \sin(\theta) d\theta d\phi}{\int_0^{2\pi} \int_0^\pi (P_{nm}(\cos(\theta)) \sin(m\phi))^2 \sin(\theta) d\theta d\phi} \quad (2.3)$$

We show that we can replace the denominators[37, p.709] by $N_{n0} = 4\pi \frac{(n+m)!}{(2n+1)(n-m)!}$ and for $m > 0$, $N_{nm} = 2\pi \frac{(n+m)!}{(2n+1)(n-m)!}$. So there's no need to numerically integrate the denominators³.

The transformation of the integrands at the numerators of A_{nm} and B_{nm} into Cartesian coordinates makes it easy to visualize the contributions of each coefficient, but it is important to use them with care in the case of integration in a volume, because they are no longer orthogonal to each other if they are not located on the sphere. Any point outside will have the effect of coupling the coefficients together, thereby degrading the results.

We obtain the following coefficients by making the substitutions $\cos(\theta) = z/r$ and $\phi = \arccos(x/\sqrt{(x^2 + y^2)})$ then we'll use the Chebycheff polynomials $\cos[n \arccos(\omega)] = T_n(\omega)$ and $\sin[n \arccos(\omega)] = U_n(\omega)$. However, during these transformations, the following areas must be respected⁴ type shape because the angles are often no longer in the correct quadrant[38].

$$\begin{aligned} a_{00} &= 1 \\ a_{10} &= z \\ a_{11} &= x \\ a_{20} &= \frac{-x^2 - y^2}{2} + z^2 \\ a_{21} &= 3xz \\ a_{22} &= 3x^2 - 3y^2 \end{aligned}$$

²If measurements are made on a sphere of radius r , normalization (sphere of unit radius) of the coefficients A_{nm} and B_{nm} is provided by the term r^n .

³The variable change $x \rightarrow \cos t$ mathematically implies $(1-x^2)^{m/2} \rightarrow |\sin t|^m$, however we can remove the absolute value and use $(1-x^2)^{m/2} \rightarrow \sin^m t$. That way we get domain problems and it is no longer $[0, \pi]$.

⁴In complex cases such as the In the equations presented on page 60, we've chosen to keep a $\cos[m \arctan(y', x')]$

$$\begin{aligned}
a_{30} &= \frac{-3(x^2 + y^2)z}{2} + z^3 \\
a_{31} &= \frac{-3x(x^2 + y^2)}{2} + 6xz^2 \\
a_{32} &= 15(x^2 - y^2)z \\
a_{33} &= 15x(x^2 - 3y^2) \\
a_{40} &= \frac{3(x^2 + y^2)^2}{8} - 3(x^2 + y^2)z^2 + z^4 \\
a_{41} &= \frac{-15x(x^2 + y^2)z}{2} + 10xz^3 \\
a_{42} &= \frac{15(-x^4 + y^4)}{2} + 45(x^2 - y^2)z^2 \\
a_{43} &= 105x(x^2 - 3y^2)z \\
a_{44} &= 105x^4 - 630x^2y^2 + 105y^4 \\
a_{50} &= \frac{15(x^2 + y^2)^2z}{8} - 5(x^2 + y^2)z^3 + z^5 \\
a_{51} &= \frac{15x(x^2 + y^2)^2}{8} - \frac{45x(x^2 + y^2)z^2}{2} + 15xz^4 \\
a_{52} &= \frac{105(-x^4 + y^4)z}{2} + 105(x^2 - y^2)z^3 \\
a_{53} &= \frac{105x(-x^2 + 3y^2)(x^2 + y^2 - 8z^2)}{2} \\
a_{54} &= 945(x^4 - 6x^2y^2 + y^4)z \\
a_{55} &= 945x(x^4 - 10x^2y^2 + 5y^4) \\
b_{11} &= y \\
b_{21} &= 3yz \\
b_{22} &= 6xy \\
b_{31} &= \frac{-3y(x^2 + y^2)}{2} + 6yz^2 \\
b_{32} &= 30xyz \\
b_{33} &= 15y(3x^2 - y^2) \\
b_{41} &= \frac{-15y(x^2 + y^2)z}{2} + 10yz^3 \\
b_{42} &= -15xy(x^2 + y^2) + 90xyz^2 \\
b_{43} &= 105y(3x^2 - y^2)z
\end{aligned}$$

$$\begin{aligned}
b_{44} &= 420 x^3 y - 420 x y^3 \\
b_{51} &= \frac{15 y (x^2 + y^2)^2}{8} - \frac{45 y (x^2 + y^2) z^2}{2} + 15 y z^4 \\
b_{52} &= -105 x y (x^2 + y^2) z + 210 x y z^3 \\
b_{53} &= \frac{105 y (-3 x^2 + y^2) (x^2 + y^2 - 8 z^2)}{2} \\
b_{54} &= 3780 x (x - y) y (x + y) z \\
b_{55} &= 945 y (5 x^4 - 10 x^2 y^2 + y^4)
\end{aligned}$$

2.2 Conditions on the calculation of coefficients

From field measurements made on the surface of a sphere, some conditions are necessary to obtain a good accuracy in the determination of the coefficients A_{nm} and B_{nm} . A general method of calculation consists in integrating each longitude of the sphere, i.e. the part:

$$\int_0^\pi f(\theta, \phi) P_{nm}(\cos(\theta)) \sin(\theta) d\theta$$

then perform the Fourier transform of the previous integrations in order to determine the integration in $\cos(m\phi)$ and $\sin(m\phi)$ (latitude). It is thus necessary to avoid any folding (cf. FFT in signal processing) of higher orders[42]. We will choose a radius r of sphere for the measurement equal to half the radius of placement of the generators. It is a compromise between the determination of lower orders that measure very well near the center and become impossible to determine if $r \approx r'$. It is exactly the opposite for higher orders.

The previous integration becomes tricky if the measuring points are not placed on regularly spaced spindles as this requires a numerical integration per variable pitch. Similarly, the radius of the point must be normalized and its value recalculated on the measuring sphere. During the measurement, it is difficult to mechanically ensure a constant radius and angular positioning at all measuring points⁵. It is therefore preferable to take equi-spacing points in a parallelepiped volume and then choose as input the nearest points of a sphere of a given radius. It is even possible, if the number of measured points

⁵There is a large number of points at the poles of the sphere if each latitude is composed of the same number of points.

is high, to independently calculate several spheres of different diameters and compare the results. As shown in Figure (2.1), the field will be measured on a cubic grid of h steps and we will choose the set of points whose distance to the center is between $R - h < \sqrt{x^2 + y^2 + z^2} < R + h$

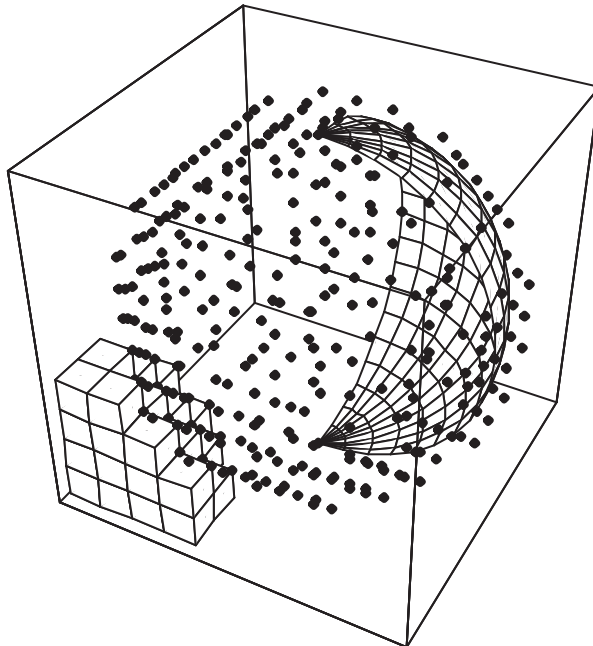


Figure 2.1: Measuring the field on a rough radius sphere $R \pm h$

Figures (2.1) and (2.2) are obtained by a $10 \times 10 \times 10$ mesh of a cube tangent to the measuring sphere. We thus obtain $(n + 1)^3$ nodes, i.e. 1331 measurement points. By taking all the points located at $\pm h$ of the sphere, we obtain a total of 350 points which will effectively intervene in the calculation of the coefficients A_{nm} and B_{nm} . The angular distribution is correct as can be seen in the Figure (2.2). However a coupling in the calculation appears since the terms in r^n are involved and are not orthogonal. The table 2.1 summarizes the accuracy of the algorithm following all the approximations and conditions indicated above. To determine this table, we have numerically created a field containing all the harmonics up to and including order 5 and with an amplitude equal to 1. The inverse problem consists in finding the value 1 from the measurement points.

An accuracy of the order of 10^{-4} is sufficient in this study, so we can consider this method of measurement satisfactory.

A_{00}	1.000047	-	-
A_{10}	1.000036	-	-
A_{11}	9.999906e-01	B_{11}	1.000087
A_{20}	9.998247e-01	-	-
A_{21}	1.000032	B_{21}	1.000026
A_{22}	9.999436e-01	B_{22}	1.000008
A_{30}	9.999918e-01	-	-
A_{31}	1.000009	B_{31}	1.000042
A_{32}	9.999989e-01	B_{32}	9.999925e-01
A_{33}	1.000030	B_{33}	9.999934e-01
A_{40}	1.000123	-	-
A_{41}	9.999818e-01	B_{41}	9.999873e-01
A_{42}	1.000000	B_{42}	1.000002
A_{43}	9.999972e-01	B_{43}	9.999989e-01
A_{44}	9.999971e-01	B_{44}	9.999983e-01
A_{50}	1.000039	-	-
A_{51}	9.999526e-01	B_{51}	9.999725e-01
A_{52}	9.999986e-01	B_{52}	1.000000
A_{53}	9.999994e-01	B_{53}	9.999998e-01
A_{54}	1.000000	B_{54}	9.999999e-01
A_{55}	1.000000	B_{55}	1.000001

Table 2.1: Error on the coefficients for a sampling of 350 points.

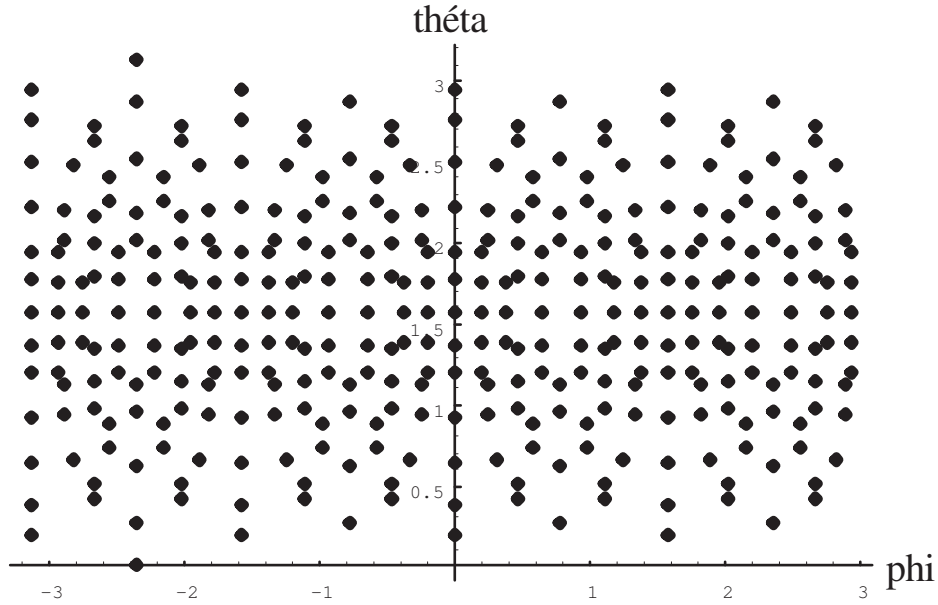


Figure 2.2: Angular distribution in θ , ϕ of the measuring points

2.3 Algorithm for calculating coefficients

We will therefore determine the coefficients that minimize the difference between the set of measurement points and the linear combination of Legendre functions. The general form of the model is

$$y(x) = \sum_{k=1}^M a_k X_k(x) \quad (2.4)$$

We are defining a merit function that we will seek to minimize:

$$\chi^2 = \sum_{i=1}^N \left[y_i - \sum_{k=1}^M a_k X_k(x_i) \right]^2 \quad (2.5)$$

The minimum of this function is given by the M normal equations:

$$0 = \sum_{i=1}^N \left[y_i - \sum_{j=1}^M a_j X_j(x_i) \right] X_k(x_i) \quad k = 1 \dots M \quad (2.6)$$

We can rewrite this system in the form of

$$\sum_{j=1}^M \alpha_{kj} a_j = \beta_k \quad (2.7)$$

with

$$\alpha_{kj} = \sum_{i=1}^N X_j(x_i)X_k(x_i) \text{ et } \beta_k = \sum_{i=1}^N y_i X_k(x_i) \quad (2.8)$$

The application of the previous general form is summarized in the algorithm *coefficients* which calculates the terms up to and including order 8. The two subroutines indicate how to calculate the order of the coefficients as a function of the index used for the linear ordering of the variables. The function *lgndr* is available in any literature dealing with the recurrence calculation of the associated Legendre polynomials (ex:[13]).

COEFFICIENTS()

```

1  nmax ← 8
2  nbvara ← 45
3  nbvarb ← 36
4  nbvar ← nbvara + nbvarb
5  nbpoints ← 350
6  for i ← 1 to nbpoints
7      do x[i] ← measured
8          y[i] ← measured
9          z[i] ← measured
10         field[i] ← measured
11
12  for k ← 1 to nbvar
13      do bet[k] ← 0.
14          for l ← 1 to nbvar
15              do u[k][l] ← 0.
16
17  for i ← 1 to nbpoints
18      do r ← √(x[i]2 + y[i]2 + z[i]2)
19          for k ← 1 to nbvara
20              do n, m ← DETANM(k)
21                  a[k] ← (-1)m rn lgndr(n, m, z[i]/r) cos(m arctan(y[i], x[i]))
22                  bet[k] ← bet[k] + field[i] × a[k]
23
24          for k ← 1 to nbvarb
25              do n, m ← DETBNM(k)
26                  a[k + nbvara] ← (-1)m rn lgndr(n, m, z[i]/r) sin(m arctan(y[i], x[i]))
27                  bet[k + nbvara] ← bet[k + nbvara] + field[i] × a[k + nbvara]
28

```

```

29         for  $k \leftarrow 1$  to  $nbvar$ 
30             do for  $l \leftarrow 1$  to  $nbvar$ 
31                 do  $u[k][l] \leftarrow u[k][l] + a[k] \times a[l]$ 
32
33
34
35     for  $l \leftarrow 1$  to  $nbvar$ 
36         do  $sol[l] \leftarrow \sum_k u^{-1}[k][l] \times bet[k]$ 
37

```

DETANM(i)

```

1  indent  $\leftarrow 0$ 
2  for  $n \leftarrow 0$  to  $nmax$ 
3      do for  $m \leftarrow 0$  to  $n$ 
4          do indent  $\leftarrow indent + 1$ 
5              if indent =  $i$ 
6                  then return  $n, m$ 
7
8
9  error " $i \notin [1, nbvara]$ "

```

DETBNM(i)

```

1  indent  $\leftarrow 0$ 
2  for  $n \leftarrow 1$  to  $nmax$ 
3      do for  $m \leftarrow 1$  to  $n$ 
4          do indent  $\leftarrow indent + 1$ 
5              if indent =  $i$ 
6                  then return  $n, m$ 
7
8
9  error " $i \notin [1, nbvarb]$ "

```

This computational technique is equivalent to the determination of the pseudo-inverse matrix of **Moore-Penrose** which allows us to construct the general solution of the problem of linear association functions. It consists in finding a matrix X minimizing the Euclidean norm $\|AX - B\|$, where A and B are two given rectangular matrices. If the lines of the matrix A are linearly independent, which is the case if the measuring points are on the same sphere, the solution is

$$X = (A^T A)^{-1} \cdot A^T \cdot B \quad (2.9)$$

2.4 Coefficients cancellation

In magnetic resonance imaging, the static magnetic field should be as homogeneous as possible. We will try to cancel up to a certain order all the coefficients. We must then create a magnetic field whose orders will be opposite to those of the main field. We have chosen for this study a device based on permanent magnets whose dimensions are much smaller than those of the machine. The correcting magnets will have a maximum volume of one cubic centimeter. As we will see later, a minimum volume of magnetized material is needed to generate a non-negligible field at the center, while respecting a multipole development⁶ rather small.

2.5 Calculation of correction magnets

Several solutions for determining the magnetic field generated by a magnet can be used. As we saw in the previous chapters, we can determine in a complete analytical form the field produced by rectangular magnets. The main advantage of this approach is a very short calculation time and a very high accuracy. On the other hand, we do not have such practical formulas for cylindrical magnets or sectors, as there is often still numerical integration to be done. However, this type of analytical approach is no longer suitable for generating a magnetic field a priori. The opposite problem consists in determining, for example, the position of magnets or the geometric characteristics and magnetizations in order to generate this type of field. The problem can be solved by a non-linear optimization with minimization of the error between the field to be obtained and the field generated by the magnets, the variables being the position of each magnet or a geometric characteristic.

It turns out that this approach does not generally give good results. A first finding is that the equations used in numerical computation are strongly coupled, so it is very difficult to reverse the problem. A second finding is that a large number of degrees of freedom is generally required (we have evaluated them at least 30) which makes it particularly difficult to optimize these parameters in a non-linear way. It is also necessary to think about the

⁶The area of interest will be limited to half the dimensions of the generator. The multipole development becomes important if $r/r' > 1/2$.

form of the functional. For example, let us take a minimization of the norm between the desired field and the field generated by the magnets, it would be very annoying if the error were large at the center while keeping the average error low.

The location of the error is therefore very important. Usually we try to locate the error as far from the center as possible. A simple idea is to cancel the successive derivatives of the magnetic field (origin of the function at the center of the machine). In Cartesian coordinates, if we want to cancel up to and including the fifth derivative:

$$\frac{\partial f}{\partial x}, \frac{\partial f}{\partial y}, \frac{\partial f}{\partial z}, \frac{\partial^2 f}{\partial x^2}, \dots, \frac{\partial^3 f}{\partial x \partial y \partial z}, \dots, \frac{\partial^5 f}{\partial x^2 \partial y^2 \partial z}, \dots$$

we obtain 215 equations to be cancelled ($(order + 1)^3 - 1$), plus an additional equation if we wish to control the value of the constant field. However, we are in the presence of a magnetic field, and several combinations of derivatives are null; this makes the problem much easier because the number of equations to be cancelled will be less. To obtain directly a base of non-zero derivatives, we will use the development of the scalar potential in Legendre polynomials.

In a volume where there is no moving electric charge and of constant permeability, which is the case in the useful area of the machine, the magnetic field is described by a law of the type $\vec{B} = -\vec{\nabla}\psi$ with

$$\nabla^2 \psi = 0 \quad (2.10)$$

A laplacian solution is a potential $\frac{1}{R}$.

In polar coordinates the laplacian is written:

$$\frac{1}{r^2} \frac{\partial}{\partial r} \left(r^2 \frac{\partial \psi}{\partial r} \right) + \frac{1}{r^2 \sin \theta} \frac{\partial}{\partial \theta} \left(\sin \theta \frac{\partial \psi}{\partial \theta} \right) + \frac{1}{r^2 \sin^2 \theta} \frac{\partial^2 \psi}{\partial \phi^2} = 0 \quad (2.11)$$

2.5.1 Legendre polynomial magnet development

The calculation will be made from a magnet whose magnetization \vec{M} is directed along the \vec{z} and we will be interested for the moment only in the z component of the \vec{B} field generated by this magnet. We will use the formula $F_{zz'}$ page 14 with the hypothesis that the magnetization is rigid and is therefore not influenced by the external field. However, it would be interesting

to determine experimentally the influence of the external transverse components H_x and H_y on the value of the M_z magnetization. According to these hypotheses, the field produced by the magnet is

$$B_z = \frac{M_z}{4\pi} \frac{\partial}{\partial z} \int_S \left[\frac{1}{R} \right]_{z_1}^{z_2} dx' dy' \quad (2.12)$$

Using the development of $\frac{1}{R}$ in spherical coordinates[31, p.1274], the development of potential can be written⁷:

$$\begin{aligned} \frac{1}{R} = & \sum_{n=0}^{n=\infty} \sum_{m=0}^{m=n} \epsilon_m \frac{(n-m)!}{(n+m)!} P_{nm}(\cos \theta) P_{nm}(\cos \theta'). \\ & \cos [m(\phi - \phi')] \begin{cases} \frac{r^n}{r'^{n+1}} & \text{si } r' > r \\ \frac{r'^n}{r^{n+1}} & \text{si } r > r'. \end{cases} \end{aligned} \quad (2.13)$$

We can then enter the derivative with respect to z into the integral and determine the integrand as follows[12, p.48][48]: for $r' > r$ (Correction magnets are placed outside the useful area):

$$\begin{aligned} \frac{\partial \frac{1}{R}}{\partial z} = & - \sum_{n=0}^{n=\infty} \sum_{m=0}^{m=n} \epsilon_m \frac{(n-m+1)!}{(n+m)!} P_{nm}(\cos \theta) P_{n+1m}(\cos \theta'). \\ & \cos [m(\phi - \phi')] \frac{r^n}{r'^{n+2}} \end{aligned} \quad (2.14)$$

We can see that the z derivation is not for the variables θ and r but for the variables θ' and r' . Using the fact that $\frac{\partial 1/R}{\partial z} = -\frac{\partial 1/R}{\partial z'}$, the identification between the coefficients A_{nm}, B_{nm} measured and the development of the field produced by the magnets is easier.

2.5.2 Approximate Surface Integration

The following x' and y' integration of the previous equation will be neglected for the moment and we will replace this integration by the A cross section of the magnet. This approximation must then be carefully evaluated so that the error committed does not contradict the desired precision when cancelling the coefficients. A_{nm} and B_{nm} .

⁷ $\epsilon_m = 1$ if $m = 0$ and 2 if $m > 0$.

We thus obtain the following development of the B_z field⁸:

$$B_z(\rho, \theta, \phi) = -\frac{M_z A}{4\pi} \sum_{n=0}^{n=\infty} \sum_{m=0}^{m=n} \epsilon_m \frac{(n-m+1)!}{(n+m)!} \left[\frac{P_{n+1m}(\cos \theta')}{r'^{n+2}} \right]_{z_1}^{z_2} \cdot r^n P_{nm}(\cos \theta) \cos [m(\phi - \phi')] \quad (2.15)$$

This development is thus valid in the case where $r < r'$. Since the sum ranges from $n = 0$ to ∞ , it is necessary to study the convergence of the series as a function of n . Figure (2.3) shows the relative error between the exact value of the field and the development (2.15) as a function of the value n . Since the magnet is at $r' = 10\text{cm}$, we clearly see that (2.15) is valid only in the domain $r \in]-r', r'[$. The limits of the interval are the asymptotes at ∞ . We also notice that the further we move from the source, the smaller the error, due to the truncation of the series. The error increases as we get closer to the source because we did not perform the x, y integration of the magnet cross section.

2.5.3 Cancellation of coefficients

By developing $\cos [m(\phi - \phi')] = \cos(m\phi) \cos(m\phi') + \sin(m\phi) \sin(m\phi')$, we can identify the coefficients A_{nm} and B_{nm} of the measured field with the corresponding coefficients of the correction magnets. By adding the field generated by the magnets to the measured field, we have the following equation:

$$\begin{aligned} & \frac{1}{4\pi} \sum_{n=0}^{N_{ordres}} \sum_{m=0}^n (A_{nm} \cos(m\phi) + B_{nm} \sin(m\phi)) r_{mes}^n P_{nm}(\cos \theta) + \\ & - \frac{M_z A}{4\pi} \sum_{n=0}^{N_{ordre}} \sum_{m=0}^{m=n} \epsilon_m \frac{(n-m+1)!}{(n+m)!} \left[\frac{P_{n+1m}(\cos \theta')}{r'^{n+2}} \right]_{z_1}^{z_2} \cdot \\ & r^n P_{nm}(\cos \theta) [\cos(m\phi) \cos(m\phi') + \sin(m\phi) \sin(m\phi')] = 0 \quad (2.16) \end{aligned}$$

We can notice that this identification is quite valid because each component of the magnetic field verifies the Laplace equation $\nabla^2 \psi = 0$. Moreover

⁸We have chosen the convention that the indices numbered z_1 and z_2 represent the start and end coordinates of the bar magnet. Strictly speaking, they should be called z'_1 and z'_2 but in order to lighten the formulation, there is no possible confusion with the coordinates of the calculation point.

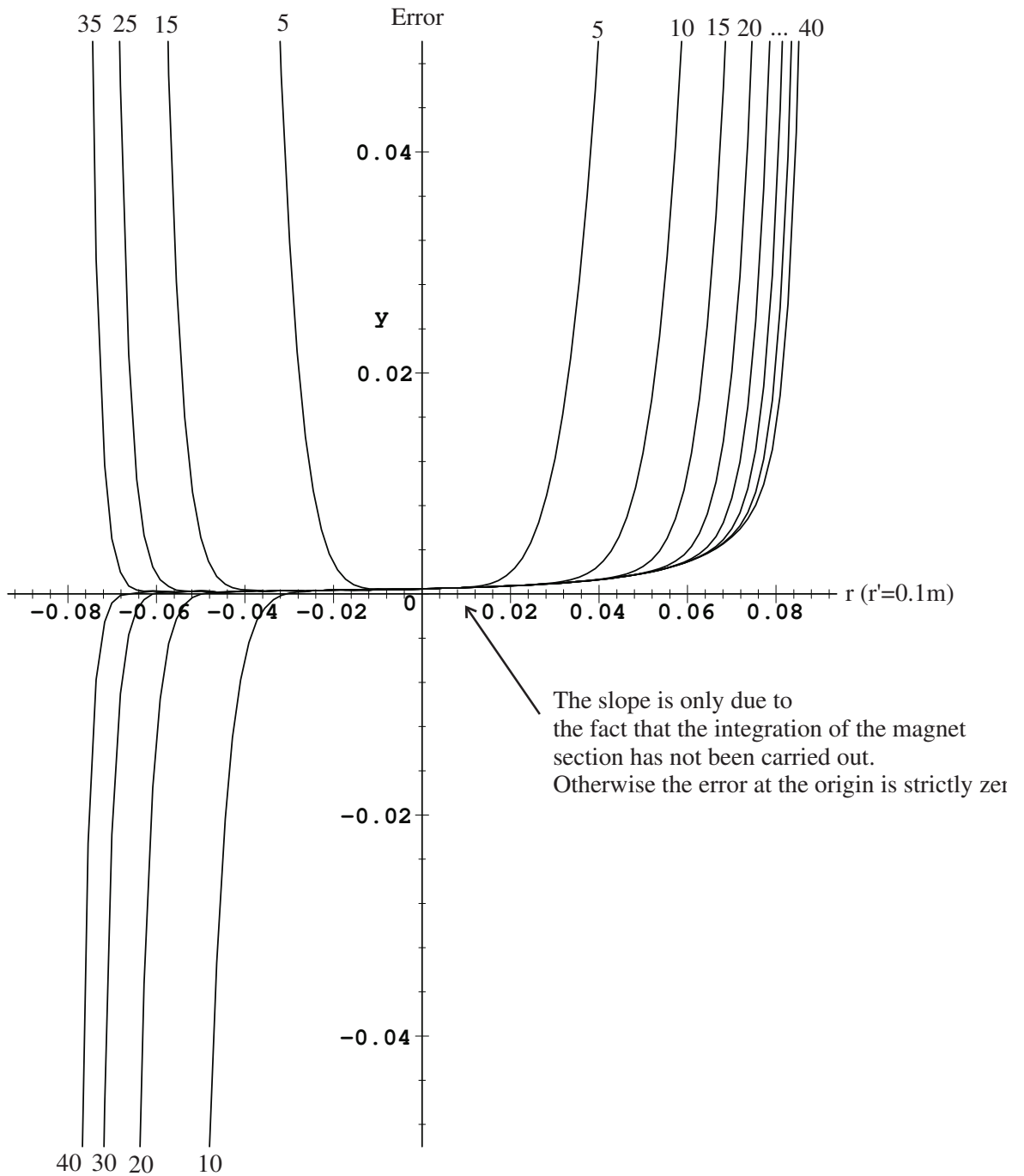


Figure 2.3: Relative error between the formula (1.14) and the development (2.15) as a function of n . The source is at $r' = 10\text{cm}$.

any integration or derivation following the spatial coordinates does not modify this property. We can therefore still approximate the field by the double series Eq(2.1).

The terms r_{mes}^n and r^n will be normalized to 1 to simplify the calculation. Using the orthogonality property of Legendre's development, we will group and cancel the factor functions of the terms into $P_{nm}(\cos \theta) \cos(m\phi)$ and $P_{nm}(\cos \theta) \sin(m\phi)$, we obtain a system of equations of the form:

$$\left\{ \frac{A_{nm}}{4\pi} - \frac{M_z A}{4\pi} \epsilon_m \frac{(n-m+1)!}{(n+m)!} \left[\frac{P_{n+1m}(\cos \theta')}{r'^{n+2}} \right]_{z_1}^{z_2} \cos(m\phi') \right\} \times P_{nm}(\cos \theta) \cos(m\phi) = 0 \quad (2.17)$$

and

$$\left\{ \frac{B_{nm}}{4\pi} - \frac{M_z A}{4\pi} \epsilon_m \frac{(n-m+1)!}{(n+m)!} \left[\frac{P_{n+1m}(\cos \theta')}{r'^{n+2}} \right]_{z_1}^{z_2} \sin(m\phi') \right\} \times P_{nm}(\cos \theta) \sin(m\phi) = 0 \quad (2.18)$$

To correct all the harmonics up to and including order 5, we have 35 such equations to solve simultaneously. We will only keep the part between brackets because these equations must be verified whatever the calculation point (θ, ϕ) is. We immediately notice that there are not enough variables to cancel out the 35 equations above. We can then add N magnets to retrieve the missing variables, so we write:

$$\begin{cases} \frac{A_{nm}}{4\pi} - \sum_{i=1}^N \frac{M_i A_i}{4\pi} \epsilon_m \frac{(n-m+1)!}{(n+m)!} \left[\frac{P_{n+1m}(\cos \theta'_i)}{r_i'^{n+2}} \right]_{z_{i1}}^{z_{i2}} \cos(m\phi'_i) = 0 \\ \frac{B_{nm}}{4\pi} - \sum_{i=1}^N \frac{M_i A_i}{4\pi} \epsilon_m \frac{(n-m+1)!}{(n+m)!} \left[\frac{P_{n+1m}(\cos \theta'_i)}{r_i'^{n+2}} \right]_{z_{i1}}^{z_{i2}} \sin(m\phi'_i) = 0 \end{cases} \quad (2.19)$$

2.5.4 Hardware configuration of the shims

We have placed the magnets on a cylinder with a radius of 10cm⁹. For a simplicity of adjustment we have allowed ourselves to fix the ϕ' angle of each magnet, thus having only the z' displacement for the adjustment¹⁰.

⁹In the whole document, r' is equal to 10cm minimum and the measurements are made at 5cm from the center. To generalize the results, we consider that the area of interest is half the dimensions of the machine.

¹⁰the letters ' are used simply to specify that these are the coordinates of the magnets and not the calculation point.

Having therefore only one degree of freedom per magnet, we have chosen to uniformly distribute 35 identical magnets in ϕ' around the cylinder and to act on their displacement in z' .

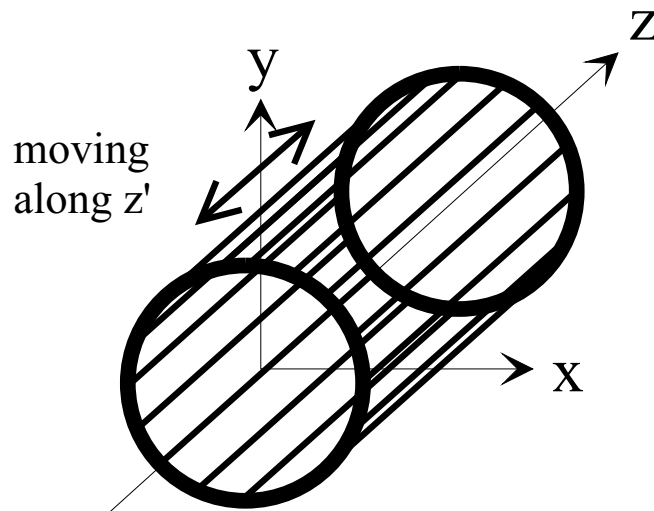


Figure 2.4: Magnet configuration

The principle of the adjustment is as follows; first, we measure the magnetic field with a Hall probe or an NMR gaussmeter. The measurement points should preferably be located on the surface of a sphere. Then, with the help of a software program, we precisely determine the coefficients of the spherical harmonics. From these coefficients, we will determine the position of the magnets which produce exactly the coefficients whose value will be opposite to those of the measured field.

The software for determining Legendre coefficients is numerically stable, the problem is almost linear. On the other hand, determining the position of magnets from Legendre coefficients is a non-linear problem. The coupling between the equations being very high, we have to use particular numerical methods that allow us to invert the equations. A chapter will be devoted to the numerical solution.

2.6 First problem solved

To validate the method, we tried to correct the homogeneity defects of the B_z field created by a small ferrite placed on a radius of 11cm and a z-displacement of 2.5cm with respect to the origin of the axes. Then we ar-

ranged the 35 magnets in the configuration explained previously (placed on a cylinder with a radius of 10cm and uniformly distributed in ϕ). The ferrite is deliberately placed on a slightly larger radius in order to avoid a possible conflict of position. In a first step, the field generated by the ferrite on the surface of a sphere must be measured. 350 points are needed to calculate the spherical harmonics with sufficient precision (see Tab 2.1) while respecting the fact that the uncalculated higher harmonics are not too high in the measurement zone. There would be, in the manner of the Fourier Transform, a folding of the higher harmonics on the lower harmonics. In our case on a measurement sphere of 5cm diameter this was not the case.

As an example, the figures (2.5) and (2.6) show a main field before correction (high curve in each figure) and after adding the correction magnets (low curve) for two axes Oz and Ox .

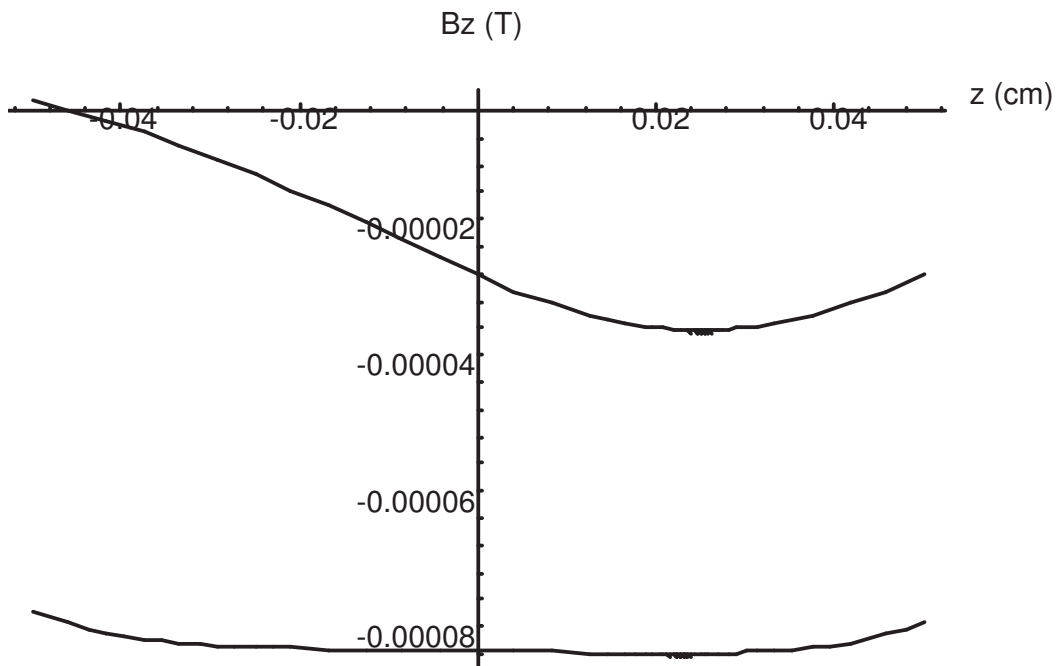


Figure 2.5: z axis field correction

These figures clearly show an improvement in the field strength between the first curve and the second, which is much more homogeneous.

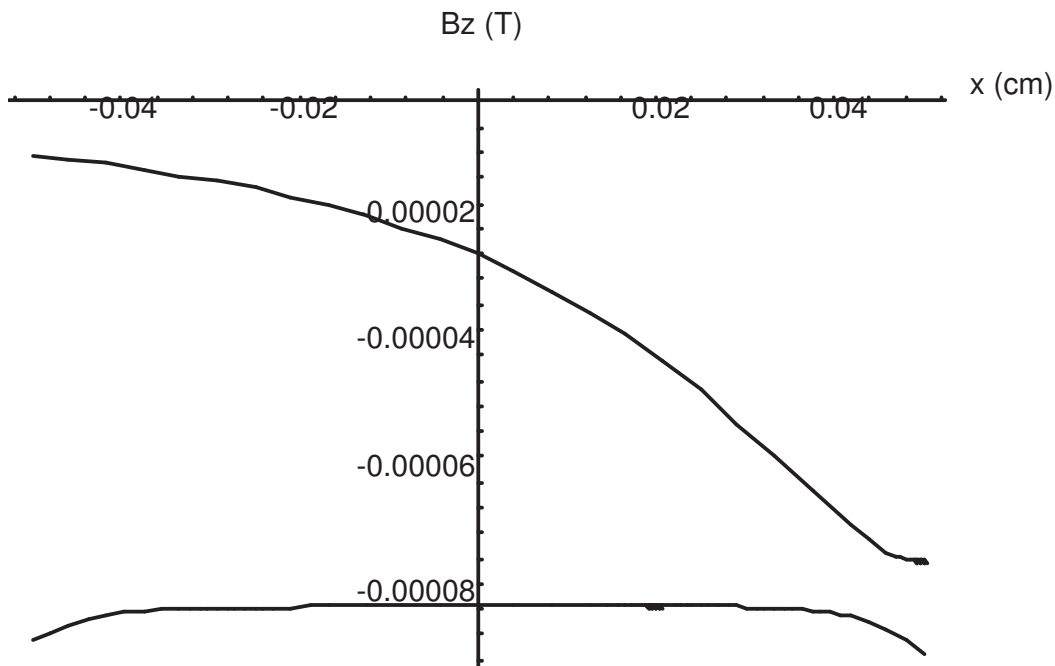


Figure 2.6: \vec{x} axis field correction

2.7 Discussion on the direction of magnetization of the magnets relative to the main field

2.7.1 All magnets in the same direction:

If we orientate all the correction magnets in the same direction we obtain a distribution of the values of the coefficients A_{nm} and B_{nm} centred on 0. However, up to and including order 5, the coefficient A_{20} escapes this rule. This is not centred on zero and one of the limits of the spread is approximately zero. To be more precise the value zero can be reached but with a very low probability. It is thus necessary to generate a field defect with a A_{20} ¹¹. So the sign of that coefficient will determine the general orientation of the correction magnets.

¹¹This coefficient expresses the difference of curvature along the \vec{z} and the average of the curvatures along the \vec{x} and \vec{y} .

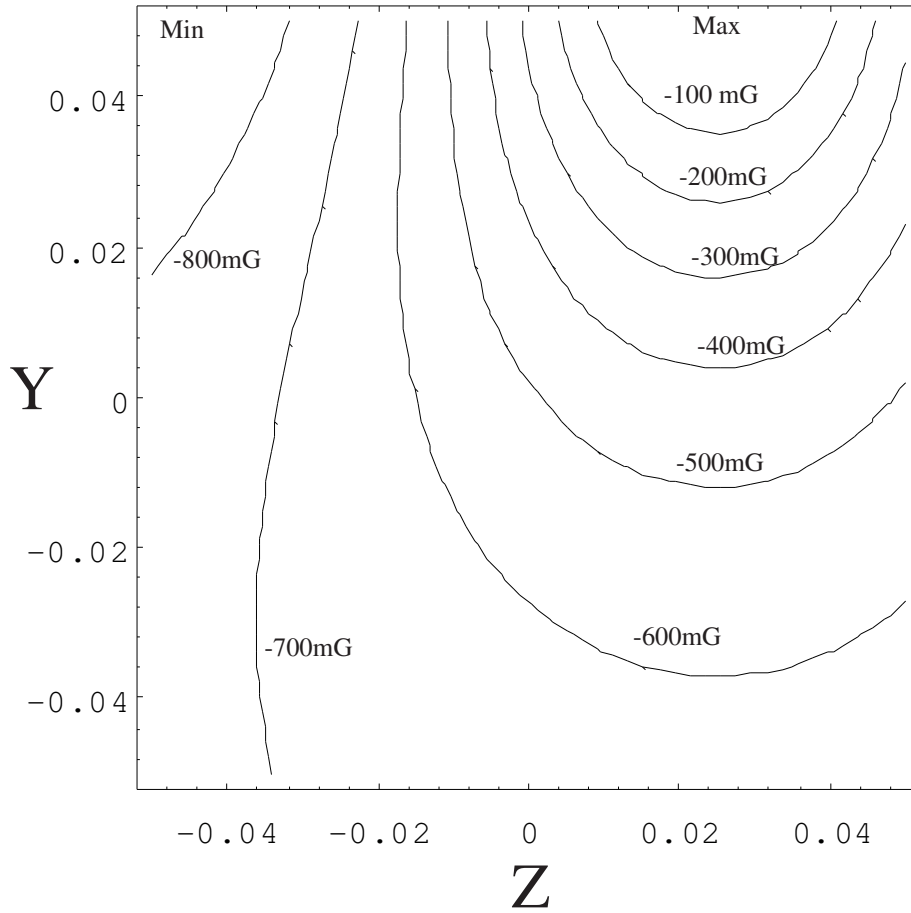


Figure 2.7: Initial field level curve

2.7.2 One every two magnets in the same direction

This time, all the coefficients are approximately centered, so we can choose the direction of variation of the main field. However, the maximum values reached by the coefficients of this configuration are 25% lower, so we have a lower power of correction.

2.7.3 One hemisphere one way and vice versa

We can also use the fact that by orienting one hemisphere in one direction and the other in the opposite direction we can shift the distribution of the corresponding gradient from the $-alpha$ to the $+alpha$ interval towards 0 to

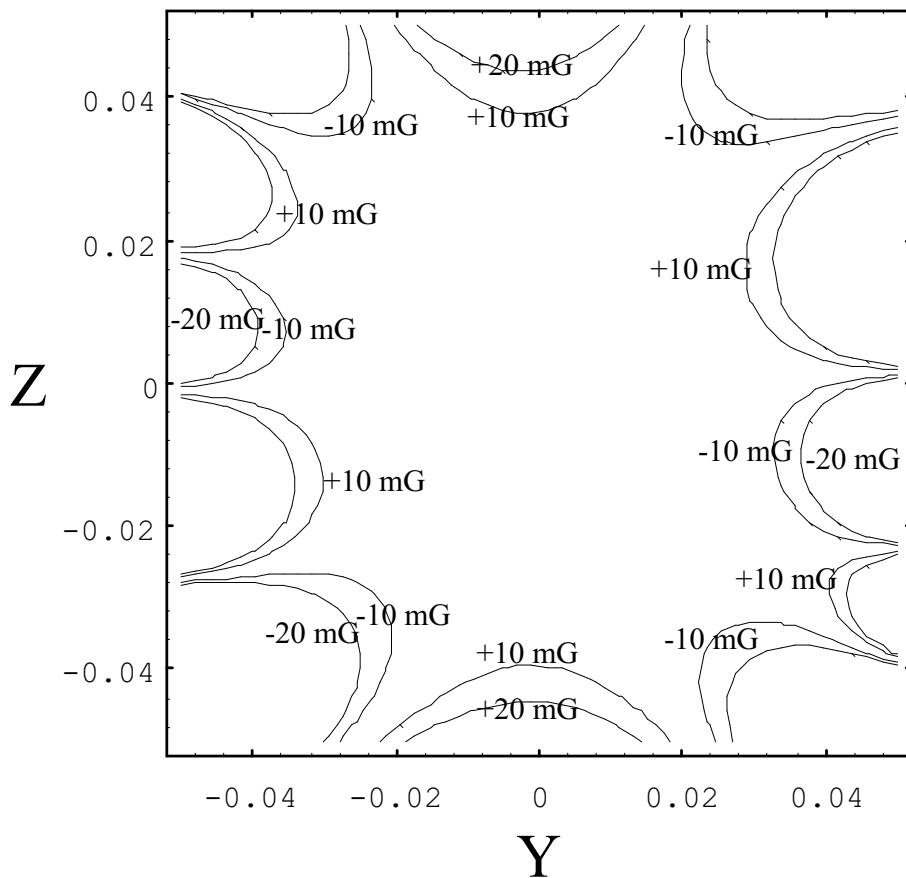


Figure 2.8: Corrected field level curve (apparent 6th order - quod erat demonstrandum)

$2\alpha^{12}$, this can possibly be used to correct an important gradient. Nevertheless we will recall that the power of correction on the other coefficients will be further decreased by 25%.

2.8 Influence on transverse components

In magnetic resonance imaging, we have hypothesized that we are only interested in the longitudinal component of the field because the radiofrequency field only captures along this axis. However, there are a contribution from

¹²For example let us orient the upper hemisphere of our configuration in the direction of the field and the lower hemisphere in the opposite direction, the distribution of the coefficient B_{11} , i.e. the following gradient y , will be shifted.

the transverse components. In rotational symmetry, conventional helmoltz coil-type configurations essentially generate a field in one direction. But our correction system does not have, except in special cases, a symmetry of revolution. It is therefore interesting to know if this system does not amplify the transverse errors, no control equation being integrated. The Figure (2.9) shows that on the contrary the field lines tend towards the direction \vec{z} . The divergence $\nabla \cdot \vec{B} = 0$ is verified because each of the derivatives $\partial B_x / \partial x$, $\partial B_y / \partial y$ and $\partial B_z / \partial z$ is null. The most important parasite term is a $\partial B_y / \partial z$ gradient.

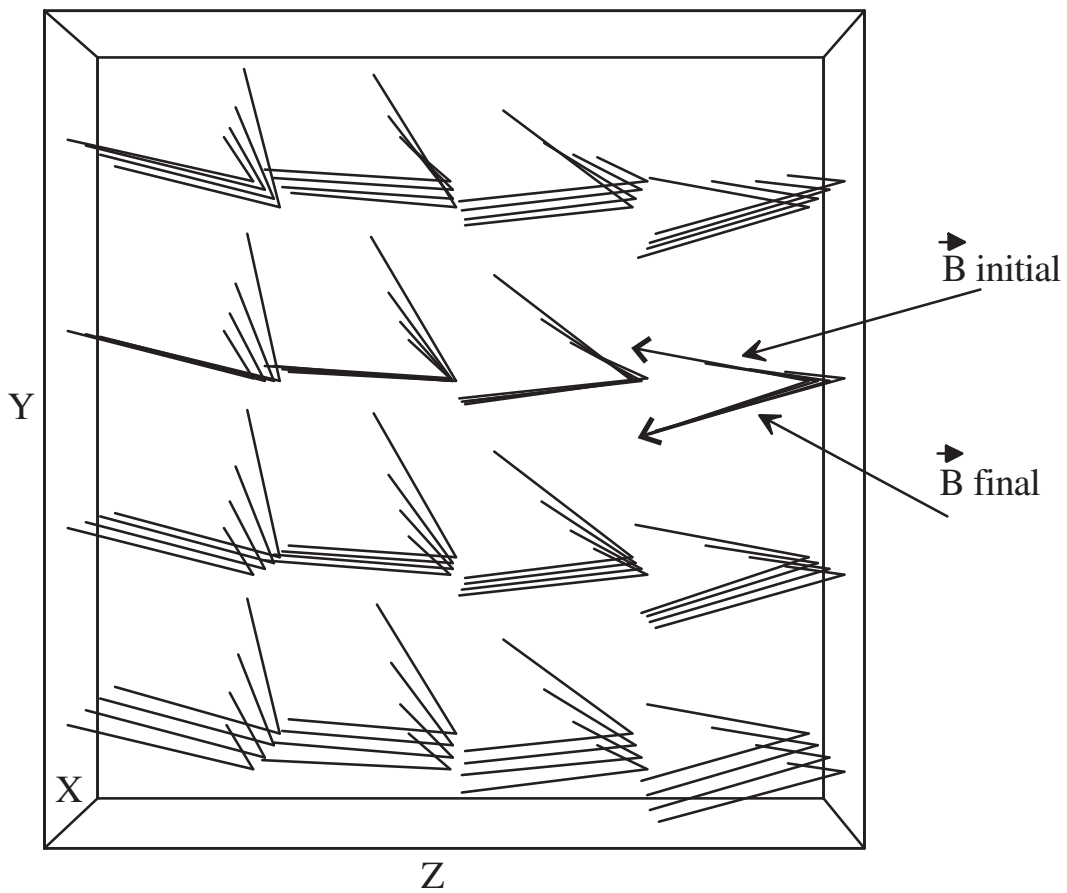


Figure 2.9: Behaviour of the \vec{B} field before and after the correction. The transverse components B_x and B_y are globally weaker.

2.9 Bessel field development

An alternative to the previous approach in cylindrical coordinates is the use of Bessel functions. We will always assume that the replacement of the integral in x' and y' by the simple surface of the magnet is accurate enough for a computation point far away from the correcting magnet.

Let's start from the development of the potential in cylindrical coordinates[24, p.118]:

$$\frac{1}{|\mathbf{x} - \mathbf{x}'|} = \frac{4}{\pi} \int_0^\infty \cos[k(z - z')] \times \left\{ \frac{1}{2} I_0(k\rho_<) K_0(k\rho_>) + \sum_{m=0}^{\infty} \cos[m(\phi - \phi')] I_0(k\rho_<) K_0(k\rho_>) \right\} dk \quad (2.20)$$

where I_0 and K_0 are the modified Bessel functions.

Then an interesting identification can be used:

$$K_0\left(k\sqrt{\rho^2 + \rho'^2 - 2\rho\rho' \cos(\phi - \phi')}\right) = I_0(k\rho_<) K_0(k\rho_>) + 2 \sum_{m=0}^{\infty} \cos[m(\phi - \phi')] I_0(k\rho_<) K_0(k\rho_>) \quad (2.21)$$

Using as before the formula $F_{zz'}$ page 14 and deriving the integrand with respect to z , we obtain the field equation B_z generated by a corrector magnet whose magnetization is M_z , the cross-section is A and the length is $z_2 - z_1$:

$$\begin{aligned} B_z(\rho, \phi, z) &= \frac{M_z A}{2\pi^2} \int_0^\infty \left[\frac{\partial \cos[k(z - z')]}{\partial z} \right]_{z_1}^{z_2} \times \\ &K_0\left(k\sqrt{\rho^2 + \rho'^2 - 2\rho\rho' \cos(\phi - \phi')}\right) dk \\ &= -\frac{M_z A}{2\pi^2} \int_0^\infty k (\sin[k(z - z_2)] - \sin[k(z - z_1)]) \times \\ &K_0\left(k\sqrt{\rho^2 + \rho'^2 - 2\rho\rho' \cos(\phi - \phi')}\right) dk \quad (2.22) \end{aligned}$$

There are therefore other possible developments in the field. By studying the convergence of the series resulting from the previous formula, we can extract the various terms from the series and form a system of equations. The next series starts at order 1 because the calculation of order 0 obliges

the use of the limits. We are in the presence of an indetermination and this indetermination is lifted, the term at order 0 is equal to zero.

$$B_z(\rho, \phi, z) = -\frac{M_z A}{2\pi^2} \sum_1^N k (\sin[k(z - z_2)] - \sin[k(z - z_1)]) \times K_0 \left(k\sqrt{\rho^2 + \rho'^2 - 2\rho\rho' \cos(\phi - \phi')} \right) \quad (2.23)$$

The Figure (2.10) shows, in the same way as the Figure (2.3), the relative error between the exact value of the field and the development (2.23) for $N = 36$ and $N = 64$. Note that the error in the useful zone is larger than the Legendre development, but there is no longer a radius of convergence. This has the advantage of creating large useful zones if a larger average error is allowed. However, it is necessary not to get too close to the source, because the higher harmonics become, like the Legendre development, predominant.

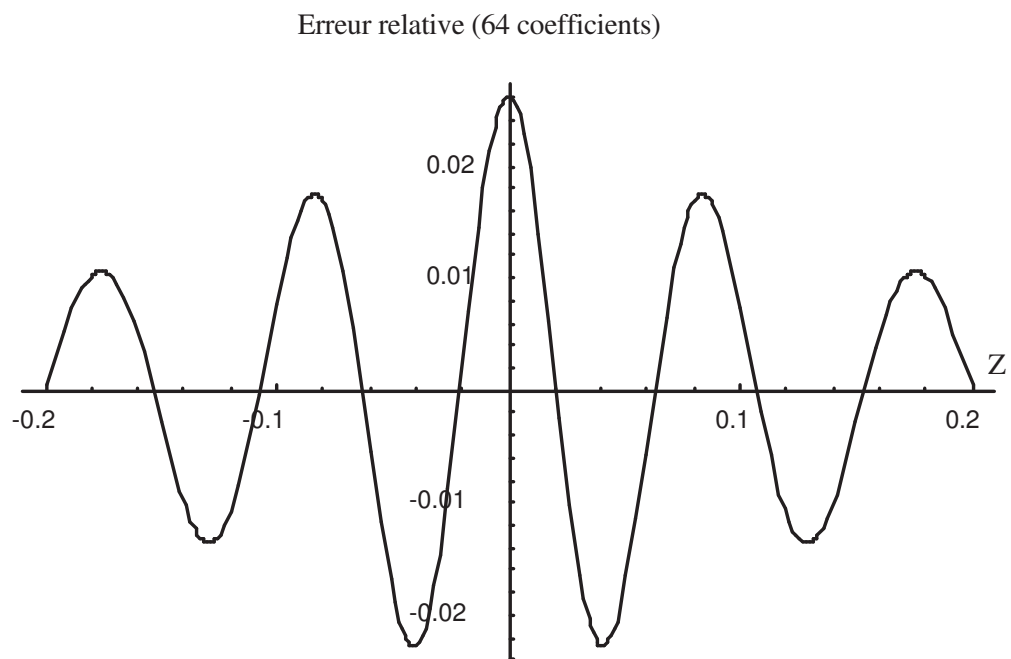
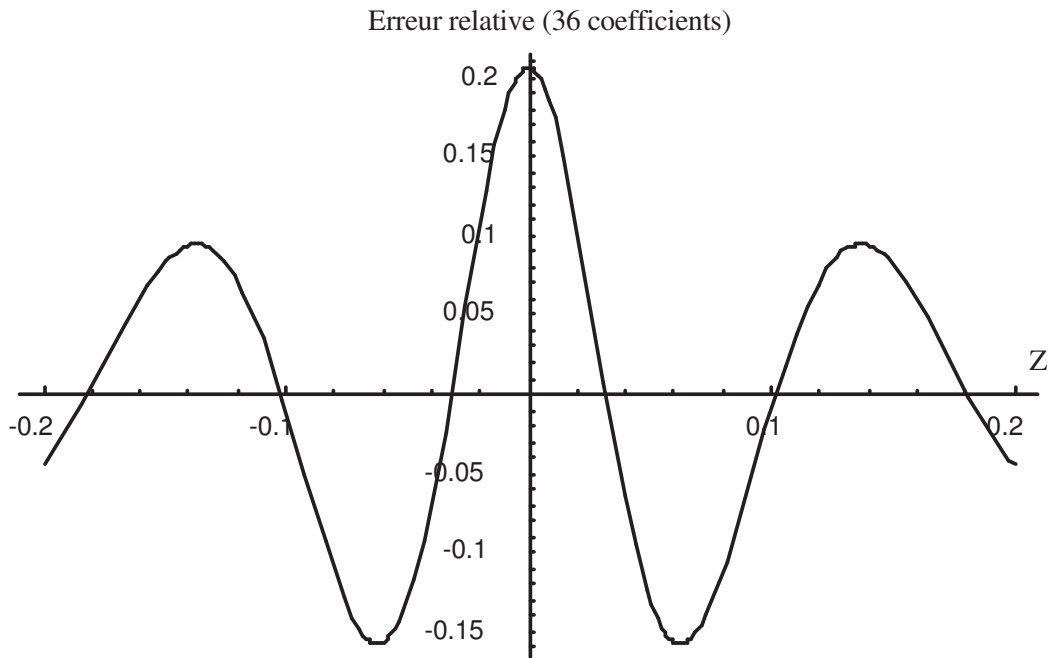


Figure 2.10: Relative error between exact field and Bessel functions approximation

Chapter 3

Non-linear resolution

The numerical resolution of Legendre's system of equations is essential. From a field expressed as Legendre coefficients, the program determines the position of the magnets that will generate this field. The main difficulty is that the different equations are strongly coupled. When we linearize the equations at each iteration, the Jacobian matrix is not invertible. It is therefore impossible to solve this system by a classical Newton-Raphson-type method. However, the method of decomposing a matrix into singular values partially solves this problem. We then created our own solution system based on this method and on the analysis of the behavior of this type of equations. This technique can be useful for inverse problems deriving from a potential in $\frac{1}{R}$.

3.1 General Newton method

We want to solve the following system by Newton's method.

$$\begin{aligned} f_1(x_1, x_2, x_3, \dots, x_n) &= 0 \\ f_2(x_1, x_2, x_3, \dots, x_n) &= 0 \\ &\vdots \\ f_n(x_1, x_2, x_3, \dots, x_n) &= 0 \end{aligned} \tag{3.1}$$

Having an initial vector $\mathbf{x} = (x_1, x_2, x_3, \dots, x_n)$, we will determine a displacement vector δ by expanding each function into a Taylor series and keeping only the linear terms.

$$f_1(\mathbf{x}) + \frac{\partial f_1}{\partial x_1}(\mathbf{x})\delta_1 + \frac{\partial f_1}{\partial x_2}(\mathbf{x})\delta_2 + \dots + \frac{\partial f_1}{\partial x_n}(\mathbf{x})\delta_n = 0$$

$$\begin{aligned}
f_2(\mathbf{x}) + \frac{\partial f_2}{\partial x_1}(\mathbf{x})\delta_1 + \frac{\partial f_2}{\partial x_2}(\mathbf{x})\delta_2 + \cdots + \frac{\partial f_2}{\partial x_n}(\mathbf{x})\delta_n &= 0 \\
&\vdots \\
f_n(\mathbf{x}) + \frac{\partial f_n}{\partial x_1}(\mathbf{x})\delta_1 + \frac{\partial f_n}{\partial x_2}(\mathbf{x})\delta_2 + \cdots + \frac{\partial f_n}{\partial x_n}(\mathbf{x})\delta_n &= 0
\end{aligned} \tag{3.2}$$

In matrix notation, the system of equation (3.2) is written as follows

$$F(\mathbf{x} + \delta\mathbf{x}) = F(\mathbf{x}) + J.\delta\mathbf{x} + O(\delta\mathbf{x}^2) = 0 \tag{3.3}$$

we calculate $\delta\mathbf{x}$ by

$$J.\delta\mathbf{x} = -F \equiv \delta\mathbf{x} = -J^{-1}.F \tag{3.4}$$

$\delta\mathbf{x}$ represents the deviation to be applied to the initial vector \mathbf{x} and if there is no singularity at the point considered[2, p.373], $\mathbf{x} + \delta\mathbf{x}$ will be the new approximation of the root of the system of equations (3.1). We will repeat the calculation until we obtain a sufficiently precise root.

3.2 Roots of Legendre's equations

To determine the position of the correction magnets, we use the system of equations (2.19) determined in the previous chapter:

$$\begin{cases} \frac{A_{nm}}{4\pi} - \sum_{i=1}^N \frac{M_i A_i}{4\pi} \epsilon_m \frac{(n-m+1)!}{(n+m)!} \left[\frac{P_{n+1,m}(\cos \theta'_i)}{r_i'^{n+2}} \right]_{z_{i_1}}^{z_{i_2}} \cos(m\phi'_i) = 0 \\ \frac{B_{nm}}{4\pi} - \sum_{i=1}^N \frac{M_i A_i}{4\pi} \epsilon_m \frac{(n-m+1)!}{(n+m)!} \left[\frac{P_{n+1,m}(\cos \theta'_i)}{r_i'^{n+2}} \right]_{z_{i_1}}^{z_{i_2}} \sin(m\phi'_i) = 0 \end{cases}$$

We have chosen to move the magnets only in z. Thus each magnet will move in one of the 35 grooves evenly distributed around the generating cylinder.

To make the variables z_i appear, the bracketed part of (2.19) will be rewritten in Cartesian coordinates, and we will determine ϕ' for each magnet i.

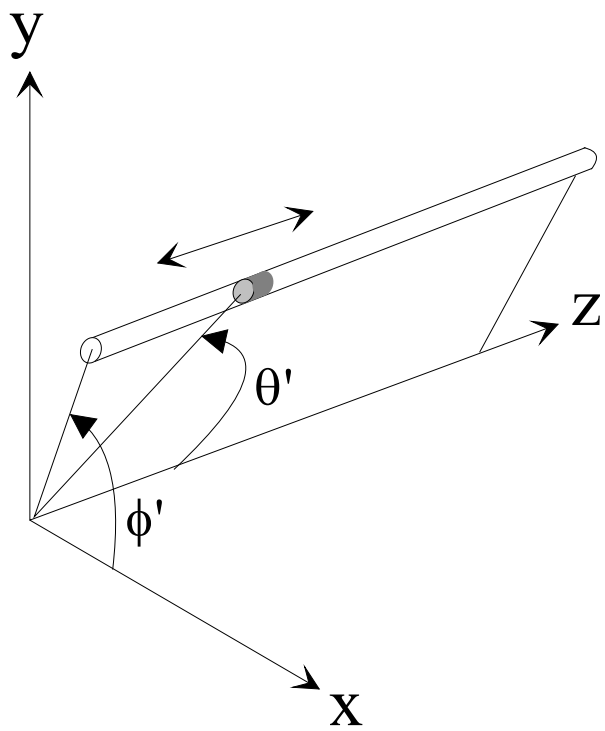


Figure 3.1: Variables used

$$\begin{cases} \frac{A_{nm}}{4\pi} - \sum_{i=1}^N \frac{M_i A_i}{4\pi} \epsilon_m \frac{(n-m+1)!}{(n+m)!} \left[\frac{P_{n+1} m \left(\frac{z'_i}{r'_i} \right)}{r_i'^{n+2}} \right]^{z_{i2}} \cos \left[m(i-1) \frac{2\pi}{35} \right] = 0 \\ \frac{B_{nm}}{4\pi} - \sum_{i=1}^N \frac{M_i A_i}{4\pi} \epsilon_m \frac{(n-m+1)!}{(n+m)!} \left[\frac{P_{n+1} m \left(\frac{z'_i}{r'_i} \right)}{r_i'^{n+2}} \right]^{z_{i2}} \sin \left[m(i-1) \frac{2\pi}{35} \right] = 0 \end{cases} \quad (3.5)$$

Now that the main equations have been set, we must determine the roots. We will calculate the Jacobian of the system (3.5) in relation to the variables z_i . Each element of the matrix is written as follows

$$\frac{\partial f}{\partial z_i} = \frac{M_i A_i}{4\pi} \epsilon_m \frac{(n-m+2)!}{(n+m)!} \left[\frac{P_{n+2} m \left(\frac{z'_i}{r'_i} \right)}{r_i'^{n+3}} \right]^{z_{i2}} \begin{matrix} \cos \\ \sin \end{matrix} \left[m(i-1) \frac{2\pi}{35} \right] \quad (3.6)$$

3.3 Inversion of the Jacobian matrix

An important step is the calculation of J^{-1} in (3.4) because the main difficulty is there. Let us suppose that we are very close to a solution vector, a difference of 10% on only one of the coordinates of the vector is enough to make the system non-invertible. The equations composing the system are thus decoupled in a region very close to the solution. The difficulty remains the choice of an initial vector. An ad-hoc method consists in randomly drawing each position of a correcting magnet within a reasonable interval¹. The probability of being close to the solution vector(s), assumption not verified is particularly low, we can consider after a rough calculation to have a chance on 10^{35} . It is thus almost impossible to find a root in an acceptable time. However the calculation time can be greatly reduced by using the method of decomposition in singular values of a square matrix.

The generic idea of the root search is based on the following hypothesis, let us take any initial vector and a number of equations much lower than the number of the general system and we will assume that the solution vector found must be close to the real solution. If we decrease the number of equations to be solved to n , the program can only provide us with the n most significant variations on the coordinates of the initial vector. The other coordinates of the vector are not affected (i.e. some magnets do not move at

¹The limits of the gap are approximately equal to the radius of the generating cylinder, beyond which the magnet no longer has any significant influence.

all), so it seems clear that the accuracy achieved will be insufficient. But in our problem, a remarkable fact is that the found vector can be used efficiently in the search for a new solution to the system on which we increase the number of equations to be solved. The process ends when we have reached the full number of equations and found the solution vector.

3.4 Singular value decomposition of a square matrix

This very powerful technique is used for inversion of singular matrices. Gaussian elimination or LU decomposition² cannot be used because of their sensitivity to rounding errors. Singular value decomposition is often used in linear least squares calculations, matrices are generally poorly conditioned because the aim is to minimise the difference between a model and a set of points greater than the number of variables needed to fully determine a solution. The problem in this case is oversized. In this study, we will not use least squares but a root search, because the equations already generate a non-invertible matrix when the number of unknowns equals the number of equations. Using a greater number of variables does not provide better results.

The singular value decomposition is based on the following linear algebra theorem: Any matrix A whose number of rows is greater than or equal to the number of columns can be decomposed into a product of three matrices U , W , V^T . The matrix U is the same size as the matrix A and its column vectors are orthogonal to each other. The W matrix is a diagonal matrix composed of positive or zero values, its size is equal to the number of columns of A . Finally the V^T matrix is an orthogonal square matrix, so we have:

$$A = U \cdot [diag(w_i)] \cdot V^T \quad (3.7)$$

The numerical routines used are derived from an algorithm proposed by Forsythe[15] originally created by Golub and Reinsch[18].

In our case, the matrix A is square, so the three matrices will be as square and of the same size as A . Since U and V are orthogonal matrices, the transpose of each of these matrices is equal to their inverse. The inverse of the matrix A is written as follows

²Lower Upper triangular matrix.

$$A^{-1} = V. [diag(1/w_i)].U^T \quad (3.8)$$

In the case of the search for roots of a system deriving from a potential in $1/R$, the equations (represented by the main equation of the field a_{00} and successive derivatives) cancel each other at infinity. Given the size of our system (radius of the generating cylinder equal to 10cm), at more than 30cm from the center we can consider that the magnets are placed at infinity. As the matrix to be inverted is precisely the Jacobian of these equations with respect to the spatial coordinates, the system will be made non-invertible in the case where magnets are ejected far from the area of interest. Many elements of this matrix will be cancelled and thus the row or column vectors of the matrix A^{-1} become linearly dependent. The classical consequence of a divergent system is to provide no result. This general tendency is moreover the main difficulty encountered in the inverse problems related to the positioning of sources.

The coefficients of the diagonal matrix W^{-1} indicate whether the matrix is well conditioned. If the ratio $w_{max}/w_{min} > 10^6$ in the case of 4-byte floats and $w_{max}/w_{min} > 10^{12}$ in the case of 8-byte floats, rounding errors become very large when inverting the matrix A by a Gauss pivot method.

By setting a limit value where any lower value w_i will be replaced by zero³, we remove some lines from the matrix A . They are either coupled together or close to zero. Calculating the inverse by this method will solve $AX = B$ by a method of least squares, it will then be a matter of determining X such that $||AX - B||$ is minimum.

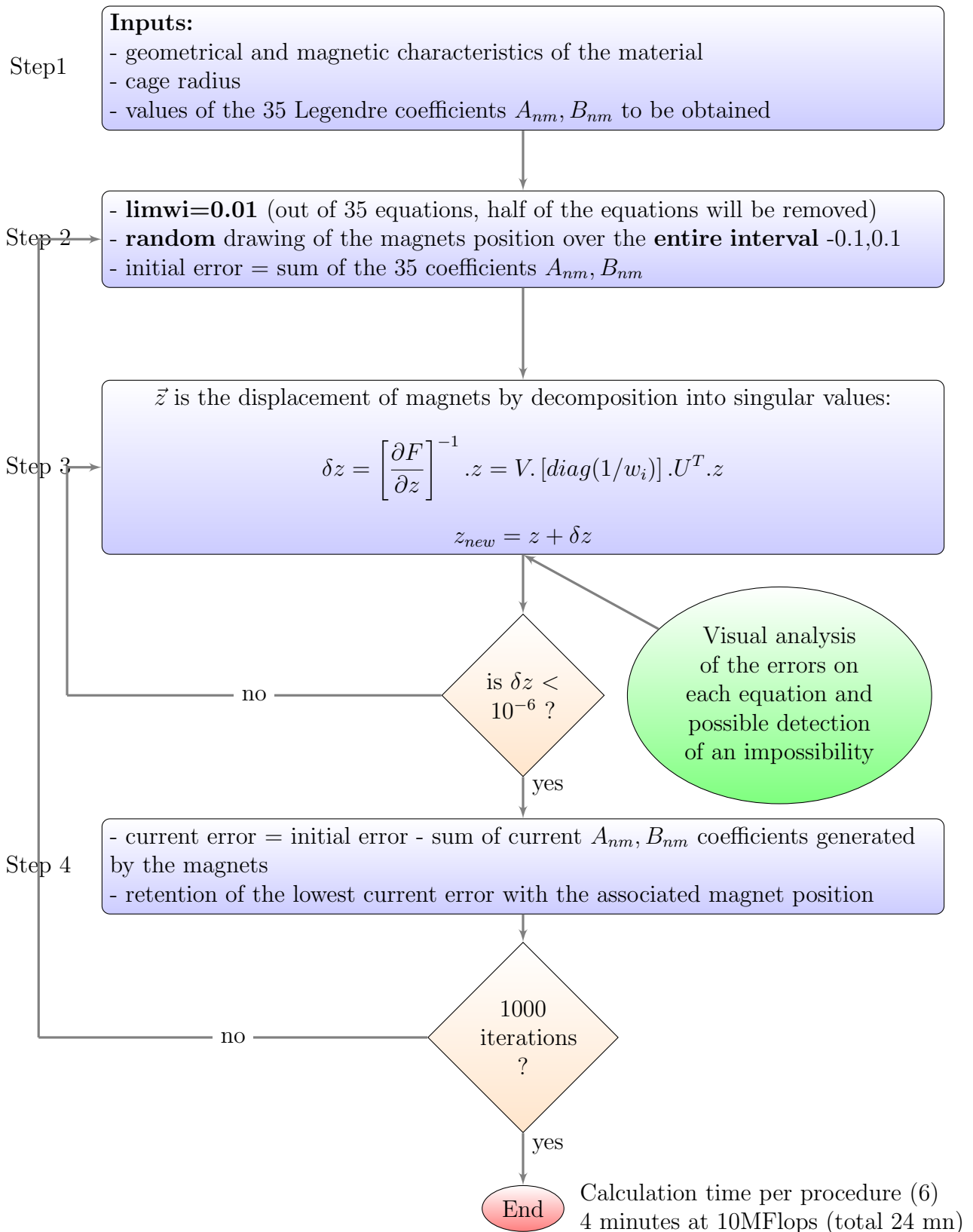
3.5 Software flowchart

The positions of magnets generating the field opposite to the field determined by the coefficients A_{nm} , B_{nm} , themselves derived from the measurements, are given by the algorithm in the Figure (3.5).

The 5 following procedures consist in repeating the initial procedure and reusing the solution vectors found previously by dividing by 10 in each procedure the coupling coefficient $limwi$. The random draw will be centered on the previous solution vector $\pm 1cm$.

Iteration 2 is therefore written by taking the initial algorithm and replacing step 2 by the Figure below (3.2).

³We will transgress a mathematical rule $w_i = 0 \rightarrow 1/w_i = \infty = 0$, an infinity that we have replaced by zero!



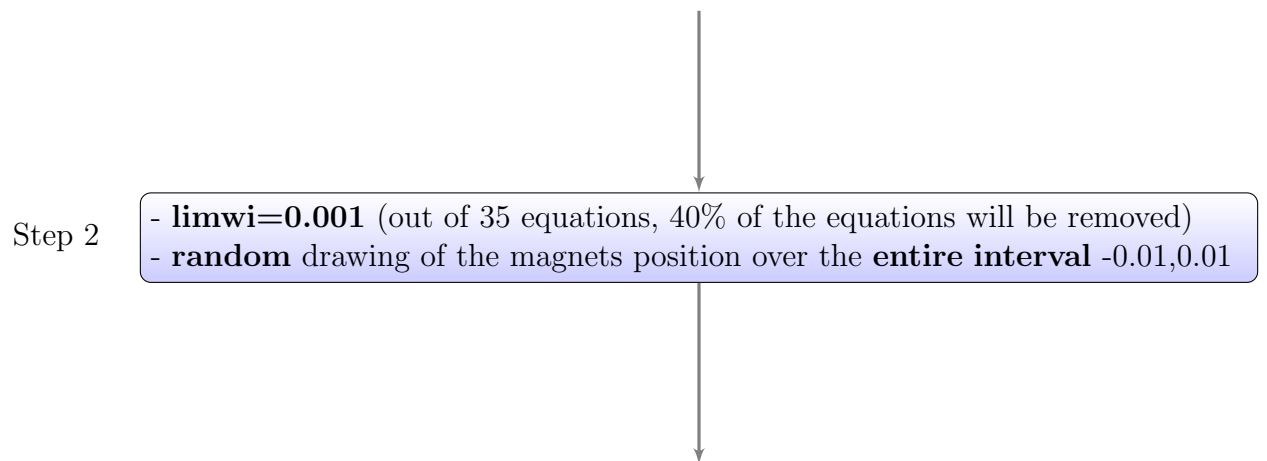


Figure 3.2: Modification of Step 2 to refine the \vec{z} magnets positioning

Chapter 4

Bivariates application

To illustrate the algorithm of the previous chapter by a graphical method, we will determine the position of two magnets that will generate a homogeneous field on the \vec{z} axis. These 2 magnets are in the first configuration Figure (4.1) and the characteristics of the magnets are given in chapter 1.5. As we are only interested in the B_z field on the axis, their position in ϕ' is unimportant. This study is instructive because we can transpose this two-dimensional case to the more complicated n-dimensional examples.

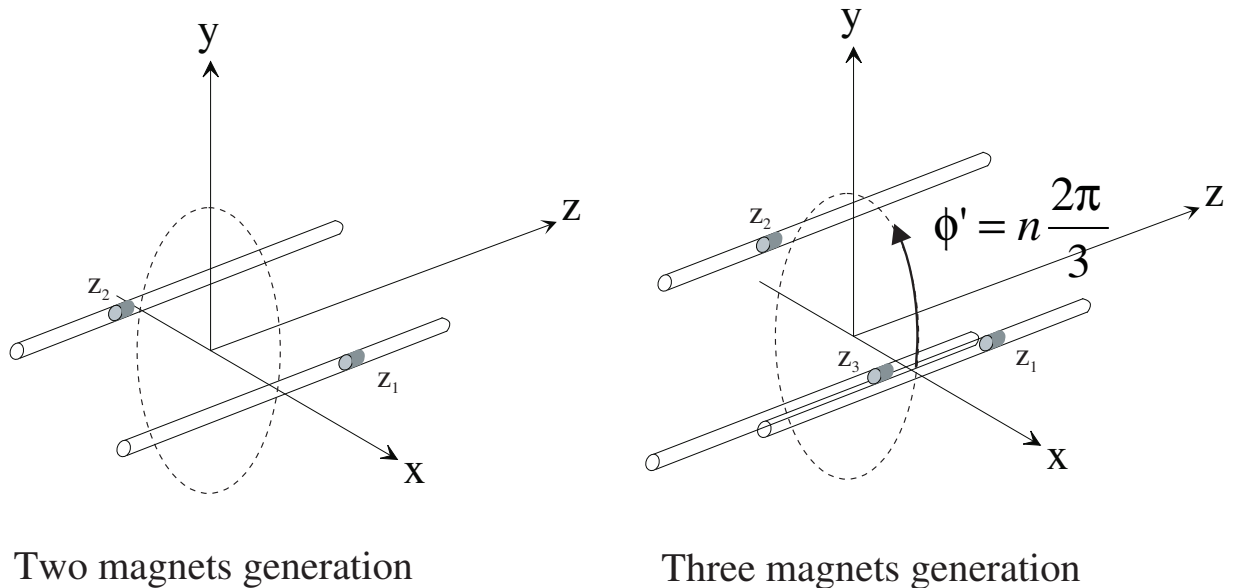


Figure 4.1: Two and three magnets configuration

4.1 Curve appearance a_{00} , a_{10} , a_{20}

The curve $a_{00} = cste$ is represented in 2 and 3 dimensions (2 and 3 magnets), the coordinates of the axes are the positions of the magnets. We notice that the transposition is easy because the curve $f(z_1, z_2) = cste \equiv f(z_1, z_2, z_3 = 0) = cste$. We find the curve with 2 magnets by a section of the curve with 3 magnets. The curve $a_{00} = 0$ is subtle, the axes \vec{x} and \vec{y} are asymptotes to infinity, there is also a virtual curve when $z_1 = z_2 = \infty$. However these remote solutions do not interest us, so we will limit the study to $\pm 20cm$ ¹.

The Figure (4.3) shows the two curves $a_{10} = 0$ and $a_{20} = 0$. It is a matter of finding the points of intersection of the simultaneous solutions. The particularity of the first equation is that it consists of a $z_2 = -z_1$ line and curves tangent to the solution points of a_{20} . Algorithms of the multidimensional Newton type will fail because the next solution vector is determined by the intersection of the hyperplanes, themselves tangent to the curves at the current point. It is therefore imagined that a solution determined by two tangent curves cannot be found. In this case, the solution is not in doubt because the second curve is automatically intersected by the line. The dotted polyline represents the path followed in the search for solutions. We notice that the 4th segment is very close to the solution but is subsequently ejected. The second approach is made using the SVD algorithm, as a hyperplane is suppressed if it is parallel to another². The solution is then found. However, if the initial vector answers $z_2 = -z_1$, a solution will be found very quickly, even with a Newton-Raphson method.

4.2 Selection of initial vectors

During a simple field generation, many Legendre development coefficients are null. We often find a line³ of the type $z_1 \pm z_2 \pm \dots \pm z_n = 0$, it is well indicated to choose an initial vector whose components are made up of the same absolute value chosen randomly and of sign in accordance with the equation of this line. In this way the vector clings to the plane, and is thus less subject to the phenomenon of tangent curves. In physical terms we can relate this to the different symmetries, but the mental effort becomes

¹We remind that throughout the document, we have normalized the dimensions of the generator to $r' = 10cm$. This is absolutely not restrictive because it is a dimensional ratio between r and r' , so we have chosen that the magnets could move a maximum of $\pm 2r'$.

²Two lines of the Jacobian are identical, so the singular value decomposition will remove one of the lines and continue as a least squares resolution.

³Some equations even contain several lines such as $a_{31} = 0$.

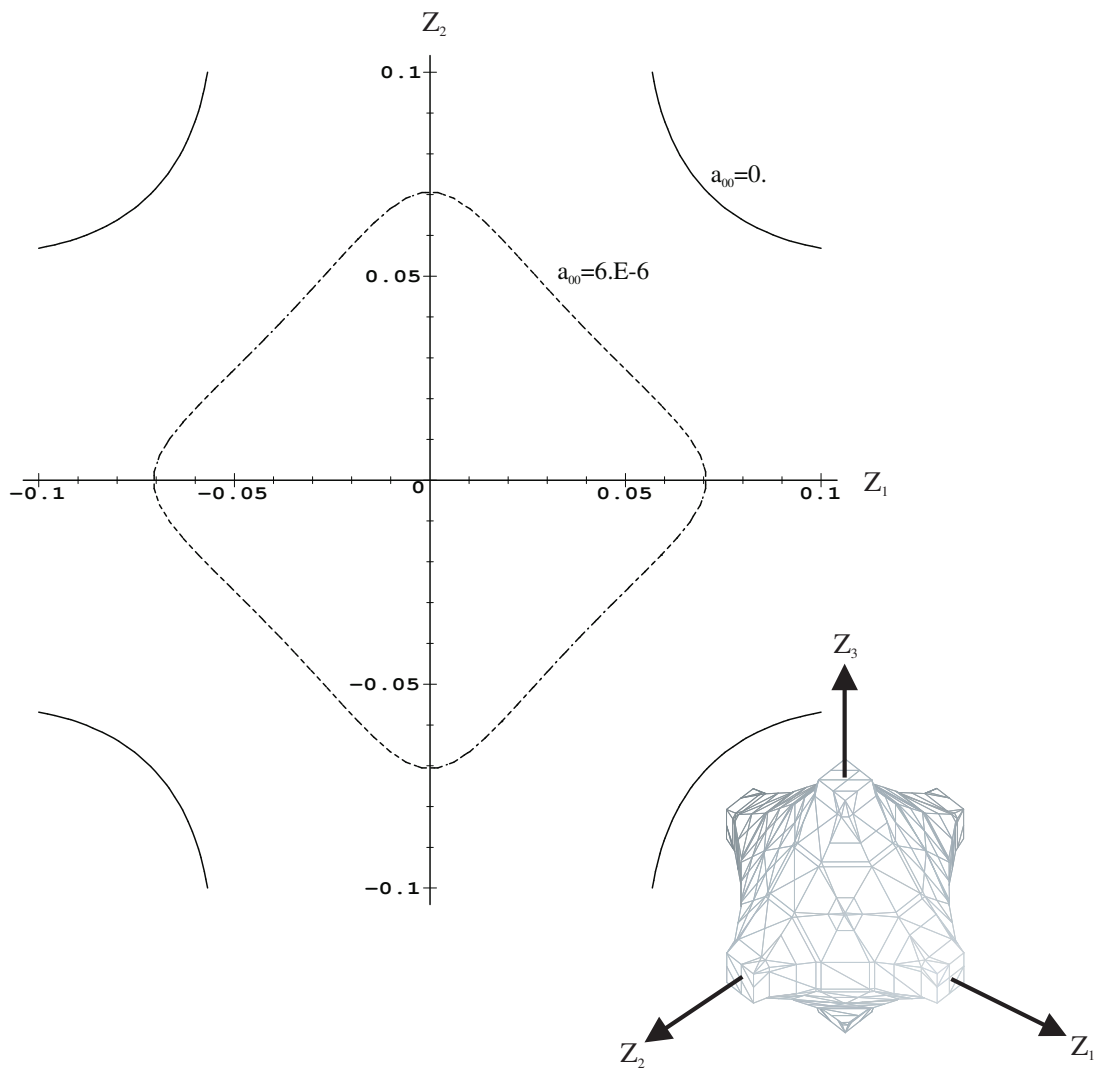


Figure 4.2: a_{00} for two and three magnets. The axes represent the positions of the magnets along the slides.

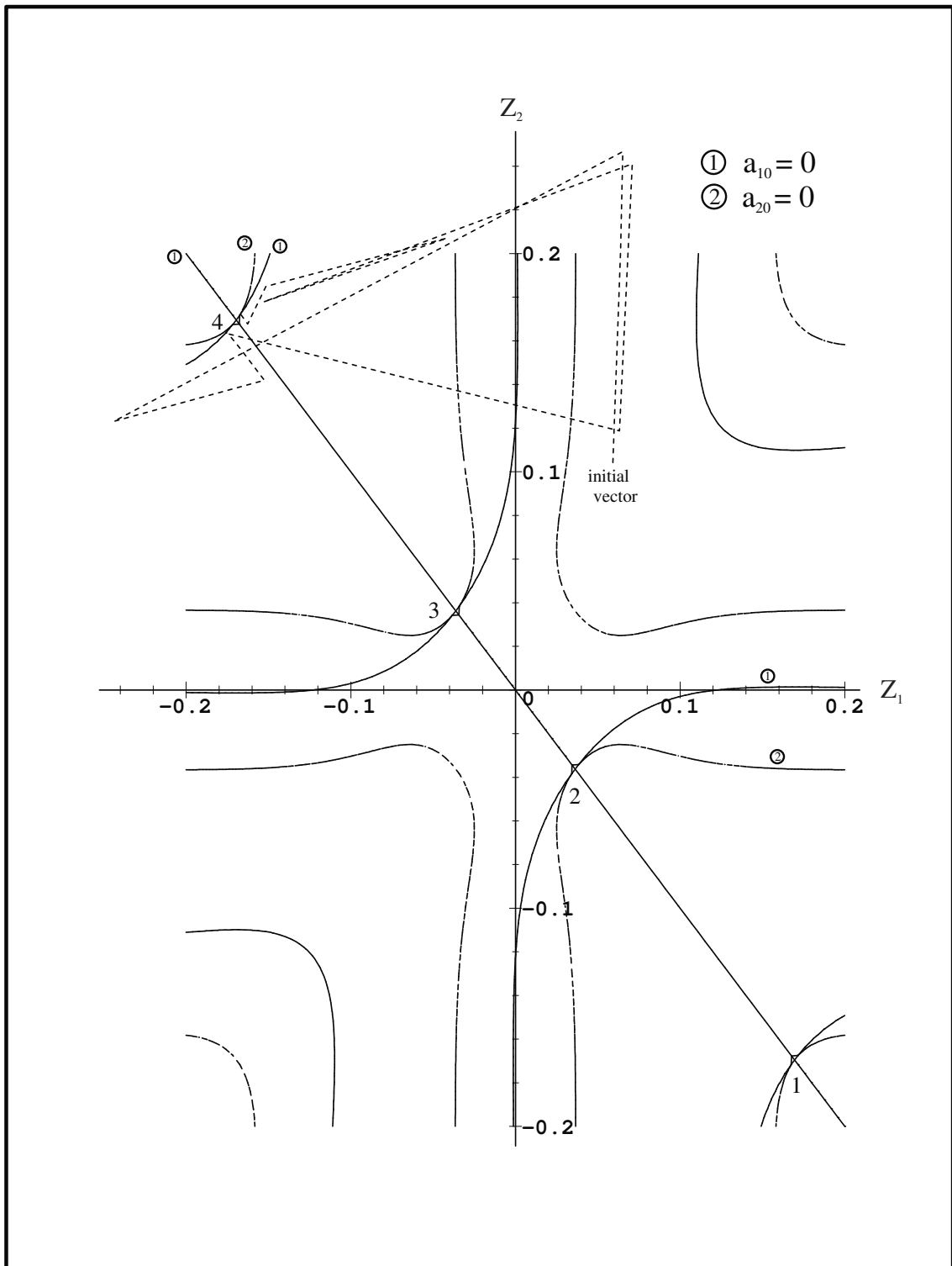


Figure 4.3: Search for solutions using Newton's algorithm for the first 4 segments. After failure, the final approach is performed by eliminating the tangent planes.

important when the number of orders to be corrected is large. It would then be interesting to review the different equations of the straight lines and test different initial vectors. A rough method consists in trying all the combinations of signs, but for 35 equations we get $2^{34} = 17\,179\,869\,184$ initial vectors.

However, these considerations are valid only in the case of cancelling the coefficients, otherwise the lines disappear as we can see in the Figure (4.4). Therefore, there is only no pure symmetry if the coefficient considered is not zero.

However, it seems difficult to search for solutions cancelling some of the coefficients because the function is not derivable everywhere⁴. Experience shows that it is simpler to correct a magnetic field where none of its coefficients is zero than to generate a particular field profile with a priori many zero coefficients.

We have thus demonstrated the interest of eliminating one of the tangent planes by our algorithm. By side effect, we also avoid getting too close to the solution in order to avoid an erroneous calculation of the jacobian, as some functions are not derivable at these points. It is thus the approach of the solution in the sense of least squares that eliminates this difficulty.

⁴It is precisely at solution points 1,2,3,4 of the figure (4.3) that one of the functions is not derivable.

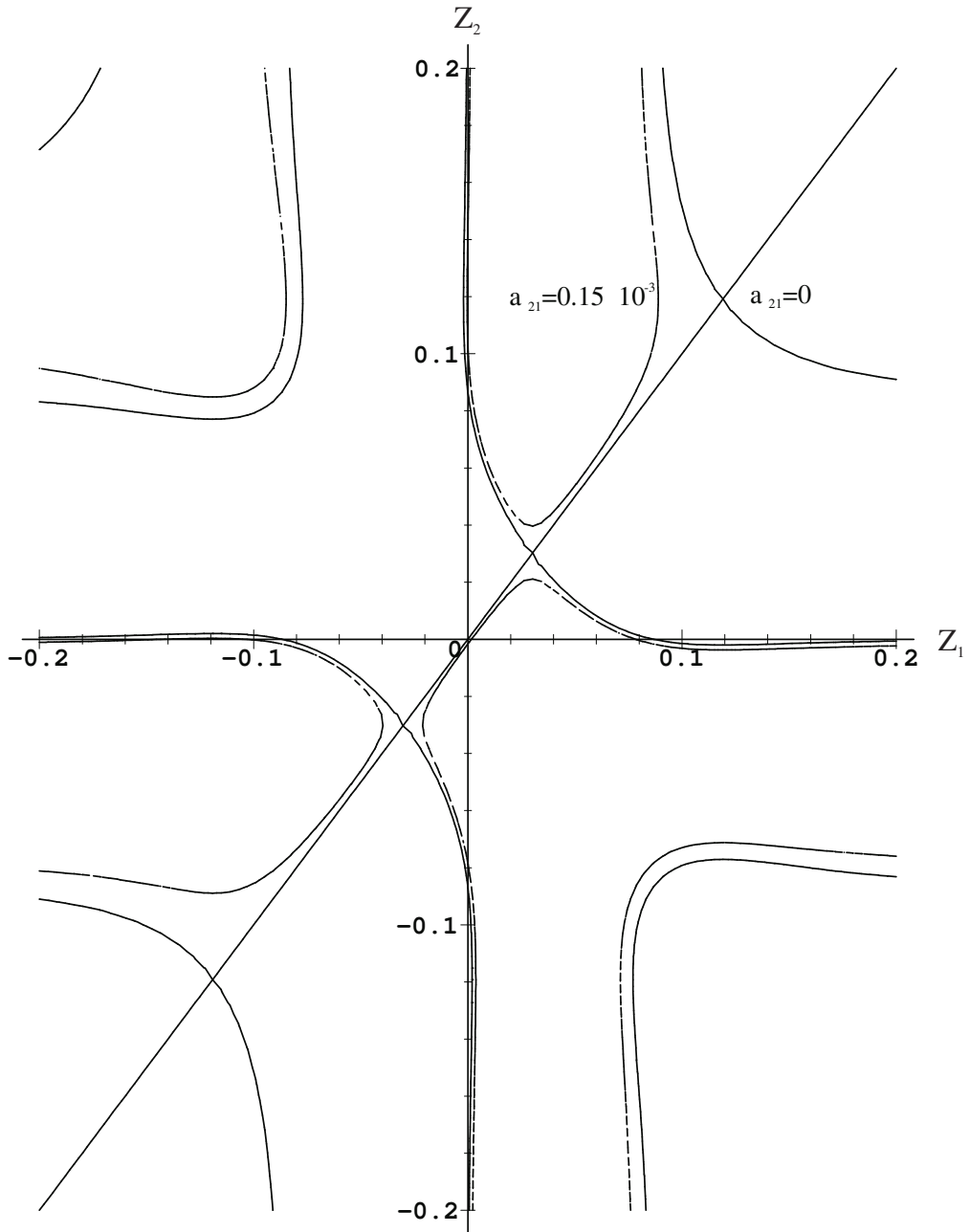


Figure 4.4: Symmetries exist only in the case of zero coefficients.

Chapter 5

Field generation by means of current wires.

The initial hypothesis is that we can generate a large number of configurations from straight current lines. We have initially chosen the simplest possible conductor shape and tried to generate arbitrary fields. If this is not possible, as the functions from the potential development may not be independent in the case of a line segment, we will choose another form of current line. Passing from line segments to B-splines for example does not pose any difficulty because the equations of the current elements are defined in the parametric form $x' = f(t)$, $y' = f(t)$ and $z' = f(t)$. This allows later numerical integration of the infinitesimal elements \vec{dl} between the starting point and the end point of the current arcs.

Generally speaking, the potential vector \vec{A} created by an element of current \vec{dl} and intensity I is written:

$$\vec{A} = \frac{\mu_0}{4\pi} I \int_l \frac{\vec{dl}}{R} \quad (5.1)$$

and the magnetic field \vec{B} is written:

$$\vec{B} = \text{rot} \vec{A} \quad (5.2)$$

These equations allow us to directly use Legendre's polynomial development.

5.1 Field development of a wire segment

5.1.1 Calculation of component B_z (see Fig 5.1)

Let's first consider a line segment carried by a $z = cste$ plane and let's look at the only one z component of the field generated by this coordinate wire $(x_1, y_1; x_2, y_2)$:

$$B_z = \int_l (y_2 - y_1) \frac{\partial \frac{1}{R}}{\partial x} - (x_2 - x_1) \frac{\partial \frac{1}{R}}{\partial y} \quad (5.3)$$

Taking up the development of $1/R$ (2.13), the integration along the wire relates to the coordinates x' and y' . The various coefficients out of integration are written¹:

$$a_{nm} = \frac{1}{\sqrt{x'^2 + y'^2 + z'^2}^{n+2}} \epsilon_{m-1} \frac{(n-m+2)!}{(n+m)!} (1 + \delta_{m-1}) \\ (- (y_2 - y_1) \cos [(m-1) \arctan(y', x')] - (x_2 - x_1) \sin [(m-1) \arctan(y', x')]) \\ P_{n+1m-1} \left[\frac{z'}{\sqrt{x'^2 + y'^2 + z'^2}} \right] + \epsilon_{m+1} \frac{(n-m)!}{(n+m)!} (1 - \delta_{m+1}) \\ ((y_2 - y_1) \cos [(m+1) \arctan(y', x')] - (x_2 - x_1) \sin [(m+1) \arctan(y', x')]) \\ P_{n+1m+1} \left[\frac{z'}{\sqrt{x'^2 + y'^2 + z'^2}} \right]$$

$$b_{nm} = \frac{1}{\sqrt{x'^2 + y'^2 + z'^2}^{n+2}} \epsilon_{m-1} \frac{(n-m+2)!}{(n+m)!} (1 + \delta_{m-1}) \\ (- (y_2 - y_1) \sin [(m-1) \arctan(y', x')] + (x_2 - x_1) \cos [(m-1) \arctan(y', x')]) \\ P_{n+1m-1} \left[\frac{z'}{\sqrt{x'^2 + y'^2 + z'^2}} \right] + \epsilon_{m+1} \frac{(n-m)!}{(n+m)!} (1 - \delta_{m+1}) \\ ((y_2 - y_1) \sin [(m+1) \arctan(y', x')] + (x_2 - x_1) \cos [(m+1) \arctan(y', x')]) \\ P_{n+1m+1} \left[\frac{z'}{\sqrt{x'^2 + y'^2 + z'^2}} \right]$$

with

$$\epsilon_m = \begin{cases} 0 & \text{si } m < 0 \\ 1 & \text{si } m = 0 \\ 2 & \text{si } m > 0 \end{cases}$$

¹We voluntarily wrote $\arctan(y', x')$ which returns the angle in all four quadrants, this syntax is similar to the form $\arctan(\frac{y'}{x'})$ defined only on the interval $[-\pi/2, \pi/2]$.

et

$$\delta_m = \begin{cases} 1 & \text{si } m = 0 \\ 0 & \text{si } m \neq 0 \end{cases}$$

To calculate the different coefficients, we perform the following substitution $x' = x_1 + (x_2 - x_1) \times t$, $y' = y_1 + (y_2 - y_1) \times t$. We recognize the parametric equations of a line segment. We then integrate Bz following t varying from $[0,1]$. This step can therefore be modified by replacing the parametric equations in the program by other equations in the numerical integration routine and by taking care to modify the terms in $(x_2 - x_1)$, $(y_2 - y_1)$, $(z_2 - z_1)$ by the local derivative of the integration path. The above-mentioned terms are obtained in this way by deriving the two parametric equations with respect to t .

Analytical integration is possible for all coefficients, however a coefficient of order 4 requires 20 million characters to be represented. Order 5 cannot be reasonably written analytically, so we will choose numerical integration, which is much faster.

5.1.2 Calculation of the B_x component (see Fig 5.1)

After considering the z component of the field generated by the wires, we will determine the x component of the field. Currently, many publications[8][22][23][32] dealt with the control of the field components parallel to the plates (in our reference the x and y components). It is essentially about the generation of field gradients.

$$B_x = \int_l \underbrace{(z_2 - z_1)}_{=0} \frac{\partial \frac{1}{R}}{\partial y} - (y_2 - y_1) \frac{\partial \frac{1}{R}}{\partial z} \quad (5.4)$$

Since the wire segments of coordinates $(x_1, y_1; x_2, y_2)$ are all at $z' = cste$, the first term of the integral is null. Writing the B_x field is similar to that used for correction magnets:

$$a_{nm} = \frac{1}{\sqrt{x'^2 + y'^2 + z'^2}^{n+2}} \epsilon_m \frac{(n - m + 1)!}{(n + m)!} \times -(y_2 - y_1) \cos [m \arctan(y', x')] P_{n+1m} \left[\frac{z'}{\sqrt{x'^2 + y'^2 + z'^2}} \right]$$

$$b_{nm} = \frac{1}{\sqrt{x'^2 + y'^2 + z'^2}^{n+2}} \epsilon_m \frac{(n - m + 1)!}{(n + m)!} \times -(y_2 - y_1) \sin [m \arctan(y', x')]$$

$$P_{n+1m}\left[\frac{z'}{\sqrt{x'^2 + y'^2 + z'^2}}\right]$$

with $x' = x_1 + (x_2 - x_1) \times t$, $y' = y_1 + (y_2 - y_1) \times t$ et $z' = cste$.

The Figure (5.1) shows the dimensions we have chosen for the field generator. In this study, only the wires generating a B_x field are represented, so there are no transverse arcs drawn in the drawings. However, to measure the B_y and B_z fields, they will actually be used in the calculation.

Physically the current lines are closed and we consider that the return arcs are far from the area of interest. This point can be criticized because it forces a plate of important dimension. However this omission is not essential at first, because it is a question of showing the possibility of generating field configurations from rectilinear wires. If it proves possible, the inventoried cases can be studied for practical realization knowing that in the case of a gradient $\partial B_x / \partial x$ there are no return arcs. We can form coils on the same plate, the directions of the currents being opposite by symmetry along the \vec{y}

5.1.3 Calculation of the B_y component (see Fig 5.1)

This component does not interest us because it is parallel to the active conducting wires. However, when calculating the vector \vec{B} , it is necessary to take into account the transverse arcs which generate a B_y component. To calculate the coefficients a_{nm} and b_{nm} relative to this component, we permute the x' , y' from the coefficients relative to the B_x component.

$$a_{nm} = \frac{1}{\sqrt{x'^2 + y'^2 + z'^2}^{n+2}} \epsilon_m \frac{(n-m+1)!}{(n+m)!} \times -(x_2 - x_1) \cos [m \arctan(x', y')] \\ P_{n+1m}\left[\frac{z'}{\sqrt{x'^2 + y'^2 + z'^2}}\right]$$

$$b_{nm} = \frac{1}{\sqrt{x'^2 + y'^2 + z'^2}^{n+2}} \epsilon_m \frac{(n-m+1)!}{(n+m)!} \times -(x_2 - x_1) \sin [m \arctan(x', y')] \\ P_{n+1m}\left[\frac{z'}{\sqrt{x'^2 + y'^2 + z'^2}}\right]$$

with $x' = x_1 + (x_2 - x_1) \times t$, $y' = y_1 + (y_2 - y_1) \times t$ and $z' = cste$.

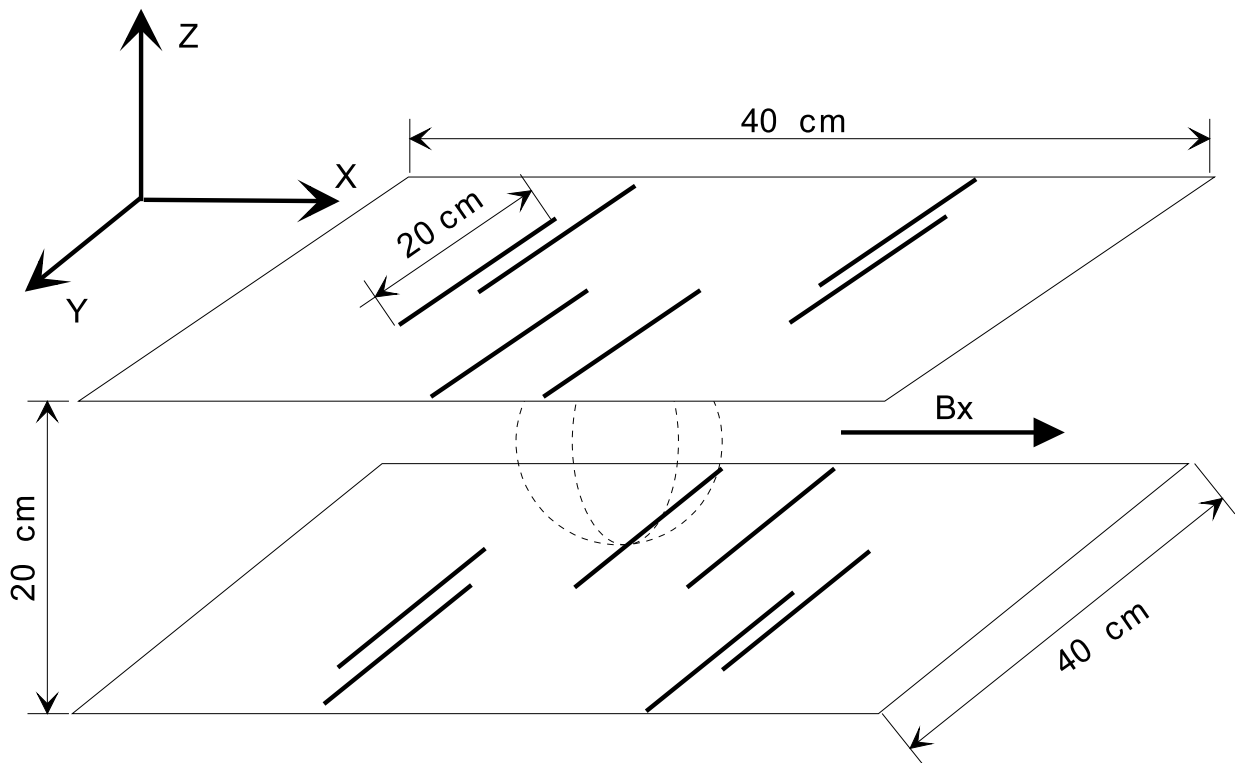


Figure 5.1: Generation of a B_x field profile (the sphere of radius 5cm indicates the area of interest).

5.2 Uniform field generator

We are going to compute a uniform B_x field configuration in a sphere of 10cm diameter. This case is interesting from a numerical point of view, because the values of the coordinates of the table 5.1 cancel perfectly all the coefficients up to order 5 included. For this reason we have kept a very high precision for the values of the table. However this case is only of theoretical interest because the dimension of the plates in the y direction is important.

In the case of a very homogeneous field as shown in the field map Fig(5.2), we always obtained this configuration with a current ratio of 4. We cannot conclude on the uniqueness of this solution, but after several tests, we did not find other configurations. The ratio of 4 is a condition we imposed, the system already finding a solution from a current ratio of 3.2. However, it is simpler to have whole ratios in order to make turns with the same current, so we chose the value 4. Higher values work but the size of the plates becomes prohibitive, because the outer conductors must be kept away from the central area.

Analyzing the Figure (5.3) and the coordinates of the table 5.1, the configuration is relatively astonishing because there is no axial symmetry. There is simply a point symmetry at the origin between the two plates. There are also conductors placed outside carrying important currents compared to those in the center. If we ask the system to find a position with a lower current ratio, the coefficient $a_{20} = -r^2/2 + z^2$ cannot be cancelled. Referring to the study of correction by a cage of permanent magnets, this coefficient was already proving to be crucial for the realization of the correction system. This coefficient expresses the lack of uniformly distributed sources around the area of interest. Remember that inside a sphere of magnetized material, for example, the field is perfectly uniform. But for the sake of accessibility we cannot place sources all around the useful area. How then can we simulate the uniform distribution of charges that can only be distributed on two parallel planes? The system has chosen to increase the distance of the outer wires from the origin, and therefore the angle of incidence of these conductors becomes smaller. However, the wire must carry a higher current in order to simulate a nearby wire, virtually placed between the two planes. This behaviour is preponderant, and keeping it in mind allows us to develop initial configurations more quickly. From the point of view of feasibility, we must therefore seek to distribute the sources uniformly around the area and when this is not possible, simulate the missing sources by other sources that are stronger because they are further away. Each of them will be positioned at the θ and ϕ angles of the replaced source and at a mechanically permissible

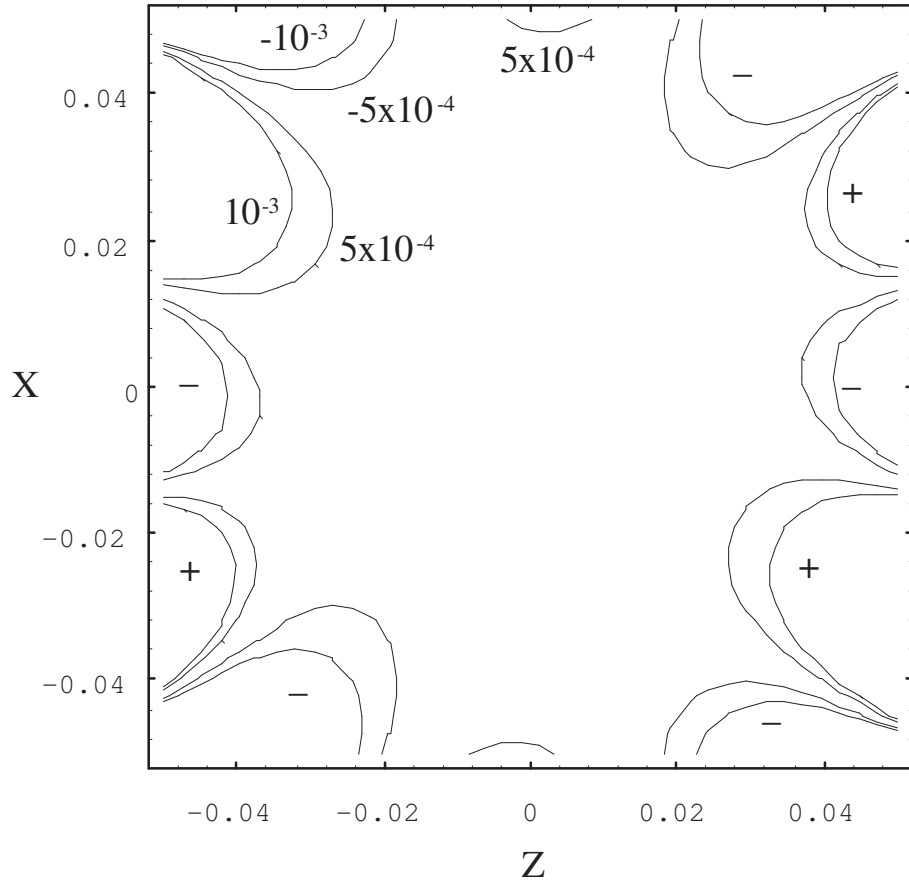


Figure 5.2: Homogeneity of the B_x field. Relative error with respect to the central field.

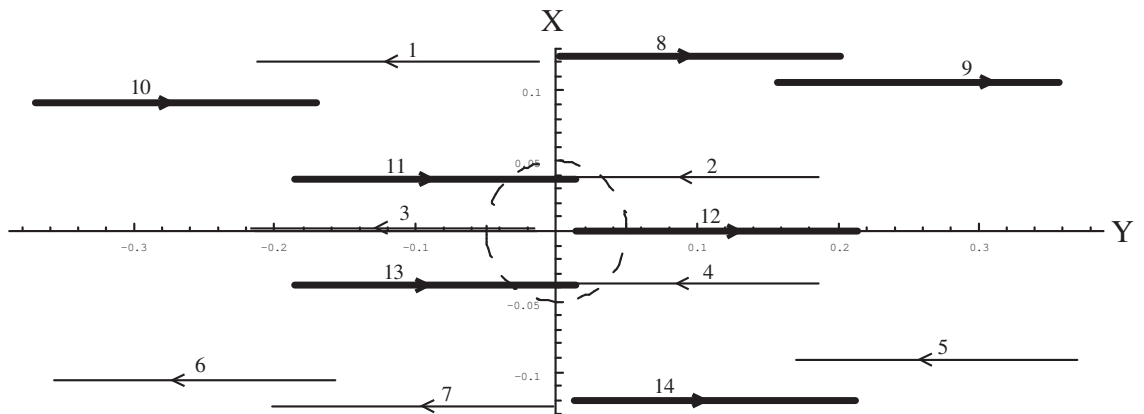


Figure 5.3: Top view of the upper and lower plates. B_x directed upwards and homogeneous up to and including order 5.

distance.

ref	plane ($z=\pm 0.1\text{m}$)	x (m)	y (m)	relative current
1	down	0.120873	-0.211988	4
2	down	0.0387396	-0.0140289	1
3	down	0.	-0.213914	1
4	down	-0.0376243	-0.0137464	1
5	down	0.091118	0.169644	4
6	down	-0.105396	-0.357483	4
7	down	-0.124105	-0.202016	4
8	up	0.124105	0.00201545	-4
9	up	0.105396	0.157481	-4
10	up	0.0911151	-0.369644	-4
11	up	0.0376243	-0.186254	-1
12	up	0.	0.0139139	-1
13	up	-0.0387396	-0.185971	-1
14	up	-0.120873	0.0119882	-4

Table 5.1: Wire position and intensity for an homogeneous B_x

5.3 Field gradient generation $\frac{\partial B_x}{\partial x}$

We will now study a series of gradients, the first of which will be along the \vec{x} axis. These configurations are proving harder to find for a reason that we have been able to elucidate. The calculation consists of cancelling all coefficients except A_{11} . However, the program cannot undo the coefficient $a_{31} = 3x(-r^2/2 + 2z^2)$. However, we have already encountered this difficulty with the coefficient A_{20} for homogeneous fields. It is the same problem because we can recognize a form of the type $a_{31} \sim xa_{20}$ knowing that the coefficient x cannot cancel because it is the value of the gradient. It is thus the second term very close by its form to a_{20} but with a coefficient 2 applied to z^2 . The problem of the lack of sources placed around the useful area becomes even more troublesome. We have not been able to completely cancel this coefficient with current ratios below 6, which is already very detrimental to the energy efficiency of the system².

The following configuration is determined for external wires carrying twice as much current. As we will see, this is not sufficient to make up for the lack

²Given the strong currents they're carrying, they're moving away from the area.

of current at the periphery of the useful zone.

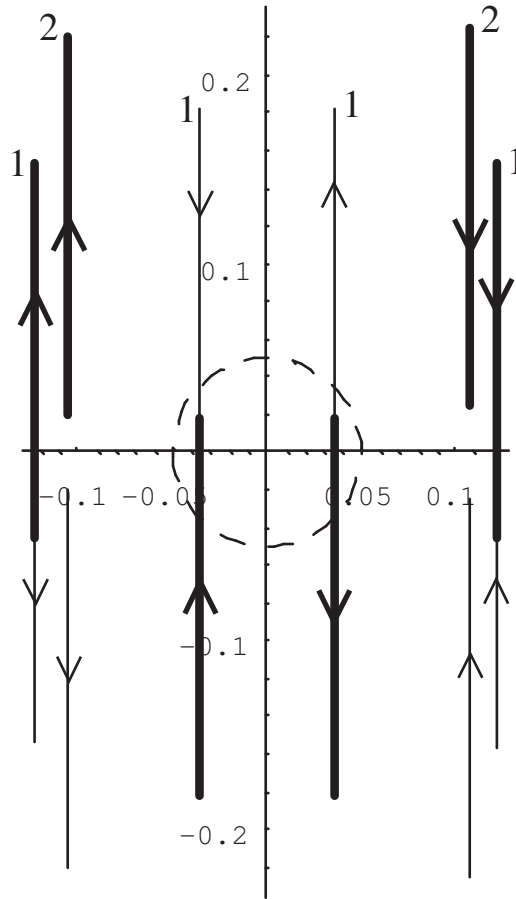


Figure 5.4: Field gradient configuration (II) $\frac{\partial B_x}{\partial x}$

The field map (5.5) clearly shows that the external conductors should carry a higher current. After trying with a current ratio of 3 and obtaining unsatisfactory results, the configuration Fig(5.6) very clearly improves the linearity of the gradient. However, the first configuration can be retained if an energy constraint exists while accepting a gradient of this precision.

The software provided the solution Figure (5.6). The coordinates on the \vec{y} axis are strictly zero, but for the sake of clarity we have slightly moved the wires away from the axis. It is obvious that at the realization the symmetrical wires with respect to the \vec{y} axis will be joined. We can then isolate 3 parameters on the 36 starting variables, the internal conductors at $x = \pm 0.038m$ and the external conductors at $x = \pm 0.1159m$ carrying a current 4 times more important.

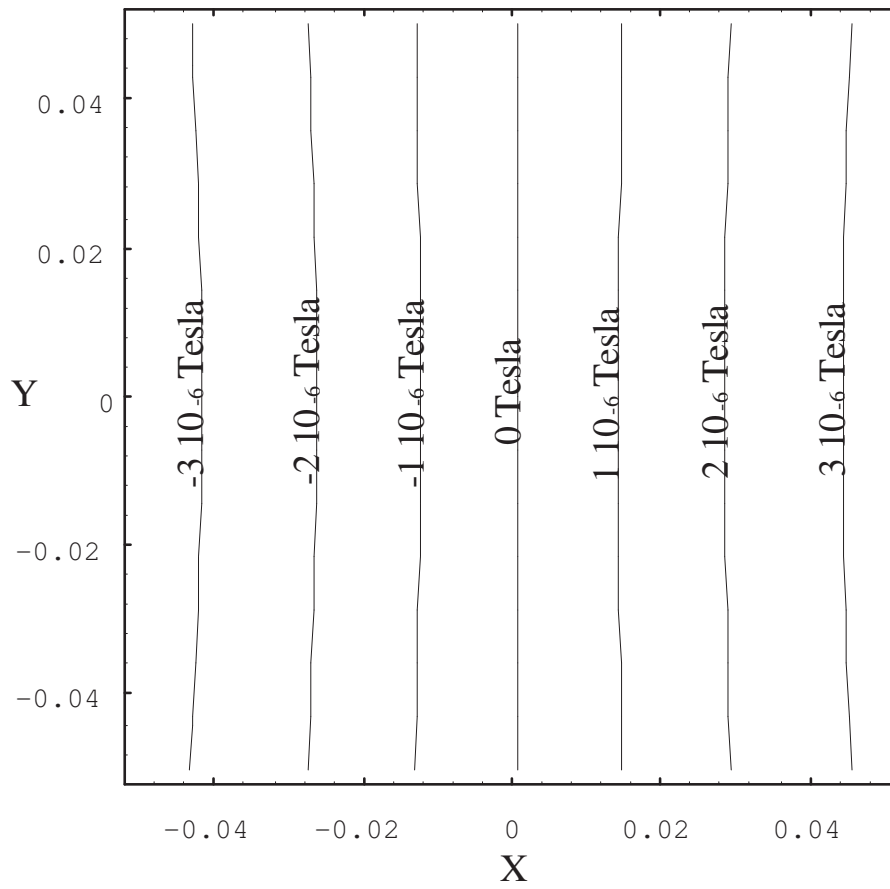


Figure 5.5: Plot (II) of the gradient $\frac{\partial B_x}{\partial x}$ for a current of 1 A. Obvious problem of a lack of current in the corners of the figure.

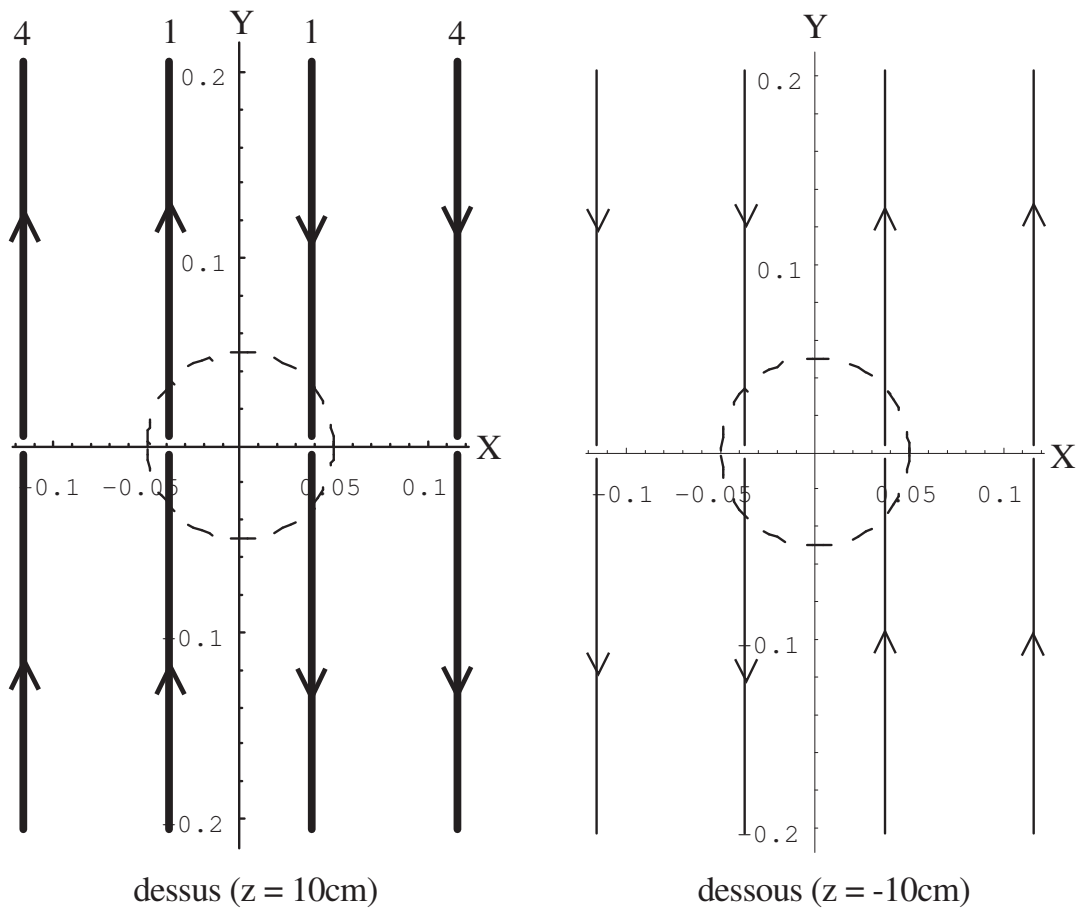


Figure 5.6: Field gradient configuration $\frac{\partial B_x}{\partial x}$

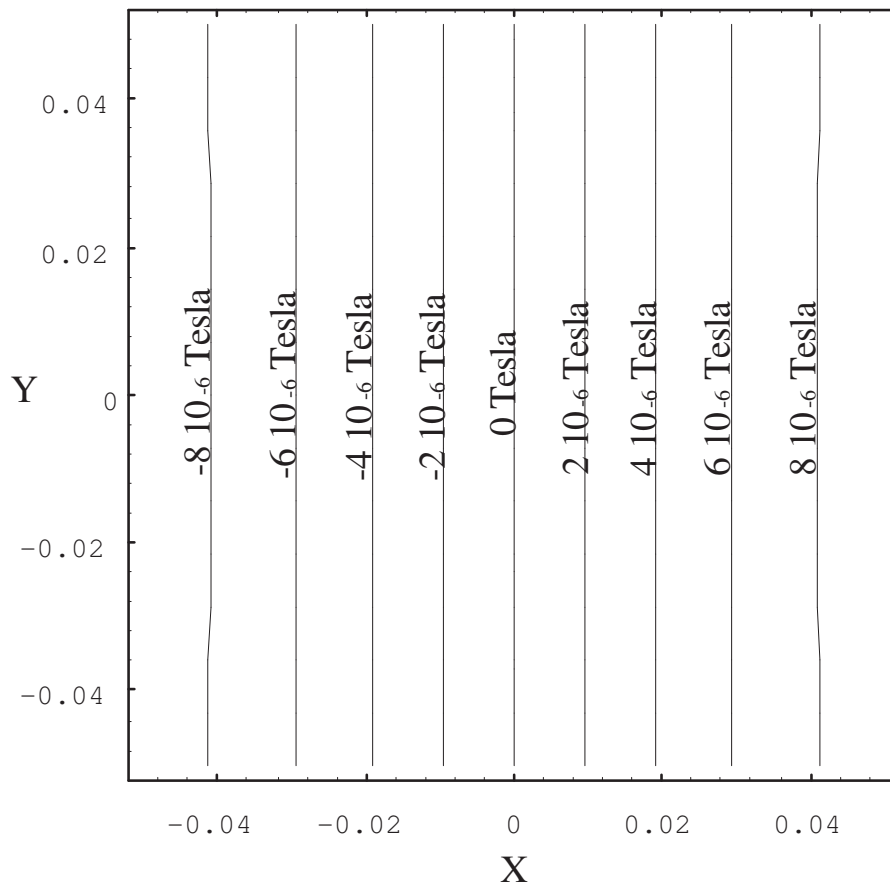


Figure 5.7: Gradient plot $\frac{\partial B_x}{\partial x} = 17 \cdot 10^{-5} \text{Tesla}/m$ for a current of 1 A.

ref	plane ($z=\pm 0.1\text{m}$)	x (m)	y (m)	relative current
1	down	-0.123	-0.154	-1
2	down	-0.105	-0.22	-2
3	down	-0.036	-0.018	-1
4	down	0.036	-0.018	1
5	down	0.105	-0.22	2
6	down	0.123	-0.154	1
7	up	-0.123	-0.046	1
8	up	-0.105	0.02	2
9	up	-0.036	-0.182	1
10	up	0.036	-0.182	-1
11	up	0.105	0.02	-2
12	up	0.123	-0.046	-1

Table 5.2: Wire position and intensity for configuration Fig(5.4)

5.4 Generation of a field gradient $\frac{\partial B_x}{\partial y}$

As in the previous examples, the coefficient $b_{31} = 3y(-r^2/2 + 2z^2)$ will be difficult to undo. It represents the lack of sources placed in the preferred y direction and away from the center³. However, we refused to increase the dimensions of the plates in order to respect a minimum space requirement. Considering that the program can give one end of a conductor at 10cm, you have to add 20cm of wire length following \vec{y} . Since the configurations are always symmetrical in the direction of the gradient, the total dimension of the plate along the \vec{y} axis can reach 60cm.

To illustrate the problem of the lack of sources following the y direction, the configuration Fig(5.8) is a solution generating the coefficients $B_{11} = 12 \cdot 10^{-5}$ and $B_{31} = 5 \cdot 10^{-4}$. The other 34 coefficients are cancelled.

The Figure field map (5.9) clearly shows a barrel shape of the gradient in the y direction. To decrease the phenomenon, we can add lines of currents in this area. Practically, we will try to decrease the current in the center and increase it towards the edges. In the Fig(5.10) configuration, eight conductors have been added, each carrying a unit current. The gradient profile is clearly improved. However, the software has not found any configuration that strictly cancels the 35 coefficients. The Figure (5.10) is very close to

³This is the same for the coefficient a_{31} , with the sources coming mainly in the x direction and away from the center.

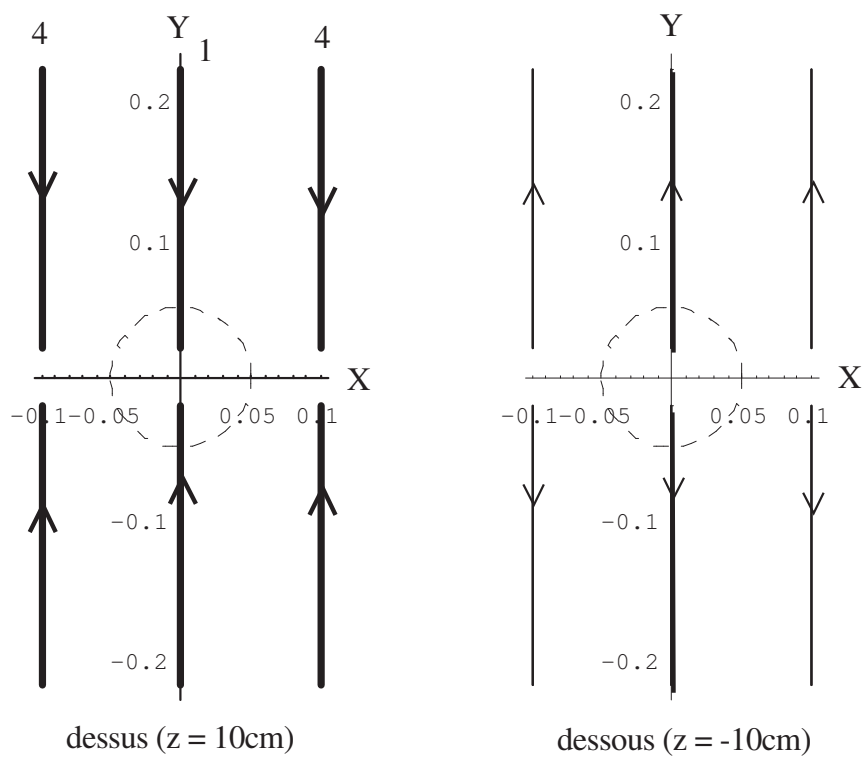


Figure 5.8: Gradient configuration (I) $\frac{\partial B_x}{\partial y}$. The coefficient B_{31} is not cancelled.

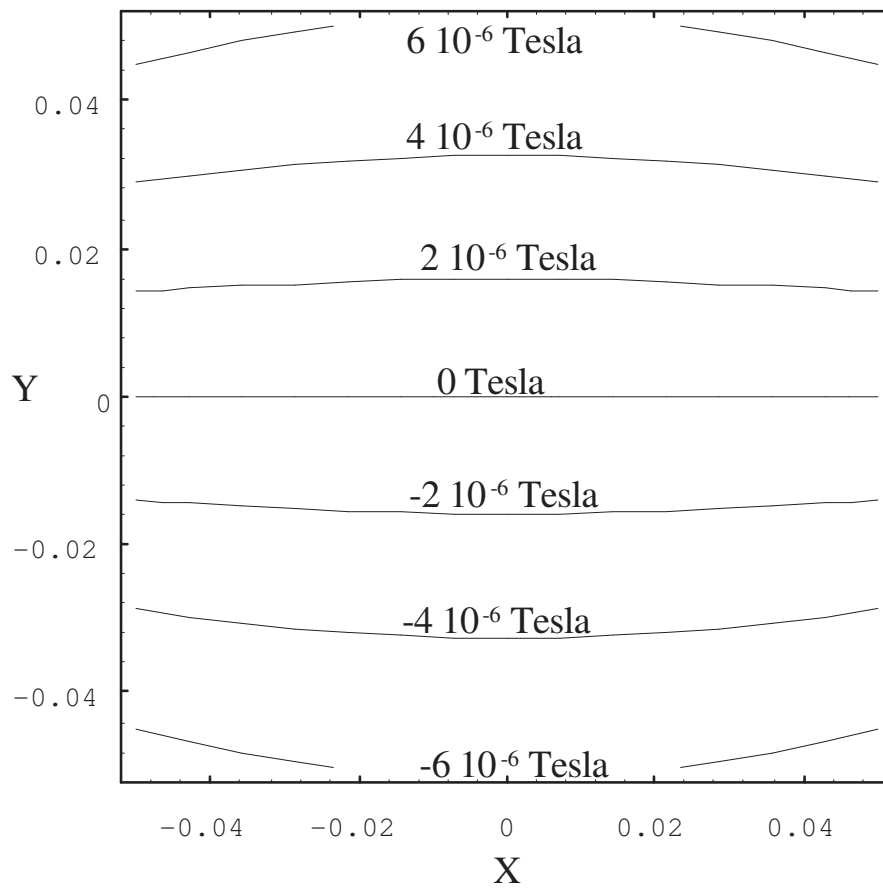


Figure 5.9: Plot (I) of the uncompensated gradient $\frac{\partial B_x}{\partial y}$ for a current of 1 A. $B_{31} \neq 0$, which explains this barrel-shaped defect.

the gradient $\frac{\partial B_x}{\partial x}$. The direction of the currents are simply modified and the conductors placed at $x = 0$ are added.

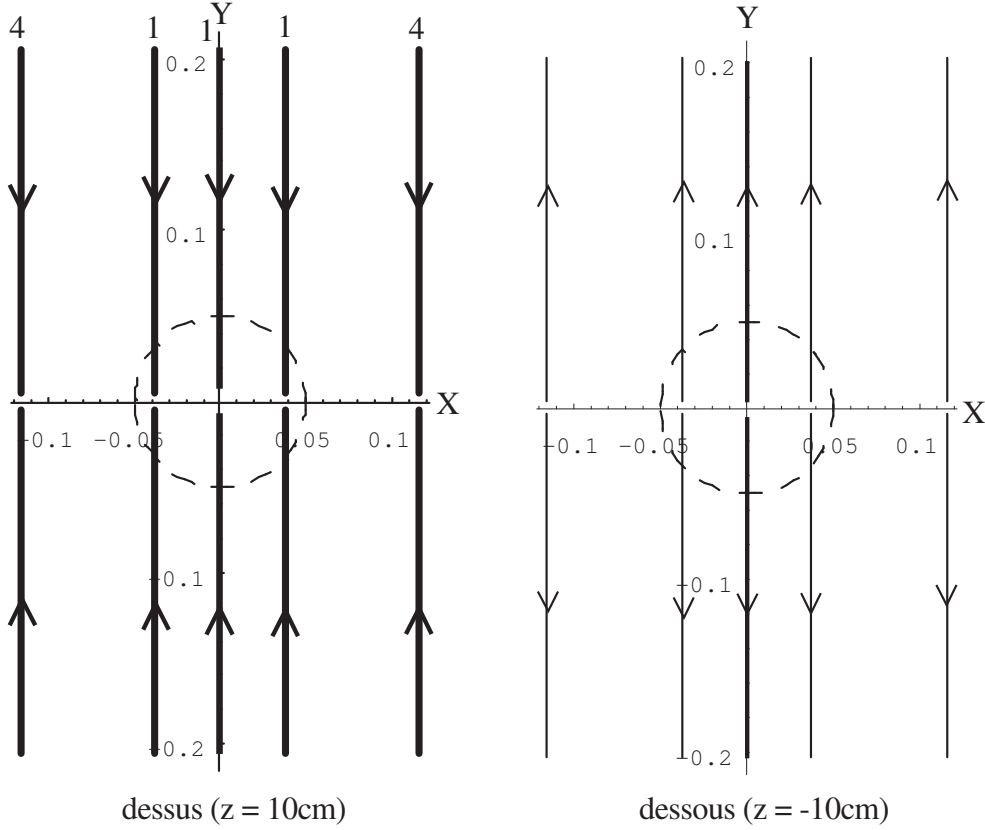


Figure 5.10: Gradient configuration (II) $\frac{\partial B_x}{\partial y}$

5.5 Field gradient generation $\frac{\partial B_x}{\partial z}$

Numerically, the search for this configuration posed no problem. The coefficient $a_{30} \sim za_{20}$ is easier to undo than a_{20} in the case of the homogeneous field due to the factor 3 applied to the term in r^2 . It is therefore not necessary to increase the current density at the periphery of the plate. However, it seems that the number of wires cannot be decreased, therefore the number of degrees of freedom is equal to the number of equations. The linearity of the gradient is excellent because the residual error made on the cancellation of the coefficients is less than 10^{-12} .

This gradient can be considered as a reference and we can see its quality on the field map.

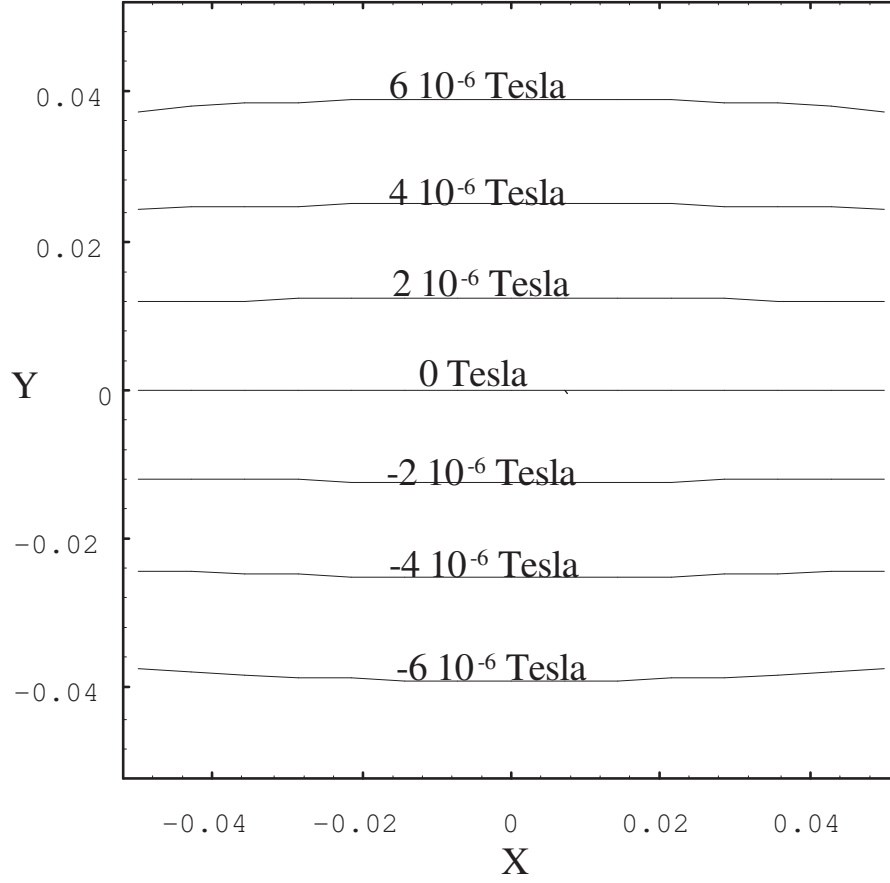


Figure 5.11: Plot (II) of the $\frac{\partial B_x}{\partial y}$ gradient for a current of 1 A. Even after compensation, this is the hardest gradient to get.

ref	plane ($z=\pm 0.1\text{m}$)	x (m)	y (m)	relative intensity
1/12	up/down	2.327160e-02	-2.162440e-01	1
2/15	up/down	1.028740e-03	-1.020940e-02	1
3/14	up/down	1.025250e-01	3.133280e-02	1
4/18	up/down	7.939740e-02	-1.931820e-01	1
5/16	up/down	-1.035660e-01	-1.312850e-02	1
6/13	up/down	-3.520900e-02	-2.014650e-01	1
7/10	up/down	6.240620e-02	-1.876790e-02	1
8/17	up/down	-9.102770e-02	-2.062440e-01	1
9/11	up/down	-6.046200e-02	2.825180e-03	1

Table 5.3: Wires position for gradient $\frac{\partial B_x}{\partial z}$.

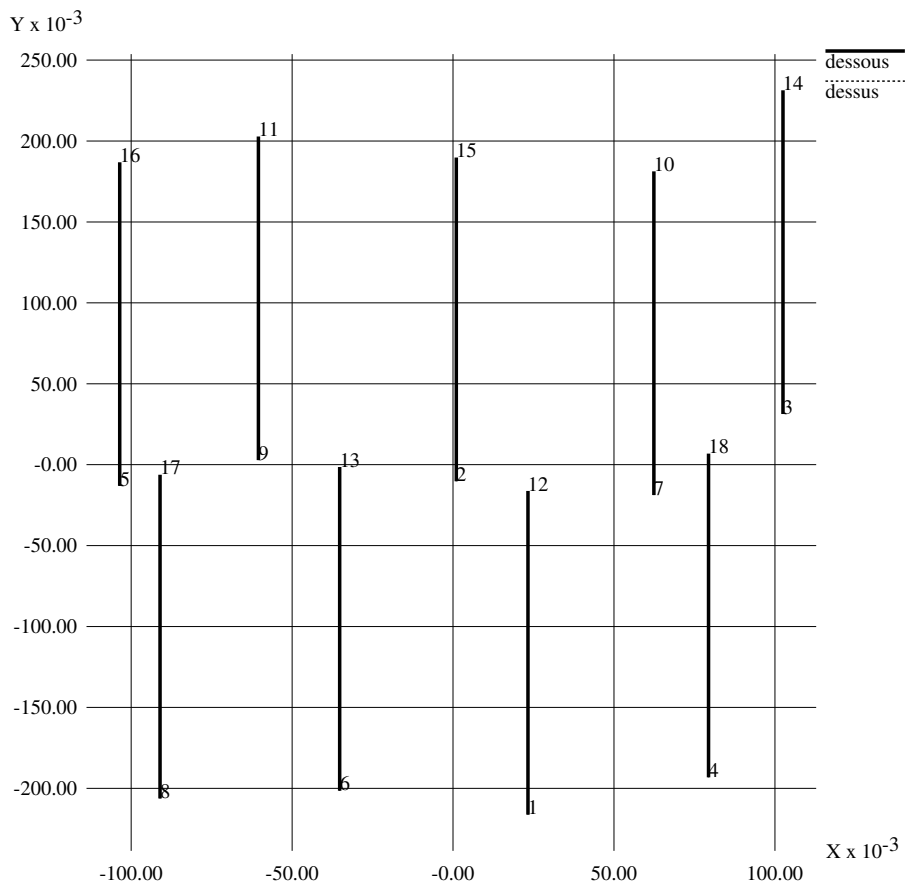


Figure 5.12: Gradient configuration $\frac{\partial B_x}{\partial z}$. The top and bottom wires are perfectly superimposed and the currents are in the same direction. The gradient is $8 \cdot 10^{-5}$ Tesla/m for a current of 1 A.

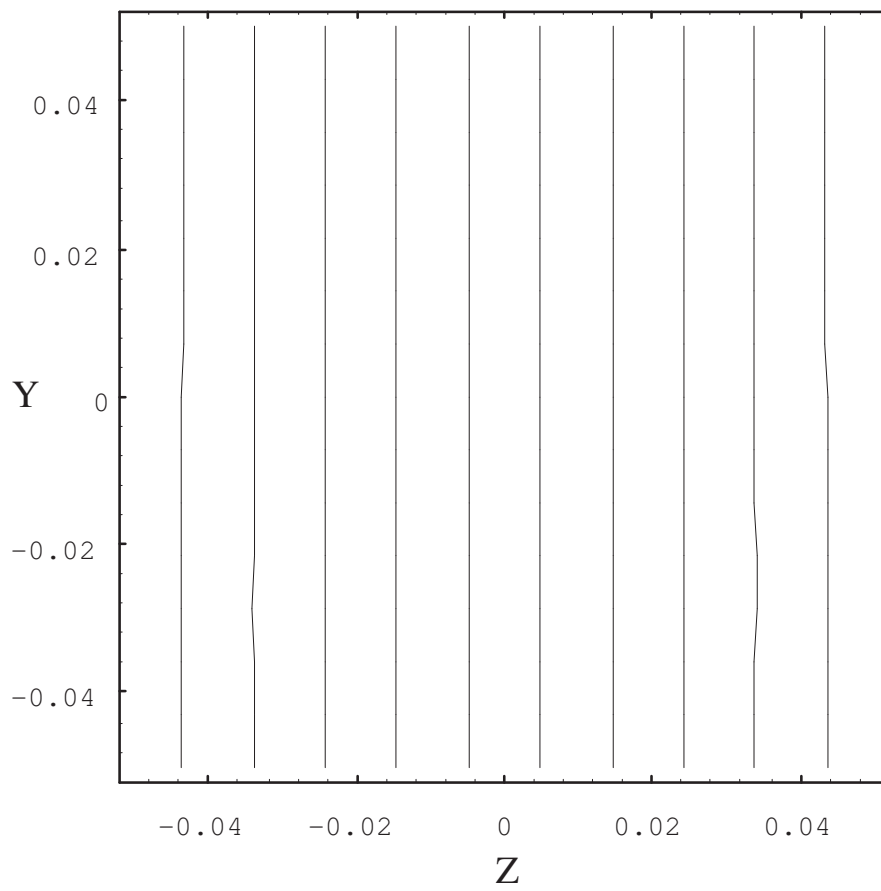


Figure 5.13: Gradient plot $\frac{\partial B_x}{\partial z}$ for a current of 1 A. The possible defects on the figure are due to the printing format. The linearity is in this case particularly good.

5.6 Return arcs

Return arcs do not pose any difficulties from a numerical point of view, but they substantially increase the dimensions of the generators and the inductance of the system. In any case, they are annoying.

In order to demonstrate the possibility of generating field profiles from straight line segments, we have considered a single straight conductor. The evaluation of the contribution of the return arc is nevertheless necessary as the current lines are closed. It is always possible to move the return arc away infinitely and neglect its effect, but in this case the inductance of the circuit increases. On the other hand, if the return arc is too close to the area of interest, the energy efficiency of the system may be degraded.

The initial program does not calculate the contributions of the return arcs because according to the profiles (see the gradient $\frac{\partial B_x}{\partial x}$), we can connect symmetrical and opposite current direction wires together. Rather, it is during a particular study that it will be necessary to add them or not.

To illustrate the feasibility of calculating return arcs, we have chosen to integrate them into the gradient configuration. $\frac{\partial B_x}{\partial z}$. On the one hand they are mechanically necessary because the currents are all in the same direction. On the other hand this configuration is very precise, so it's easy to compare the contribution of the arcs.

At first we added the return arcs without modifying the position of the conductors. It appears that the error committed on the profile is of the order of 1%. However this is not checked on all the profiles because the error of the homogeneous field becomes completely false. On the other hand to respect the very high precision of the profiles, we recalculated a new configuration taking into account the return arcs.

We have formed rectangular turns, while keeping the outer edge along the \vec{x} at $\pm 20cm$. This arbitrary value was chosen because, in this way, the plates are roughly square. In the Figure (5.14), we have only mentioned a few return arcs for the sake of clarity. The value of the gradient is 8.10^{-5} Tesla/m for a current of 1 A and the other coefficients are perfectly cancelled out, so we can refer to the previous field map Figure (5.13). The return arcs move along the ordinate corresponding to their active arc. We can thus underline the fact that we do not have additional variables because the return arcs are an integral part of the active arc since we have voluntarily decided to freeze the abscissa.

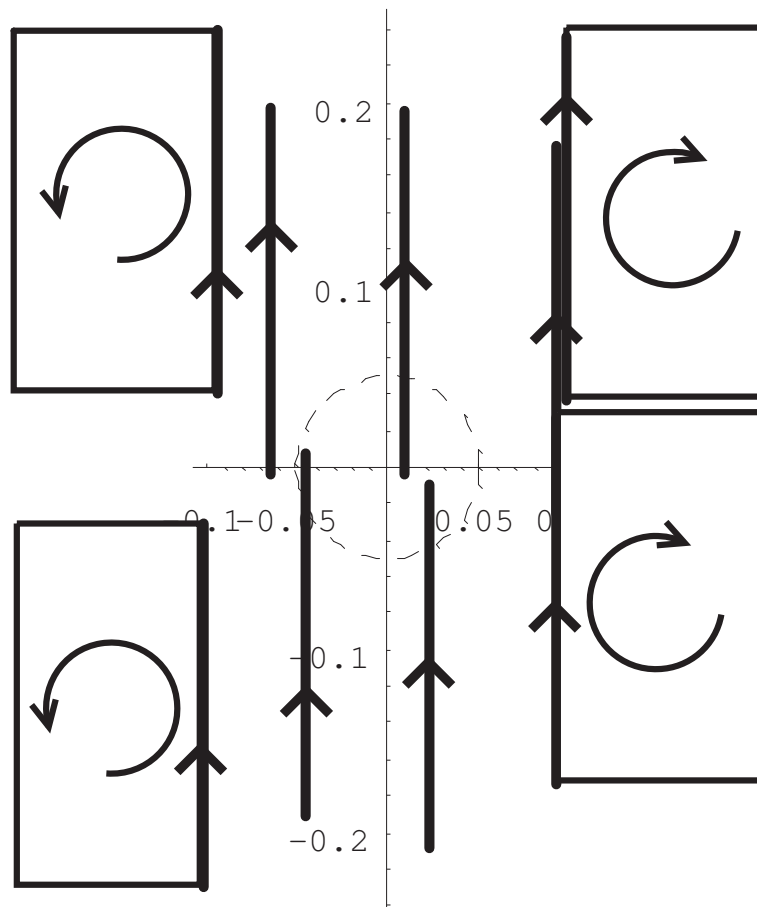


Figure 5.14: Gradient configuration $\frac{\partial B_x}{\partial z}$ with return arcs (only some are shown).

plane ($z=\pm 0.1\text{m}$)	x (m)	y (m)	relative intensity
up/down	2.181870e-02	-2.095720e-01	1
up/down	8.933420e-03	-4.407990e-03	1
up/down	9.891050e-02	3.627250e-02	1
up/down	9.164390e-02	-1.735700e-01	1
up/down	-9.325290e-02	3.971330e-02	1
up/down	-4.403900e-02	-1.918690e-01	1
up/down	9.319660e-02	-2.408020e-02	1
up/down	-1.015300e-01	-2.298690e-01	1
up/down	-6.335610e-02	-3.737180e-03	1

Table 5.4: Wire position for a gradient $\frac{\partial B_x}{\partial z}$ with return arcs.

5.7 Generation of a sinusoidal field

To prove the versatility of the method, it is interesting to study less standard profiles. Following the 4 previous configurations, we will create a field whose variation will be sinusoidal along the \vec{x} axis and if possible homogeneous along the different planes YZ . This profile is often found in travelling wave tubes and free electron lasers. The spatial period then determines the frequency of the emitted wave. In our case, we have chosen a spatial period equal to 20cm (= at the distance between plates). The software has provided the configuration Fig(5.15), the currents are all unitary. We can notice that there are no return arcs since we can connect the symmetrical and opposite current wires.

Theoretically, we cannot control the profile of a field outside the sphere of radius 5cm (half the radius of the generators). However, we have been able to extend the zone along the \vec{x} axis up to $\pm 10\text{cm}$. Harmonics greater than 5 remain weak if we do not approach the wires. However, along the \vec{y} and \vec{z} axes, the constraints remain identical to the previous configurations. The useful zone is therefore approximately cylindrical.

It appears on this example that the coefficient A_{33} cannot be perfectly mastered just like the coefficient A_{20} for the realization of the homogeneous field. This is identified by the slight curve along the \vec{y} axis at $x = \pm 10\text{cm}$, Figure(5.16). This case is certainly more intended for Bessel functions. As this is a spatial sinusoidal field with a priori several periods on concrete examples, it is preferable to control the quality of the field over the whole area rather than moving the error from the center to the edges.

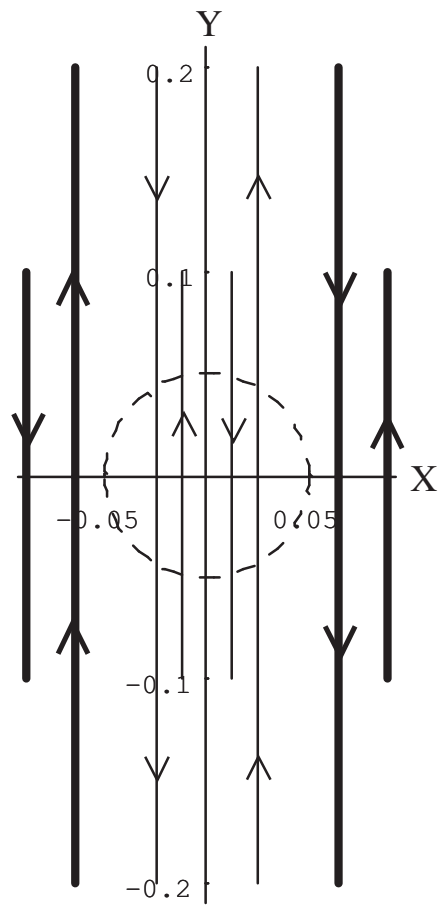


Figure 5.15: Configuration for a sinusoidal field.

plane ($z=\pm 0.1\text{m}$)	x (m)	y (m)	relative intensity
down	0.025	0.	1
down	-0.025	0.	-1
down	0.025	-0.2	1
down	-0.025	-0.2	-1
down	-0.0116	-0.1	1
down	0.0116	-0.1	-1
up	0.0883	-0.1	1
up	-0.0883	-0.1	-1
up	-0.0639	-0.2	1
up	0.0639	-0.2	-1
up	-0.0639	0.	1
up	0.0639	0.	-1

Table 5.5: Position of the wires for a sinusoidal field. Return arcs are not necessary due to the symmetry and direction of the currents.

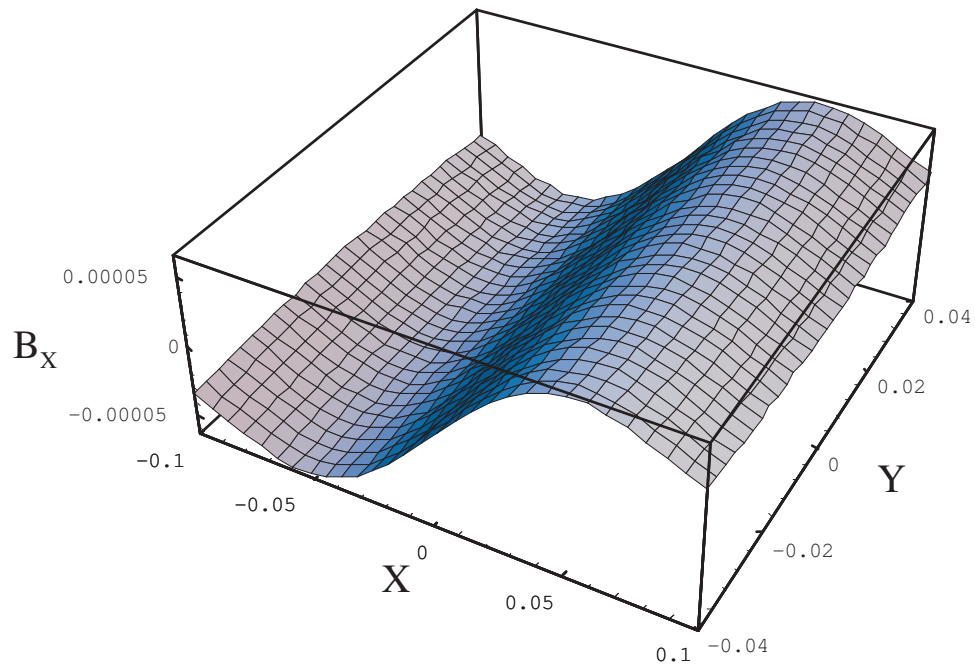


Figure 5.16: Sinusoidal field plot for a current of 100 A.

Chapter 6

Experimentation

In order to prove the validity of the field generation method, we have experimented with some field configurations. It is mainly a question of checking the direct field calculations and their accuracy, because the inverse method cannot be questioned. The only error of the inverse calculation as we have presented it is to provide no result if the physical arrangement does not allow to realize the requested field. If the result is given, it is particularly simple to check the direct chain. The behavior is almost binary, the solution exists or not and in the last case what are the compromises to be made. However, for the mechanical aspect, it is interesting to evaluate the positional tolerances. If, for example, a tolerance in the micron range is required, this correction (or generation) system will be more difficult to achieve.

6.1 Measuring environment

Chronologically, we have verified the field generation by conductors, as this turns out to be experimentally very simple. Obviously, we have chosen two non-conductive and non-magnetic plates (wood) spaced 20cm apart and brass screws. The presence of the latter is not annoying in static calculations, but in the case of field switching, the eddy currents in the body of the screws are no longer negligible. We pointed out in the introduction that the magnetic or ferromagnetic environment was the most delicate point, so we chose a location for the measurements with a high homogeneity of the Earth's field and placed the probe perpendicular to this field. After moving the probe in a 10x10x10cm cube and checking that the variation did not exceed the mG, we measured the field generated by our configurations.

To set a few orders of magnitude, the Earth's field strength is approxi-

mately 450mG. The perpendicularity of the probe is therefore critical. Moving a car 50 meters from the zone generates a variation of 0.1mG. A set of keys placed at 1 meter produces a variation of 5mG and a small correction magnet produces the same variation at 40cm. In Paris and as of October 1, 1997, the Earth's magnetic field has as components 210.59mG North, -8.45mG East, 422.44mG vertical and the annual variation is 0.4mG (according to the National Geophysical Center Boulder, Colorado USA). If we analyse these values, the largest field value is in the vertical direction. We have encountered the following mechanical problem: the Hall probe at the end of an arm does not remain perpendicular to the Earth's vertical field, because depending on the position of the probe, the mechanical deflection varies and leads to a variation of 5mG. A more robust measurement setup is therefore required.

6.2 Gradient measurement a_{11} version I

The coefficient a_{11} represents the gradient $\frac{\partial B_x}{\partial x}$. We applied a current of 350 mA so that the wire would not heat up. Since the ohmic resistance of copper varies with temperature, we recorded a field drift using a stabilized voltage supply and a high current. This is not inconvenient with the use of a stabilized power supply, but we do not have one available for currents below one ampere. We have therefore chosen to limit the joule effect.

We think we have respected a positional tolerance of about 1 mm. We have also moved the threads by playing on their elasticity and we have not recorded any significant variation. This is therefore a reassuring statement about the feasibility of the system in accordance with the numerical calculation of the positional tolerance estimated at $\pm 1mm$.

We therefore measured a gradient corresponding to the chosen characteristics, but there are still some measurement errors of the order of mG, mainly due to magnetic pollution. The homogeneity along the other axes is excellent, the gaussmeter did not provide us with any significant deviation. The measured inductance is $13\mu H$ for a gradient value of 677mG/m/A. The dimensions of the system are given on page 71.

6.3 Gradient measurement a_{11} version II

The ratio of the external to internal currents is 4, so we can expect an increase in inductance compared to the first gradient (ratio of 2), however

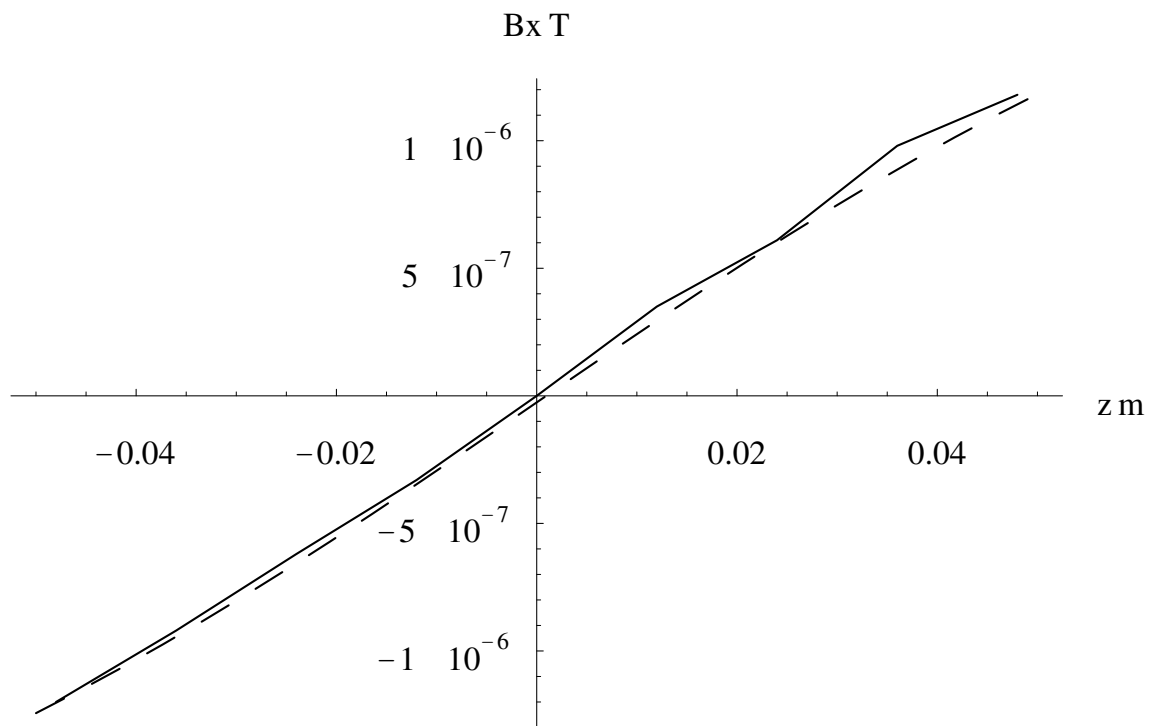


Figure 6.1: Actual and theoretical dotted gradient curve a_{11} version I. Errors are due to the imperfect rigidity of the measuring system. Homogeneity along the other axes is excellent.

the efficiency will also increase. We will analyse more closely the advantages and disadvantages of these two structures.

This gradient has been measured and we noticed its very high linearity. We were unable to detect the slightest defect compared to the theoretical curves. It is therefore a gradient that deserves to be retained for future applications.

We have measured an inductance of $48\mu H$ for a gradient value of 1710mG/m/A , which is very interesting because the inductance is low. To compare with the first gradient configuration a_{11} , the gradient II is 2.5 times higher. So we have to at least double the first configuration to get the same field value, the inductance will then increase¹ at the minimum of n and at the maximum of n^2 .

6.4 Magnet cage validation

We first measured the value of the remanent field of each magnet according to the conditions cited on page 19. Then we compared a field map generated by the magnet cage and its theoretical model. The differences found are in agreement with the necessary precision. The direct calculation is therefore sufficient proof when validating a configuration found by the inverse calculation. We remind that in the case of the cage, the direct calculation is not expensive because it is based on formulas in arctan and in the case of wire sections, the calculation is derived from Biot and Savart's law and is fully analytical.

We have made two configurations, the first where all the magnets are in the same direction and placed at $z = 0$ and the second where every other magnet is reversed. As the number of magnets is odd, and given the disparity in remanent field values, on the \vec{z} axis, we must find a shape equivalent to a single magnet placed at $z = 0$. The first configuration gives a central field strength of 2.2 Gauss, so the Earth's field is not disturbing in the case of a perpendicularity defect of the probe. On the other hand, the second configuration is more difficult to measure because the value of the central field is 50mG. We then see in the Figure (6.2) a defect in the positioning of the probe at $z = 0.05m$.

¹This consideration is empirical, the calculation of inductances is always very difficult to perform. However if we double a structure, the inductance will be at least multiplied by two because the flow is twice as strong. But at the maximum it will reach a factor of 4, the coupling between turns is not equal to unity because each turn sees only a part of the flow of the other turns.

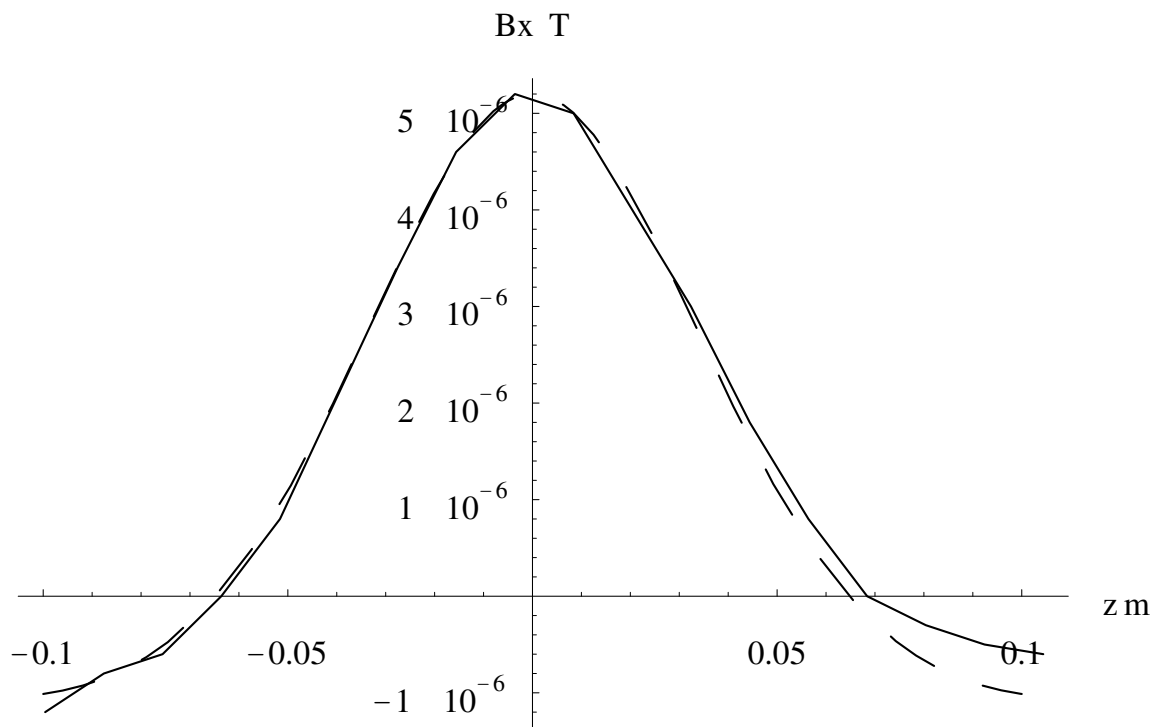


Figure 6.2: Physical and theoretical dotted curve of the magnet cage. The measurement errors are of the same type as those seen on the gradients, the low rigidity of the measuring system is certainly to blame.

Conclusion

We have presented an alternative using Bessel functions, and there is also an approximate method, the use of Fourier-Bessel development of the magnetic field. For a given field profile, it is a question of finding a surface current distribution carried by a cylinder or a plane[46]. On this principle, the publications[53][7][47] show achievements in gradients, homogeneous field generators, etc...

For the purpose of comparison the article[32] shows a series of gradients and isovalent profiles (supposed to represent a sequence of parallel lines in the case of gradients). In addition to the complexity of the current lines, we have gained a factor of 100 in gradient accuracy for a lower inductance than the one presented in the article, so we have not found any drawback to our structure.

we pointed out at the beginning of the paper, it is a matter of choosing the location of the error. Methods derived from Taylor series development are very precise at the center but if the truncation of the series is at n , the error is in r^{n+1} . Deviating from the center, the error suddenly becomes very large. On the other hand, articles using Fourier-Bessel functions provide a larger useful area but the error is larger in this region.

The concept of a current density seems to us to be rather risky in the case of precise profiles, because at the time of realization, it is necessary to approximate this density by a series of wires. If the sampling step is small, the precision will be higher but the number of wires will also be higher. The inductance can then reach prohibitive values. The reverse approach is not precise. As it happens, articles using this technique are faced with the problem of sampling and apodization[32][8].

There are also very interesting methods based on neural networks and genetic algorithms. The application to the inverse calculation of electromagnetic fields is justified in view of the complexity of the inversions. These two methods are essentially generic. On problems deemed to be insolvent, these techniques have given very good results.

behaviour of their natural counterparts. After a sometimes very long learning process, the connections (e.g. synapses) are calibrated in the form of coefficient calculations. These more or less modulate the signal from the previous neuron to the next neuron. The simulation of logic functions, however complex they may be, are trivial neural network problems. Once the network is calibrated, the calculation time of a response is very fast, hence its growing usefulness in the real time domain.

The article[3] proposes to teach the neural network where to place sources according to the field they generate. The training is simple, we choose a large number of randomly chosen source positions in space and we provide by an direct calculation of the magnetic field corresponding to the neural network. Therefore, during the learning phase, at the input of the network, the characteristics of the field are provided and at the output the position of the sources. A classical algorithm used for the calculation of the synaptic coefficients is the error backpropagation. After initialization, the extraordinary fact is that the network is able to give an approximately coherent source position even if the entered field is not in the learning domain. This is the main interest of inverse problems, other applications rather exploit the learning memory function. Even if the accuracy is currently nothing like the one needed for our applications, it is a very promising method.

Genetic algorithms, on the other hand, work very differently. They are used in complete NP problems, i.e. combinatorial explosion problems. If the search space is absolutely gigantic, like the exhaustive search of all valid positions of the chess game (greater than the number of particles in the universe), they find their interest by selecting very quickly the locally winning combinations. As Nature operates a selection of viable DNA helices, the algorithms have at their disposal the possibility to multiply, destroy or mutate the most significant combinations of the problem. They perform these operations with a given probability.

In field synthesis, we have a probability criterion stated on page 48 concerning the search for positions that are statistically closer and closer to the solution. We have chosen a purely numerical method in order to considerably reduce the number of random vectors. But it is also possible to make this choice among this space using genetic algorithms. It is still a method that lets the computer search alone for a solution based on a local law. This can be in the case of the magnet cage, the choice of the magnets to be moved at step n . Then depending on the best configurations, this law can cross the positions (cross-over). However, we have doubts about the efficiency of the method in this particular case, because by moving a single magnet all the other positions have to be retouched. It is therefore a strongly coupled

problem. It appears that mixing two parts of the two most significant configurations has no chance of giving a more efficient configuration. On the other hand, weakly coupled problems give very good results.

The use of Legendre polynomial potential development is well suited if a high accuracy of a spatially limited profile is required. The use of Legendre polynomial potential development is well suited if high accuracy is required from a space-limited profile. However, it is imperative to use a powerful root search algorithm. In order to correctly understand the chosen inversion method, we have explained how to solve a simple problem in two and three dimensions, which allows the graphical representation of the equations.

First, we created a fictitious field from generators and then we inverted the problem. Knowing that at least one solution exists, the algorithm was refined until we obtained a solution in a reasonable calculation time. We noticed that the number of solutions is very limited or even unitary because we always found the initial position of the generators and only this one. Uniqueness is further demonstrated[35]. If a field is defined in space, there is only one source position capable of producing it. But at a given precision several configurations can be equivalent.

The main difficulty encountered during the study is the physical possibility of a given structure to generate the required field profile. The choice of the magnet cage and the displacement in z alone does not necessarily prove the existence of the solution even if it is in the correction domain. A mathematical study of the coupling between equations in the case of a given structure would certainly allow us to raise this question. To reach this problem we have not obtained with great precision for all flat gradients. Some coefficients pose difficulties because we deliberately limit the location of sources to restricted areas.

The equations composing the system are fractions of polynomials, it is therefore possible to analytically invert these equations and rewrite them on the form of a Groebner base. However, putting these fractions on the same denominator provides a polynomial of very high degree. If this track is followed, it is imperative to continue to the Groebner base, otherwise we will be back to the search for polynomial roots, which we are already doing.

Bibliography

- [1] N. N. Abdelmalek. On the solution of least squares problems and pseudo-inverses. *Computing*, 13:215–228, 1974.
- [2] Forman S. Acton. *Numerical Methods That Work*. Mathematical Association of America, 1990.
- [3] Kishimoto Sakasai Ara. Solution of electromagnetic inverse problem using combinational method of hopfield neural network and genetic algorithm. *Journal of Applied Physics*, 79:1–7, 1996.
- [4] Artley. *Fields and Configurations*. Holt, Rinehart, Winston, New York, 1965.
- [5] Saint-Jalmes Taquin Barjoux. Optimization of homogeneous electromagnetic coil systems: application to whole body nmr imaging magnets. *Review Of Scientific Instruments*, 52:1501–1508, 1981.
- [6] Bertram. On the convergence of iterative solutions of the integral magnetic field equation. *IEEE Transactions on Magnetism*, 11:928–933, 1975.
- [7] Turner Bowley. Passive screening of switched magnetic field gradients. *J Phys:Scientific Instruments*, 19:876–879, 1986.
- [8] Crozier Dodd Luescher Field Doddrell. The design of biplanar, shielded, minimum energy, or minimum power pulsed b0 coils. *MAGMA*, 3:49–55, 1995.
- [9] O Dwyer O Donnell. Choosing the relaxation parameter for the solution of nonlinear magnetic field problems by the newton-raphson method. *IEEE Transactions on Magnetism*, 31, 1995.
- [10] Durand. *Magnétostatique*. Masson, 1968.
- [11] L. Eldén. A weighted pseudoinverse, generalized singular values, and constrained least squares problems. *BIT*, 22:487–502, 1983.

- [12] D. I. Hoult F. Romeo. Magnet field profiling: Analysis and correcting coil design. *Magnetic Resonance in Medicine*, 1:44–65, 1984.
- [13] Press Vetterling Teukolsky Flannery. *Numerical Recipes in C*. Cambridge University Press, 1992.
- [14] R. Fletcher. *Practical Methods of Optimization*. JOHN WILEY & SONS, 1987.
- [15] G. E. Forsythe, M. A. Malcolm, and C. B. Moler. *Computer Methods for Mathematical Computations*. Prentice-Hall, Englewood Cliffs, N.J., 1977.
- [16] Philip E. Gill, Walter Murray, and Margaret H. Wright. *Practical Optimization*. Acpress, 1981.
- [17] G. H. Golub and W. Kahan. Calculating the singular values and pseudo-inverse of a matrix. *SIAM Journal on Numerical Analysis*, 2:205–224, 1965.
- [18] G. H. Golub and C. Reinsch. Singular value decomposition and least squares solution. *Numerische Mathematik*, 14:403–420, 1970.
- [19] I. J. Good. Some applications of the singular decomposition of a matrix. *Technometrics*, 11, 1969.
- [20] S. J. Hammarling. The singular value decomposition in multivariate statistics. *ACM SIGNUM Newsletter*, 20:2–25, 1985.
- [21] Hawksworth. New magnet designs for mr. *Magnetic Resonance in Medecine*, 17:27–32, 1991.
- [22] Ersahin Hinks Bronskill Henkelman. Biplanar gradient coil for interventional open-concept superconducting magnet. In *Fourth ISMRM Meeting, New York, 124*, 1996.
- [23] Ersahin Hinks Bronskill Henkelman. Gradient coil design for interventional open configuration magnet with pole pieces. In *Fifth ISMRM Meeting, Vancouver, British Columbia, Canada*, 1997.
- [24] J.D. Jackson. *Classical Electrodynamics*. John Wiley & Sons, 1975.
- [25] Kenneth Levenberg. A method for the solution of certain non-linear problems in least-squares. *Quarterly of Applied Mathematics*, 2(2):164–168, July 1944.

- [26] Donald W. Marquardt. An algorithm for the least-squares estimation of nonlinear parameters. *SIAM Journal of Applied Mathematics*, 11(2):431–441, June 1963.
- [27] Labiche Taquin Momy. Correction d’un champ magnétique statique par aimants permanents. In *Numelec’97, Ecole Centrale de Lyon*, 1997.
- [28] Nakata Fujiwara Okamoto Muramatsu. Method for determining relaxation factor for modified newton-raphson method. *IEEE Transactions on Magnetism*, 29:1962–1965, 1993.
- [29] Rheinboldt Ortega. *Iterative Solution of Nonlinear Equation In Several Variables*. New York: Academic Press, 1970.
- [30] Ostrowski. *Solutions of Equations and Systems of Equations*. New York: Academic Press, 1966.
- [31] H. Feshbach P. M. Morse. *Methods of Theoretical Physics*. Mc Graw-Hill Book Compagny, 1953.
- [32] Martens Petropoulos Brown Andrew Morich Patrick. Insertable bipolar gradient coils for magnetic resonance imaging. *Rev Sci Instrum*, 62(11):2639–2645, 1991.
- [33] G. Peters and J. H. Wilkinson. Inverse iteration, ill-conditioned equations, and Newton’s method. *SIAM Review*, 21:339–360, 1979.
- [34] Bank Rose. Parameter selection for newton-like methods applicable to non-linear partial differential equations. *SIAM Journal of Numerical Analysis*, 17:806–822, 1980.
- [35] Roubine. *Compléments d’électromagnétisme*. Ecole Supérieure d’Electricité, 1980.
- [36] Albanese Rubinacci. Numerical procedures for the solution of non linear electromagnetic problems. *IEEE Transactions on Magnetism*, 28:1228–1231, 1992.
- [37] Tikhonov Samarskii. *Equations of mathematical physics*. Dover Publications, Inc, 1990.
- [38] Saint-Jalmes Darrasse Taquin Sauzade. Etudes de bobines de gradients commutés, de bobines de déplacements de champs et de bobines de correction pour imageurs de rmn. *Rapport final du contrat ANVAR, IEF Orsay*, 84460200, 1987.

- [39] Souza Vidigal Momy Taquin Sauzade. Nonlinear calculations of three-dimensional static magnetic fields. *IEEE Transactions on Magnetism*, 33:2486–2491, 1997.
- [40] Souza Vidigal Taquin Sauzade. Optimal design of a self shielded magnetic resonance imaging magnet. *Journal de Physique II*, pages 2121–2132, 1993.
- [41] M. Souza. *Etude d'un système magnétique pour IRM de grand volume et d'accès facile à la zone homogène*. PhD thesis, Université de PARIS-SUD, Centre d'Orsay, 1992.
- [42] P. N. Swarztrauber. On the spectral approximation of discrete scalar and vector functions on the sphere. *SIAM J. Numer. Anal.*, 16, December 1979.
- [43] Labiche Taquin. Magnetic field profile generation software. In *Computomag, Rio de Janeiro*, 1997.
- [44] Torset Labiche Momy Taquin. Gradient design for an imager n.m.r with flat magnet. In *ESMRMB*, 1996.
- [45] Simkin Trowbridge. Optimizing electromagnetic devices combining direct search methods with simulated annealing. *IEEE Transactions on Magnetism*, 28:1545–1548, 1992.
- [46] Turner. A target field approach to optimal coil design. *Journal of Applied Physics*, 19:L147–L151, 1986.
- [47] Turner. Gradient coil design: A review of methods. *MRI*, 11:903–920, 1993.
- [48] R. Vadovic. Magnetic field correction using magnetized shims. *IEEE Transactions On Magnetism*, 25(4):3133–3139, 1989.
- [49] J. M. Varah. On the numerical solution of ill-conditioned linear systems with applications to ill-posed problems. *SIAM Journal on Numerical Analysis*, 10:257–267, 1973.
- [50] Y.Semezis V.Drivas, L.Rosenthal. *La pratique des tenseurs*. Eyrolles, 1987.
- [51] C. E. Vidigal. *Méthode de calcul de champ magnétique pour IRM avec aimant permanent et fer*. PhD thesis, Université de PARIS-SUD, Centre d'Orsay, 1992.

- [52] Nestor Sepulveda Wikswo. A numerical study of the use of magnetometers to detect hidden awes in conducting objects. *Journal of Applied Physics*, 79:2122–2135, 1996.
- [53] Yoda. Analytical design method of self-shielded planar coils. *Journal of Applied Physics*, 67:4349–4353, 1990.